

**Universität  
Basel**



Master Thesis, M.Sc in Nanosciences

Submitted by

Benjamin Bellon

b.bellon@stud.unibas.ch

Basel, 18 December 2015

# ***In vitro* Evaluation of the Relevant Properties of Different Bone Graft Materials**

Supervised by

Prof. Dr. Dr. Jens Fischer

University of Basel, University Hospital  
of Dental Medicine

Prof. Dr. Thomas Pfohl

University of Basel, Department of  
Chemistry

## Abstract

Different bone graft materials are commercially available varying in origin, chemical composition, surface morphology, porosity, and grain size. The most popular synthetic products chemically belong to the family of calcium orthophosphates. Recently, novel synthetic composite materials of electrospun PLGA fibers doped with amorphous tricalcium phosphate are being developed that offer promising properties for successful bone augmentation. Degradation behavior and bioactivity are considered to be key factors for the performance of a bone graft material upon transplantation. The bioactivity of materials is commonly tested *in vitro* by immersion of the material in solutions with ion concentrations near or equal to human blood plasma (simulated body fluid). Precipitation of HA on the materials upon immersion is proposed to be a measure of bioactivity and therefore facilitates bone augmentation.

In this study, the degradation and precipitation behavior of 13 different bone graft materials was investigated by immersion of the materials in simulated body fluid for different time intervals (12 h, 24 h, 168 h, and 336 h). Weight changes upon immersion were measured and physicochemical analysis was performed before and after different immersion times (SEM, XRD, EDS, MIP, and ICP-OES). Five commercially available products were investigated. Two of them were sintered biphasic calcium phosphates (BCP) with a HA/ $\beta$ -TCP ratio of 60/40 wt%, one material was composed of 76 wt% HA embedded in an amorphous silica matrix, and two were single phase HA materials. Furthermore, four BCPs with a  $\beta$ -TCP content between 80 and 50 wt% and the corresponding single phase HA material were investigated. Moreover, two of the mentioned composite materials with a PLGA/ATCP ratio of 80/20 wt% and 60/40 wt% and pure PLGA fibers were used for the bioactivity test.

A mass gain due to precipitation of HA was measured for every sample, although the amount of precipitated HA differed significantly among the materials. The most significant mass gain of 10 % of the initial sample mass after 168 h of immersion was observed in the 40 wt% ATCP doped PLGA fibers. Significant mass gain between 3 % and 6 % was measured in the single phase HA materials after 336 h of immersion. The unsintered BCPs and the corresponding HA material showed the most prominent mass gain, in 80 wt%  $\beta$ -TCP, of 5 % after 336 h immersion, followed by the single phase HA material with a weight gain of 3 %. A weight gain below 3 % was measured in the BCP with HA/ $\beta$ -TCP ratios in between. The sample of HA embedded in amorphous silica showed a weight gain of 1.5 % after 12 h and then a continuous mass loss compared to the initial sample weight before immersion. The two sintered BCPs both induced minimal HA precipitation and therefore a weight gain below 1.5 % was measured after 336 h of immersion.

The findings indicate that factors favoring HA precipitation are high surface roughness, porosity and surface area in combination with a release of  $\text{Ca}^{2+}$  and  $\text{PO}_4^-$  from the material. Sintered materials admittedly alter mechanical properties but the smooth surface, arising from the high temperature procession, seemed to inhibit HA precipitation. The relations between physicochemical properties and the performance in the bioactivity test, may be useful for the development of novel bone graft materials with controllable dissolution and integration behavior.

# Content

1.	Introduction	1
1.1.	Bone Anatomy	1
1.2.	Principles of Bone Regeneration	2
1.3.	Requirements for Bone Graft Materials	3
1.4.	Classification of Bone Graft Materials	4
1.4.1.	Autograft	4
1.4.2.	Allograft	4
1.4.3.	Xenograft	4
1.4.4.	Synthetic Bone Graft	5
1.4.4.1.	Calcium Phosphates and Calcium Phosphate Ceramics	5
1.4.4.2.	Calcium Sulfates	6
1.4.4.3.	Silicon Based Compounds	6
1.4.4.4.	Composite Materials	6
1.5.	Dissolution and Precipitation of Calcium Phosphates	7
1.5.1.	Solubility	7
1.5.2.	Apatite Formation in Simulated Body Fluid	9
1.6.	Aim of the Study	11
2.	Materials	12
2.1.	Commercial Products	12
2.2.	Biphasic Calcium Phosphate Series	12
2.3.	Composite Materials	13
3.	Methods	14
3.1.	Material Characterization	14
3.2.	In vitro Bioactivity Test	14
4.	Results	16
4.1.	Commercial Materials	16
4.1.1.	Surface Morphology	16
4.1.2.	Phase and Elemental Composition	17

4.1.3. In vitro Bioactivity Test	19
4.2. AlgOss® Series	22
4.2.1. Surface Morphology	22
4.2.2. Phase and Elemental Composition	23
4.2.3. In vitro Bioactivity Test	25
4.3. Composite Materials	27
4.3.1. Surface Morphology	27
4.3.2. Phase and Elemental Composition	28
4.3.3. In vitro Bioactivity Test	28
5. Discussion	33
5.1. Commercial Materials	33
5.1.1. Commercial BCP	33
5.1.2. Nanobone®	34
5.1.3. Commercial HA Based Materials	34
5.2. AlgOss® Series	35
5.3. Composite Materials	36
6. Conclusion and Outlook	39
7. Acknowledgments	41
8. References	42
9. Appendix	45

# 1. Introduction

Bone is the most common tissue for surgical transplantation procedures right after blood. It is estimated that alone in the United States 500,000 bone augmentation procedures are performed every year, which illustrates the importance of bone transplantation and the financial costs arising for healthcare<sup>1,2</sup>. In general, bone grafting is used whenever natural bone is missing or deficient and needs to be replaced or augmented. The materials used in such regenerative surgeries are so called “bone graft substitutes”. In short, a bone graft substitute is described as a material that promotes bone healing after transplantation into the defect site. The applications range from spine fusion<sup>3</sup> over plastic surgery after accidents with massive bone lost<sup>4,5</sup> to the use in oral surgery<sup>2</sup>. The role of bone graft substitutes in oral surgery has become more and more important over the last decades and they are an important tool in augmentative surgery, implantology, and periodontology<sup>6-11</sup>.

## 1.1. Bone Anatomy

Bone is considered as a nanocomposite composed of an organic and an inorganic phase<sup>12</sup>. The organic phase consists mainly of collagen fibers, a small amount of other proteins, and some incorporated water<sup>13,14</sup>. The collagen fibers act as a framework for the minerals in the inorganic phase and are responsible for tensile strength and flexibility of bone tissue. The inorganic phase of bone consists mainly of highly structured hydroxyapatite nanocrystals

**Table 1:** The composition of bone<sup>2</sup>

Inorganic phase	wt%	Organic phase	wt%
Hydroxyapatite	~ 60	Collagen	~ 20
Carbonate	~ 4	Water	~ 9
Citrate	~ 0.9	Non-collagenous proteins	~ 3
Sodium	~ 0.7		
Magnesium	~ 0.5		
Other traces: Cl <sup>-</sup> , F <sup>-</sup> , K <sup>+</sup> , Sr <sup>2+</sup> , Pb <sup>2+</sup> , Zn <sup>2+</sup> , Cu <sup>2+</sup> , Fe <sup>2+</sup>			

with traces of other minerals. Those minerals are responsible for toughness and rigidity of bone tissue. An overall composition of human bone can be seen in table 1. It has to be mentioned that the proportions of organic and inorganic phases can vary from bone to bone depending on their function and the age. It is fascinating how nature managed to build such a hard and tough material like bone considering that this material is made out of very soft collagen and brittle hydroxyapatite. One reason for that is the nanocomposite feature of bone that combines beneficial properties of both ingredients in one material. But the key that makes bone such a sophisticated material is its complex structural hierarchy<sup>15,16</sup>. Newly built bone is rather unorganized and shows weak mechanical properties. It is called woven bone and is formed during embryonic development, fracture repair, or after bone

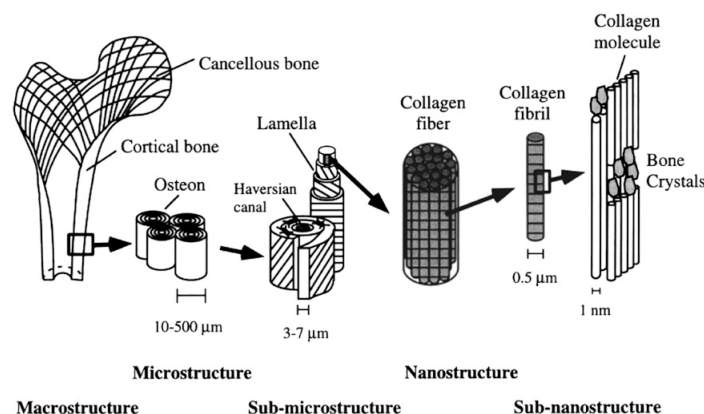


**Figure 1:** The hierarchial structure of bone<sup>16</sup>

graft incorporation<sup>17</sup>. To become such a hard and tough tissue it is organized in a highly complex structure (fig. 1). At the nanostructural level bone consists of collagen fibrils to which hydroxyapatite (HA) nanocrystals are bound via non-collagenous proteins. Those non-collagenous proteins are very important for cellular attachment and for the biomineralization process, since minerals are not directly bound to collagen. Those hydroxyapatite enriched collagen fibrils are organized to bundles of mineralized collagen fibers that are the main unit of every bone<sup>12,15</sup>. Depending on the type of bone, those collagen fibers organize at the microstructural level either to so called osteons or to trabeculae. Osteons are found in compact or cortical bone whereas trabeculae are found in spongy or cancellous bone. Compact bone is much denser than spongy bone and resists high mechanical forces like tension, compression, or torsion. Spongy bone is much more porous and therefore lighter than cortical bone, but it is weaker and only resists to compression.<sup>2</sup>

## 1.2. Principles of Bone Regeneration

Bone is a living tissue that undergoes permanent remodeling and adaption to mechanical stress. Furthermore, it exhibits excellent self-healing properties after a disruption, like a fracture. Provided that the individual is healthy, that the disruption is not too severe and that the disruption site is stabilized during healing, bone tissue is capable of repairing the defect within months without losses of its mechanical properties<sup>17</sup>. The process of fracture healing can be divided into different stages (fig. 2). The first reaction of the body after a bone fracture is the formation of a hematoma at the fracture site caused by injured blood vessels. The function of this hematoma is to clog the injured site so that the blood stream is stopped building a fibrovascular tissue around the fracture site. Furthermore, it recruits a number of cytokines, growth factors and inflammatory cells to remove necrotic tissue. Cells near the fracture site differentiate into chondroblasts forming a cartilaginous matrix. Then, pluripotential mesenchymal cells migrate to the fracture site to proliferate and differentiate into osteoblasts forming woven bone within the matrix. Osteoblasts secrete collagen and coat those fibers with non-collagenous proteins which are capable of binding minerals like calcium and phosphate from the blood stream building new bone.<sup>2</sup> This process goes on until the fracture gap is filled with cartilaginous matrix and woven bone and is then called fracture callus. The last and longest step is called remodeling and involves the replacement of the cartilaginous matrix and woven bone into structured lamellar bone.<sup>17-19</sup> However, there are circumstances that require bone graft substitutes for proper healing, for example after traumatic injuries with severe loss of bone tissue. In such cases, a bone graft material is incorporated into the gap of the disrupted site where bone material is missing to provide a scaffold into which the new bone can grow. The graft material acts primarily as a mechanical support of the injured site but also as an osteoconductive matrix

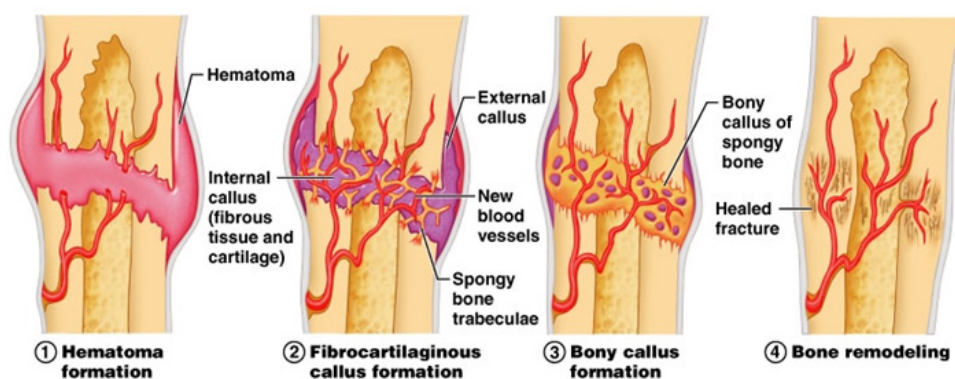


Figure 2: The different stages of bone regeneration<sup>20</sup>

for the bone regeneration process described above. During this process the bone graft material is traversed by cartilaginous matrix and woven bone and incorporated into the defect site. Depending on the material, it is then either reabsorbed by the body and replaced with bone material or it stays incorporated into the defect site. With the help of bone graft materials, it is possible to replace large amounts of missing bone where the body would not have been able to perform natural bone regeneration.<sup>20-27</sup>

### **1.3. Requirements for Bone Graft Materials**

Osteoconduction, osteoinduction and osteogenesis are the three most important elements of bone regeneration.<sup>28,29</sup> Probably the most important of these components is osteoconduction which is an essential property of a bone graft substitute. An osteoconductive material provides a scaffold for the newly formed bone, which osteoblasts and blood vessels from the adjacent bone can use as a matrix to facilitate bone generation. Therefore, the porosity of the material plays an important role in osteoconductive behavior, since blood vessels and cells have to be able to grow through the pores of the material<sup>30</sup>. Porosity also plays an important role in degradation and resorption processes<sup>31</sup>. Furthermore, an osteoconductive material stabilizes the cavity and prevents soft tissue from filling the defect. For bone augmentation, a bone substitute should at least be osteoconductive. Osteoinduction is the ability of a bone graft substitute to actively induce undifferentiated or progenitor cells from the surrounding tissue to differentiate into osteoblasts.<sup>32</sup> The induction of surrounding cells into osteoblasts is mainly facilitated by growth factors like bone morphogenetic proteins (BMPs).<sup>33</sup> Osteogenesis can be achieved by the incorporation of vital osteoblasts or osteoblast progenitor cells into the bone graft that survive the transplantation process. These cells are able to synthesize new bone material directly at the defect site.<sup>21,32</sup> Another important property of bone graft substitutes is called osseointegration, which is the ability of a material to chemically bind to the natural bone without creating a vulnerable boundary layer. Osseointegration is strongly influenced by the surface morphology and chemical composition of the transplanted material.<sup>32,34</sup> Furthermore, an ideal bone graft substitute should be biocompatible and biodegradable, which means that the substitute is harmless to the surrounding tissue and is, eventually, completely replaced by natural bone. Biodegradability is based on degradation via dissolution and on active cellular phagocytosis.<sup>4,19,35</sup> Porosity, surface morphology, chemical composition, and crystallinity of a bone graft material have a strong influence on dissolution properties and therefore on the ability to biodegrade.<sup>36,37</sup> Another important feature of bone graft materials is called bioactivity. Generally, this term refers to a material's capability of inducing a specific biological activity. Regarding to bone graft materials, bioactivity can be facilitated by a materials capability of binding to natural bone via the formation of apatite crystals on its surface upon implantation. The formation of apatite crystals on the surface of a bone graft material can therefore be seen as a measure of osseointegration capability.<sup>38-40</sup> Non-bioactive materials, for example metal alloys, are often encapsulated by fibrous tissue after implantation which weakens the performance of the implant and is not desired in bone regeneration.<sup>39</sup> Therefore, bioactivity facilitates osseointegration of a bone graft material. Since biodegradability and bioactivity are considered to be key factors in the performance of bone graft substitutes, this study concentrates on the *in vitro* evaluation of those features. Furthermore, the material should be chemically and structurally similar to natural bone, it should be easy to handle and cost effective.

## **1.4. Classification of Bone Graft Materials**

Bone graft materials are classified in four groups according to their origin. The four groups are called autograft, allograft, xenograft and synthetic bone graft.

### **1.4.1. Autograft**

The gold standard for the treatment of bone defects is the harvest of cortical and cancellous bone from the patient and the transplantation of the obtained material into the defect.<sup>16,41</sup> These transplants are called autografts and exhibit many of the desired requirements of a bone graft material. At the moment, autologous bone is the only bone graft material that is osteoconductive, osteoinductive, osteogenic, and which shows excellent osseointegration. Since the material is natural bone, all other requirements like biocompatibility, bioresorbability, as well as similar chemical and structural properties are given. Although it seems that autologous bone is the perfect bone graft material, there is one severe disadvantage which is its availability. On the one hand, sources for suitable donor bone material are rare and the amount of material that can be obtained is very limited. On the other hand, a second surgical procedure is necessary to harvest donor material, which is an additional stress factor for the patient and can lead to increased morbidity.<sup>1,5,28,42</sup> Due to the second surgery needed to harvest donor material, the procedure is unsatisfying regarding to cost- and time-efficiency.

### **1.4.2. Allograft**

To circumvent the problems associated with autografts, it is possible to harvest the donor material from another individual of the same species, which is called an allograft. However, there is a risk of negative immune response and transmission of diseases. Therefore, the material is processed prior to implantation which causes loss of osteogenic and limitation of osteoinductive behavior.<sup>18,24,43</sup> There are different methods used to process allogenic bone material like sterilization in antibiotics, irradiation, freezing, freeze-drying and decalcification which all minimize the risk of a disease transmission and a negative immune response.<sup>1,21</sup> After processing, the material has lost its osteogenic properties due to elimination of all cellular components. Depending on the processing method, allografts can maintain some of their osteoinductive properties. Generally, it can be said that a more aggressive processing minimizes the risk of a disease transmission and a negative immune response, but also leads to loss of osteoinductive properties.<sup>1,28,44</sup> Furthermore, the sterilization process leads to decreased mechanical properties compared to autologous bone material.<sup>45,46</sup>

### **1.4.3. Xenograft**

A xenograft is defined as tissue harvested from another species. Due to the similarities to human bone regarding chemical and structural properties, xenografts are mostly of bovine or porcine origin. Also, xenografts from coral or algae are used, but they need to be further processed to adapt to the chemical composition needed for human bone grafts.<sup>47</sup> Therefore, xenografts from coral or algae can also be placed in the group of synthetic bone grafts. Compared to allografts, xenografts exhibit very similar properties, and there are no limitations in availability. Depending on the xenograft used, there is a more aggressive processing needed to eliminate every transmission risk, or even further processing steps are needed to change the chemical and structural composition. Due to this processing, the osteoinductive properties of xenografts are completely lost.

**Table 2:** Properties of types of bone grafts<sup>48</sup>

	Osteoconductive	Osteoinductiv	Osteogenic
<b>Autograft</b>	+	+	+
<b>Xenograft</b>	+	-	-
<b>Allograft</b>	+	+/-	-

#### 1.4.4. Synthetic Bone Graft

To overcome the problems of availability, negative immune response and disease transmission, there are many synthetic bone grafts available on the market. These synthetic bone grafts can be divided in subgroups depending on their chemical composition.

##### 1.4.4.1. Calcium Phosphates and Calcium Phosphate Ceramics

Calcium phosphates and calcium phosphate ceramics serve as excellent alternatives to non-synthetic bone grafts since they are composed of the same constituents as the main components of natural bone namely calcium- ( $\text{Ca}^{2+}$ ) and phosphate ( $\text{PO}_4^{2-}$ ). They exhibit osteoconductive and osteointegrative properties with minimal fibrotic reaction, are biocompatible, no foreign body reactions are reported and effectiveness is proved in many clinical studies.<sup>2,29,44,47</sup> There are different calcium phosphate phases with variable Ca/P ratios (table 3). The main difference between these phases relevant for bone augmentation is displayed in variable resorption and dissolution properties. It has been shown that hydroxyapatite (HA), beta tricalcium phosphate ( $\beta$ -TCP) and biphasic calcium phosphate (BCP), which is a mixture of HA and TCP, are the most suitable phases for the use as bone graft materials.<sup>49,50</sup>

HA is the most stable phase in this group and is the main component of natural bone with a Ca/P

**Table 3:** Different calcium orthophosphates and their major properties.<sup>14</sup>

Ca/P molar ratio	Compound	Formula	Solubility at 25°C [-logK <sub>sp</sub> ]	Solubility at 25°C [g/L]
0.5	Monocalcium phosphate monohydrate (MCPM)	$\text{Ca}(\text{H}_2\text{PO}_4) \cdot 2\text{H}_2\text{O}$	1.14	~18
0.5	Monocalcium phosphate anhydrate (MCPA)	$\text{Ca}(\text{H}_2\text{PO}_4)_2$	1.14	~17
1.0	Dicalcium phosphate dihydrate (DCPD, "brushite")	$\text{CaHPO}_4 \cdot 2\text{H}_2\text{O}$	6.59	~0.088
1.0	Dicalcium phosphate anhydrate (DCPA, "monetite")	$\text{CaHPO}_4$	6.90	~0.048
1.33	Octacalcium phosphate (OCP)	$\text{Ca}_8(\text{HPO}_4)_2(\text{PO}_4)_5 \cdot 5\text{H}_2\text{O}$	96.6	~0.0081
1.5	$\alpha$ -tricalcium phosphate	$\alpha\text{-Ca}_3(\text{PO}_4)_2$	25.5	~0.0025
1.5	$\beta$ -tricalcium phosphate	$\beta\text{-Ca}_3(\text{PO}_4)_2$	28.9	~0.0005
1.2 - 2.2	Amorphous calcium phosphates (ACP)	$\text{Ca}_x\text{H}_y(\text{PO}_4)_z \cdot n\text{H}_2\text{O}$ , n=3-4.5	~25.7	~0.0027
1.5 - 1.67	Calcium-deficient hydroxyapatite (CDHA)	$\text{Ca}_{10-x}(\text{HPO}_4)_x(\text{PO}_4)_{6-x}(\text{OH})_{2-x}$ (0<x<1)	~85	~0.0094
1.67	Hydroxyapatite (HA, Hap or OHAp)	$\text{Ca}_{10}(\text{PO}_4)_6(\text{OH})_2$	116.8	~0.0003
1.67	Fluorapatite (FHA)	$\text{Ca}_{10}(\text{PO}_4)_6\text{F}_2$	120.0	~0.0002
2.0	Tetracalcium phosphate (TTCP)	$\text{Ca}_4(\text{PO}_4)_2\text{O}$	38-44	~0.0007

ratio of 1.67. The resorption properties of HA depend on morphological features like porosity and on processing procedures like sintering. Generally, it can be said that high porosity favors dissolution and resorption whereas sintering of HA at high temperatures leads to a highly crystalline structure and low resorption and dissolution rates.<sup>36,37</sup> Because of the low resorption rate, bone grafts consisting of pure HA cannot be fully replaced by natural bone and synthetic HA material can be found within the bone defect even years after implantation, which can affect the structure and physical properties of the regenerated bone fragment.

$\beta$ -TCP has a Ca/P ratio of 1.5 which makes it less stable than HA. The consequence is that  $\beta$ -TCP is resorbable by the human body via dissolution within 6 to 18 months.<sup>29,31</sup> Furthermore, it has been shown that  $\beta$ -TCP is able to partially convert into HA, the main component of natural bone, when implanted into the human body.<sup>51</sup> This ability is believed to arise from the fact that natural bone precursors have a similar Ca/P ratio like  $\beta$ -TCP.<sup>52</sup> Moreover, the relatively fast release of calcium phosphate ions seems to have an osteoinductive effect which is missing in pure HA materials.<sup>53</sup> On the one hand, the higher degradation rate compared to HA is an advantage because of the reasons mentioned above. On the other hand, this behavior can lead to problems when the resorption rate of  $\beta$ -TCP is higher than the rate of newly formed bone by means of volume loss and resulting inflammation reactions.<sup>29,47</sup>

BCP is a mixture of HA and  $\beta$ -TCP combining the positive properties of both materials and is therefore considered to be the gold standard within the group of synthetic bone graft materials.<sup>14,47</sup> Another great advantage of BCP is that the ratio between HA and  $\beta$ -TCP can be varied which makes it possible to trigger dissolution properties.

#### 1.4.4.2. Calcium Sulfates

There are records from the 10<sup>th</sup> century where calcium sulfates were used by the Arabs to treat fractured bones, which probably makes them one of the oldest bone graft materials.<sup>29</sup> They act as an osteoconductive matrix for blood vessels, fibrogenic, and osteogenic cells.<sup>54</sup> Calcium sulfates are rather soluble in aqueous environment and are reabsorbed by the human body within 6 to 12 weeks via dissolution.<sup>5,29</sup>

#### 1.4.4.3. Silicon Based Compounds

Bioactive glasses are mainly composed of silicon oxide ( $\text{SiO}_2$ ) with varying proportions of sodium oxide, calcium oxide and phosphorous pentoxide. The main advantage of these silicon based compounds is the strong osteointegrative behavior based on the fact that  $\text{SiO}_2$  is able to chemically bind directly to bone tissue in physiologic aqueous environment.<sup>29</sup> Bioactive glasses also have osteoconductive properties depending on the proportions of the other oxides mentioned above, which also have an influence on dissolution properties. Hence, bioactive glasses can be produced from non-resorbable to resorbable by the human body.<sup>55</sup>

#### 1.4.4.4. Composite Materials

In the last two decades polymer composites with incorporated inorganic or organic fillers have gained significance in the field of bone regeneration.<sup>56</sup> Since natural bone itself is a composite material with an inorganic HA phase and an organic collagen phase, it seems obvious to use similar composite materials for bone regeneration. Many polymers have been developed that are biocompatible and

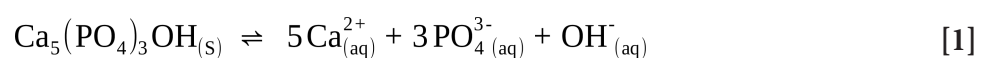
degrade in the human body to non-toxic products with a controllable and adjustable rate.<sup>14,57</sup> Most popular examples of such polymers used in tissue engineering are poly-(glycolic acid) (PGA), poly-(lactic acid) (PLA) and poly-(lactic acid-co-glycolic acid) (PLGA). These polymers can be produced with an extremely high porosity leading to a high surface area to volume ratio. Hence, they build an excellent scaffold for bone regeneration, meaning that osteoconductivity is given in such polymers. Moreover, the mechanical properties such as toughness and elasticity enable easy handling for surgeons which minimizes complications and costs for the patient. Probably the most promising advantage of such polymers in tissue engineering is the fact that there are almost no limitations for the incorporation of other materials enhancing their performance. Incorporation of HA or TCP nanoparticles leads to composite materials that exhibit the advantages mentioned for calcium phosphates combined with better handling, higher surface area, increased protein adsorption and osteoblast adhesion together with highly controllable degradation rate.<sup>56</sup> Furthermore, it is possible to incorporate osteoinductiv growth factors such as BMP, other beneficial proteins, antibiotic drugs, etc. into the polymer matrix enhancing the *in vivo* performance of the graft material.<sup>57,58</sup> Theoretically, there are no limitations for the preparation of tailored composite materials which makes it possible to combine osteoconductive, osteoinductiv, osteogenic and osteointegrative properties in one bone graft material.

## 1.5. Dissolution and Precipitation of Calcium Phosphates

As already mentioned, biodegradability of a bone substitute is facilitated by degradation via dissolution and by active cellular phagocytosis. Therefore, the dissolution properties in aqueous solutions are crucial for the performance of a bone graft material. It is considered that the formation of an apatite layer on the surface of a bone graft when implanted into the body is essential for the ability to bind to living bone.<sup>30,59</sup> Materials exhibiting this behavior are called bioactive materials and it is believed that *in vivo* bioactivity can be estimated by the formation of apatite crystals on the surface of an implant upon immersion in a solution with ion concentrations equal to human blood plasma (simulated body fluid, SBF).<sup>39,60-64</sup> Since biodegradability and bioactivity are crucial for the performance of a bone graft material and are the focus of this study, the dissolution and precipitation properties of calcium phosphates are discussed in the following section.

### 1.5.1. Solubility

The solubility of a compound in a certain solvent is a thermodynamic process and is described by the solubility product  $K_{sp}$ . When an ionic compound is dissolved in a solvent, equilibrium between the compound in solid state and the ions in dissolved state is reached eventually. In the state of equilibrium the solution is saturated in relation to the compound which means that the rate of dissolution is equal to the rate of precipitation. Based on the law of mass action, an equilibrium expression for hydroxyapatite and water can be written as it is done here:



The equilibrium expression for this reaction is

$$K_{sp} = \frac{a^5(\text{Ca}^{2+}) \cdot a^3(\text{PO}_4) \cdot a(\text{OH}^-)}{a(\text{Ca}_5(\text{PO}_4)_3\text{OH})} \quad [2]$$

where  $a$  is the activity of the compounds.

$$a = \gamma \cdot c \quad [3]$$

where  $\gamma$  is the activity coefficient and  $c$  is the concentration in the saturated solution. The activity of a solid is by definition always 1, therefore

$$K_{sp} = a^5(\text{Ca}^{2+}) \cdot a^3(\text{PO}_4) \cdot a(\text{OH}^-) \quad [4]$$

For compounds with low solubility up to 0.1 mol/L<sup>65</sup> the activity coefficients are nearly 1 which leads to the expression of the thermodynamic solubility product for hydroxyapatite

$$K_{sp} = c^5(\text{Ca}^{2+}) \cdot c^3(\text{PO}_4) \cdot c(\text{OH}^-) \quad [5]$$

and

$$pK_{sp} = -\log[c^5(\text{Ca}^{2+}) \cdot c^3(\text{PO}_4) \cdot c(\text{OH}^-)] \quad [6]$$

The solubility product  $K_{sp}$  of a compound describes the dissolved amount in a solvent at a certain temperature in equilibrium. When the ion concentrations in the solution are higher than the solubility product  $K_{sp}$  the solution is supersaturated with respect to the compound and precipitation of the compound is thermodynamically favored. When the ion concentrations are lower than  $K_{sp}$  the solution is undersaturated and the compound is fully dissolved. The driving force for dissolution or precipitation of a compound from a solution is a change in Gibbs free energy  $\Delta G$  and can be described with the following equation:

$$\Delta G = \Delta G^0 + RT \ln(K) \quad [7]$$

or

$$\frac{\Delta G}{RT} = \frac{\Delta G_0}{RT} + \ln K \quad [8]$$

where  $\Delta G_0$  is the standard free energy,  $R$  is the gas constant,  $T$  is the absolute temperature and  $K$  is the solubility product of the compound in solution (not in equilibrium).  $K$  becomes  $K_{sp}$  in the state of equilibrium where  $\Delta G = 0$ . When  $\Delta G = 0$  the process is in equilibrium, which means that the solution is saturated. In this case equation 7 becomes:

$$\frac{\Delta G_0}{RT} = -\ln K = -\ln K_{sp} \quad [9]$$

Combining equation 8 and 9 leads to the expression for the thermodynamic saturation level  $L_{sat}$

$$\frac{\Delta G}{RT} = \ln \frac{K}{K_{sp}} = \ln L_{sat} \quad [10]$$

When  $L_{sat} = 1$  the solution is saturated with the compound and  $\Delta G = 0$ . When  $L_{sat} < 1$  the solution is undersaturated and  $\Delta G < 0$ , which means that expression [1] tends to move to the right and the compound dissolves. When  $L_{sat} > 1$  the solution is supersaturated and  $\Delta G > 0$ , which means that expression [1] tends to move to the left and precipitation will occur.<sup>66</sup> The solubility behavior of calcium orthophosphates can be described with solubility diagrams. Since calcium orthophosphates are composed of a base ( $\text{Ca}(\text{OH})_2$ ) and an acid ( $\text{H}_3\text{PO}_4$ ) it is necessary to use the pH as a variable to fully describe the solubility behavior. In figure 3 the solubility phase diagrams of the ternary system  $\text{Ca}(\text{OH})_2 - \text{H}_3\text{PO}_4 - \text{H}_2\text{O}$  at 37 °C are shown. The logarithms of calcium- or phosphorus concentration in equilibrium with their saturated solution are plotted as a function of the pH. The amount of dissolved ions depends on the solubility product  $K_{sp}$  of the compound and on the pH of the solution. At pH 7.4 the solubility decreases in order of TTCP >  $\alpha$ -TCP > DCPD > DCPA > OCP >  $\beta$ -TCP > HAp. It can be seen that hydroxyapatite (HAp) is the least soluble calcium phosphate down to a pH of 4.2 followed by  $\beta$ -TCP. It is important to mention that the solubility diagrams in figure 3 are obtained for a certain compound in aqueous solution with no additional compounds such as  $\text{CO}_2$ , KOH, NaOH, or HCl that are present in human blood plasma (table 4). Those compounds can

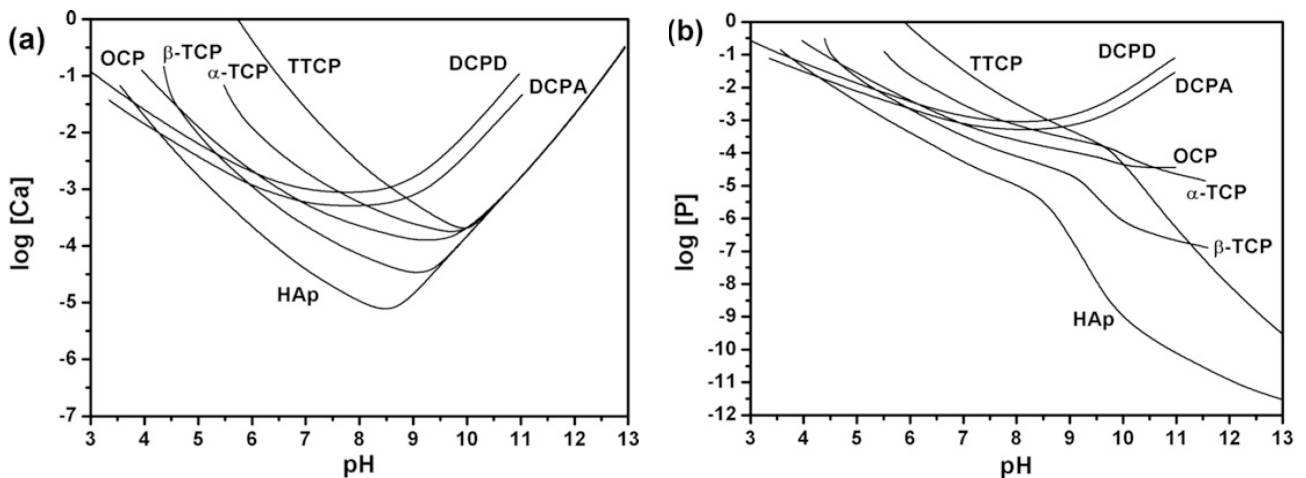


**Figure 3:** Solubility phase diagram for the ternary system  $\text{Ca}(\text{OH})_2\text{-H}_3\text{PO}_4\text{-H}_2\text{O}$  at 37°C; a) solubility isotherms showing  $\log[\text{Ca}]$  as a function of the solution in equilibrium with different calcium orthophosphates; b)  $\log[\text{P}]$  as a function of the pH of the solution.<sup>88</sup>

influence the solubility diagrams and therefore the relative stability of the calcium phosphate phases. Besides the relative thermodynamic solubility, the velocity of dissolution is a crucial factor for the development of bone graft materials. Properties like porosity or particle size strongly affect the velocity of dissolution. Generally, higher porosity or smaller particle size leads to faster dissolution rate due to the enhanced surface area in contact with the solution.<sup>38,65-70</sup>

### 1.5.2. Apatite Formation in Simulated Body Fluid

The formation of bone-like apatite crystals on the surface of bioactive materials is based on the classical crystallization theory which states that the formation of a new phase always starts with nucleation. Nucleation is defined as the process that determines the time it takes for a new phase to

occur.<sup>38</sup> When a stable crystal (nucleus) is formed spontaneously from a supersaturated solution, it has to overcome a certain energy barrier. This activation energy is a result of two processes, namely the formation of a crystal and the formation of a solid-liquid interface. The formation of a crystal in a supersaturated solution ( $L_{sat} > 1$ ) is thermodynamically favored because the system tends to a minimum in Gibbs free energy. On the other hand, the formation of a new solid-liquid interface involves a rise in Gibbs free energy and is therefore thermodynamically unfavored. The Gibbs free energy of a nucleus in a supersaturated solution as a function of its radius can be written as:

$$\Delta G = \frac{4}{3}\pi r^3 \Delta g + 4\pi r^2 \gamma \quad [11]$$

where  $r$  is the radius of the nucleus,  $\Delta g$  is the difference in free energy per volume of the newly built nucleus and  $\gamma$  is the surface tension. The first term accounts for the energy decrease due to crystal formation and is proportional to  $r^3$  assuming a spherical nucleus. The second term accounts for the rise in Gibbs free energy due to the formation of a new solid-liquid interface and is proportional to  $r^2$ . The second term dominates for small radii (fig. 4). However, for large radii, the first term dominates and the total free energy ( $\Delta G$ ) becomes negative. Therefore, a growing nucleus has to overcome a certain energy barrier ( $\Delta G_{crit}$ ) and thus a critical size ( $r_c$ ) to be thermodynamically stable. This energy barrier is the reason why a solution can be supersaturated with respect to a certain compound without precipitation to occur as it is the case for human blood plasma and for SBF. Besides the probability of a critical size nucleus to occur, the rate at which a crystal grows is important to understand crystal growth in a supersaturated solution. The nucleation rate ( $J$ ) is given by:

$$J = A \exp\left(-\Delta \frac{G_{crit}}{kT}\right) = A \exp\left[-\frac{16\pi v^2 \gamma^3 f(\Theta)}{3k^3 T^3 (\ln L_{sat})^2}\right] \quad [12]$$

where  $A$  is a kinetic factor,  $k$  is the Boltzmann constant,  $T$  is the absolute temperature,  $v$  is the volume of the critical size nucleus,  $f(\theta)$  is the contact angle function and  $L_{sat}$  is the supersaturation level defined as  $K/K_{sp}$ . It can be seen that HA crystal growth on a bioactive materials in a supersaturated solution can be facilitated by basically three strategies. One strategy is to raise the supersaturation level towards HA. Another strategy is to lower the surface tension term by providing a surface with a low interfacial energy with hydroxyapatite.<sup>38</sup> The last and most obvious strategy is to provide hydroxyapatite nuclei that remove the need for the formation of a critical size nucleus. The first strategy explains why bioactive glasses are rapidly covered with apatite crystals upon immersion in SBF. Bioactive glasses are basic and locally raise the pH of SBF which leads to a major decrease of hydroxyapatite solubility. The second strategy explains why compounds like TCP are covered with hydroxyapatite when immersed in SBF. The last strategy mentioned explains why HA is rapidly covered with new apatite crystals in SBF.<sup>12,38,62,65,66,69,70</sup>

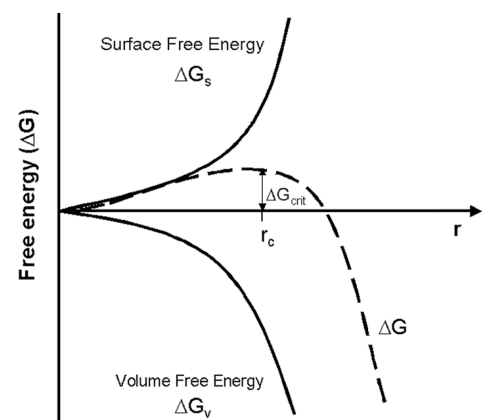


Figure 4: Diagram showing the free energy as a function of the radius of a forming nucleus.<sup>86</sup>

## 1.6. Aim of the Study

Bone graft materials become more and more important and many manufacturers offer different synthetic bone graft solutions. There are a lot of different products on the market varying in production route, chemical composition, surface morphology, porosity, grain size, etc. All the commercially available products have shown ability for bone regeneration in various *in vitro* tests and clinical trials. The fact that there are many different approaches for synthetic bone graft materials indicates that the tests are not standardized and it is not fully understood which material properties lead to which reaction in the augmentation process. The aim of this study was to evaluate the chemical and morphological properties of the tested materials which are relevant for bone augmentation. Therefore, a series of selected bone graft materials were chemically and structurally investigated. To test bioactivity and biodegradation the materials were immersed in cell culture medium for different time periods with subsequent characterization by XRD, SEM, EDS, and gravimetrically. In this study, cell culture medium was used for the bioactivity test since it offers a more accurate representation of human blood plasma than conventional SBF due to the presence of vitamins and amino acids.<sup>64</sup> The goal of the study was to find correlations between chemical and morphological properties of the materials and the performance in the bioactivity test. The results of the *in vitro* bioactivity test are considered to give a hint for the bioactivity and biodegradability properties of the different materials *in vivo*.

## 2. Materials

In this study 13 different bone graft materials were used that can be subdivided into three groups. The first group contained five commercial products, one of which was a xenograft and the other four were synthetic bone graft materials. Of the commercially available synthetic materials, two were biphasic calcium phosphates (BCP) and two were single phase HA materials. The second group contained BCPs with different ratios of HA/ $\beta$ -TCP and a pure HA material with the same structural properties. The third group contained three composite materials made of amorphous TCP incorporated into electrospun PLGA fibers with different ratios. All materials used were in granular form except the three composite materials that had a cotton wool-like appearance. The following specifications were obtained from the manufacturers unless otherwise specified.

### 2.1. Commercial Products

BioOss® (Geistlich Pharma AG, Wolhusen, Switzerland) is a xenograft derived from deproteinized and sterilized bovine bone with grain size of 250 – 1000  $\mu\text{m}$  and a porosity of around 80 %. The organic components of the bone are removed by chemical and thermal treatment ( $<350^\circ\text{C}$ ) leaving only the inorganic hydroxyapatite phase. Since the material is processed at temperatures below  $350^\circ\text{C}$  it is not sintered. Due to its similarities to human bone BioOss® is the gold standard for bone augmentation as shown by many studies<sup>7,71-74</sup>.

BoneCeramic® (Straumann AG, Basel, Switzerland) is a fully synthetic biphasic calcium phosphate with grain size of 500 – 1000  $\mu\text{m}$  and a porosity of around 90 %. It consists of 60 wt% fully crystalline HA and 40 wt%  $\beta$ -TCP sintered at temperatures of  $>1100^\circ\text{C}$ .<sup>75,77</sup>

Maxresorb® (Straumann AG, Basel, Switzerland) is a fully synthetic biphasic calcium phosphate with grain size of 500 – 1000  $\mu\text{m}$  and a porosity of around 80 %. It consists of 60 wt% fully crystalline HA and 40 wt%  $\beta$ -TCP sintered at temperatures  $>1000^\circ\text{C}$ .<sup>76</sup>

Nanobone® (Artoss GmbH, Rostock, Germany) is a synthetic nanocrystalline HA embedded in a silica gel matrix (amorphous  $\text{SiO}_2$ ) with grain size of 600 – 2000  $\mu\text{m}$  and a porosity of around 50 %. The ratio of HA/ $\text{SiO}_2$  is 76/24 wt%. The material is prepared in a sol-gel process at temperatures  $<700^\circ\text{C}$  and is therefore not sintered.<sup>78</sup>

Algipore® (Dentsply Friadent GmbH, Mannheim, Germany) is a bone graft material derived from calcium carbonate ( $\text{CaCO}_3$ ) forming red algae with grain size of 500 – 1000  $\mu\text{m}$  and a porosity of around 65 %. The calcium carbonate is transformed to HA in a hydrothermal process with addition of ammonium phosphate ( $(\text{NH}_4)_3\text{PO}_4$ ) at temperatures  $<700^\circ\text{C}$  and is therefore not sintered.<sup>42</sup>

### 2.2. Biphasic Calcium Phosphate Series

AlgOss® (AlgOss® Biotechnologies GmbH, Vienna, Austria) is also a bone graft material derived from algae and exhibits similar features as Algipore®. For this study the company AlgOss® Biotechnologies prepared five different materials with different ratios of HA/ $\beta$ -TCP. AlgOss®100 is basically the same material as Algipore® where the calcium carbonate from the algae is fully transformed to HA. AlgOss®50/50, AlgOss®40/60, AlgOss®30/70 and AlgOss®20/70 have a HA/ $\beta$ -TCP ratio of 50/50, 40/60, 30/70 and 20/80 respectively.

### **2.3. Composite Materials**

Bonewool® (Zurich Biomaterials LLC, Zurich, Switzerland) is a novel composite bone graft material made of amorphous TCP (ATCP) particles incorporated into electrospun poly(lactic-co-glycolic acid) (PLGA) fibers with an ATCP/PLGA ratio of 40/60 wt%. The ATCP particles are prepared by flame spray synthesis and have a grain size in the submicron range. The composite material exhibits a cotton wool-like appearance, is flexible, easy to shape, and therefore facilitates the surgical procedure. It combines the high bioactivity of ATCP particles with the flexibility and biodegradability of PLGA. Beside the standard product with an ATCP/PLGA ratio of 40/60, a material with an ATCP/PLGA ratio of 20/80 and pure electrospun PLGA were used for this study.

### 3. Methods

#### 3.1. Material Characterization

Inductive Coupled Plasma-Optical Emission Spectroscopy (ICP-OES) was carried out to determine the elemental concentrations of Ca and P for all materials in granular form prior to the bioactivity tests. All measurements were carried out on a Spectroblue-SOP spectrometer (SPECTRO Analytical Instruments GmbH, Kleve, Germany) with radially-viewed plasma source. Prior to analysis approximately 10 mg of every granular material was weighed on a high precision balance XP2U (Mettler-Toledo GmbH, Greifensee, Switzerland) and completely dissolved in 0.5 ml concentrated nitric acid (65 %). The stock solutions were diluted 1:50 so that the material concentrations were in the detection range of the spectrometer namely 1 – 1000 mg/L.

X-ray diffraction (XRD) was used to determine the calcium phosphate phase and the ratio of phases in case of biphasic materials. Furthermore, crystallinity and possible phase impurities could be detected. X-ray diffraction patterns were recorded on a D2 Phaser (Bruker AXS, Karlsruhe, Germany) with Co-K $\alpha$  radiation ( $\lambda = 1.78897 \text{ \AA}$ ) at a current of 10 mA and a voltage of 30 kV. The spectra were recorded from 20° to 40° (2 $\theta$ ) where the most intense peaks for HA and TCP were present, with step size of 0.02° at a scanning speed of 2 s per step. Prior to analysis the samples were pestled to obtain a fine powder which altered the signal to noise ratio in XRD analysis. Since the volume of a single sample was too low for XRD analysis, the sample triplets were measured together. The obtained patterns were compared to the patterns from the International Centre for Diffraction Data (ICDD) database (PDF-2, 2010) and from the Crystallographic Open Database (COD). Semi-quantitative phase analysis was carried out by adjusting the height of the PDF patterns to the height of the most intense peak for HA and  $\beta$ -TCP respectively.

Mercury Intrusion Porosimetry (MIP) was used to determine the porosity of the samples in granular form. All measurements were carried out on a Poremaster 60° (Quantachrome Instruments GmbH, Odelzhausen, Germany) with a pressure range of 0.7 – 5000 PSI. In this pressure range, pores with sizes between approximately 300 and 4.2  $\mu\text{m}$  could be detected.

Scanning electron microscopy (SEM) was used to determine the changes in surface topography of the materials before and after the bioactivity test and for qualitative elemental analysis with element dispersive X-ray spectroscopy (EDS). All images were recorded on a Nova NanoSEM 230° (FEI, Hillsboro, USA). The device is equipped with a field-emission Schottky emitter and an Everhart-Thornley secondary electron detector working in the field-free mode. The images were recorded with an acceleration voltage of 5 kV. Prior to analysis the samples were sputtered with 50 nm gold in a Leica EM ACE 600 high vacuum coater (Leica Microsystems AG, Heerbrugg, Switzerland).

To analyze the inorganic components of the composite materials, PLGA was removed via combustion at 650° C for 6 hours.

#### 3.2. *In vitro* Bioactivity Test

The bioactivity test was carried out to evaluate changes of the materials in physiological environment after different time intervals. Cell culture medium was prepared from Dulbecco's Modified Eagle

Medium (DMEM) powder (Sigma-Aldrich GmbH, Buchs, Switzerland, catalog number: d2902) with sodium bicarbonate added according to the manufacturer's preparation instructions and sterilely filtered through a 0.22  $\mu\text{m}$  filter. The composition of the final medium is listed in table 4. The pH of the medium was adjusted to the physiological pH of 7.4 with 1 M NaCl. Prior to immersion, the materials were dried at room temperature in a desiccator for 24 h and plasma cleaned for 2 min with oxygen plasma at a RF-level of 29.6 W to ensure sterile conditions. Approximately 0.3  $\text{cm}^3$  of the materials were measured in a clipped off 1 ml plastic syringe with 0.01 ml calibration marks and weighed with an analytical balance with an accuracy of  $\pm 0.1$  mg ( $W_0$ ). The materials were then immersed in 20 ml medium in Falcon<sup>TM</sup> 50 ml conical polypropylene tubes for different time periods (12 h, 24 h, 168 h and 336 h) at  $36.5 \pm 1.5^\circ$  C. Every 24 h the tubes were shook slightly to ensure a homogeneous distribution of the ions around the material. Additionally, 10 ml medium was changed every 48 h to ensure constant ion concentrations and to adjust the pH between 7.2 and 7.6. Before the medium was changed, the samples were centrifuged (2 min at 2500 rpm) to ensure that no granules were removed during exchange of the medium. The used DMEM medium was carbonate buffered which is why a humidified atmosphere with 5%  $\text{CO}_2$  would have been required to keep up the buffer effect. Since it was not possible to generate such an atmosphere with the available facilities, the pH rose up to a pH of around 7.6 within 48 h. This effect was compensated by changing 10 ml of the medium with DMEM adjusted to pH 7.1 every 48 h. As already mentioned, the pH of the medium was  $7.4 \pm 0.2$  over the whole immersion time with this procedure. For the 12 h and 24 h experiments, the medium was not changed. After each time period the samples were centrifuged, the medium was removed carefully in order not to remove any granules, rinsed with nanopure water, and dried in a desiccator for 48 h to a constant weight ( $W_{dry}$ ). The dried samples were weighed again and the weight change was calculated. For statistical analysis, all the experiments were carried out in triplets with every material.

**Table 4:** Ion concentrations of human blood plasma<sup>39</sup>, conventional SBF and DMEM.

	Blood plasma		c-SBF	DMEM
	Total	Dissociated		
$\text{Na}^{2+}$	142.0	142.0	142.0	155.3
$\text{K}^+$	5.0	5.0	5.0	5.3
$\text{Mg}^{2+}$	1.5	1.0	1.5	0.8
$\text{Ca}^{2+}$	2.5	1.3	2.5	1.8
$\text{Cl}^-$	103.0	103.0	147.8	119.3
$\text{HCO}_3^-$	27.0	27.0	4.2	44.0
$\text{HPO}_4^{2-}$	1.0	1.0	1.0	0.9
$\text{SO}_4^{2-}$	0.5	0.5	0.5	0.8
pH	7.2 - 7.4	7.2 - 7.4	7.4	7.2 - 7.6
Amino acids	+	+	-	+
Vitamins	+	+	-	+

## 4. Results

### 4.1. Commercial Materials

#### 4.1.1. Surface Morphology

BioOss® particles looked like typical bone material with macropores between 10 µm and 100 µm in diameter and micropores in the submicron range (fig. 5a). The total porosity obtained with MIP was  $74 \pm 1 \%$ . The surface of the particles appeared rough and the fracture planes of the bovine bone were visible.

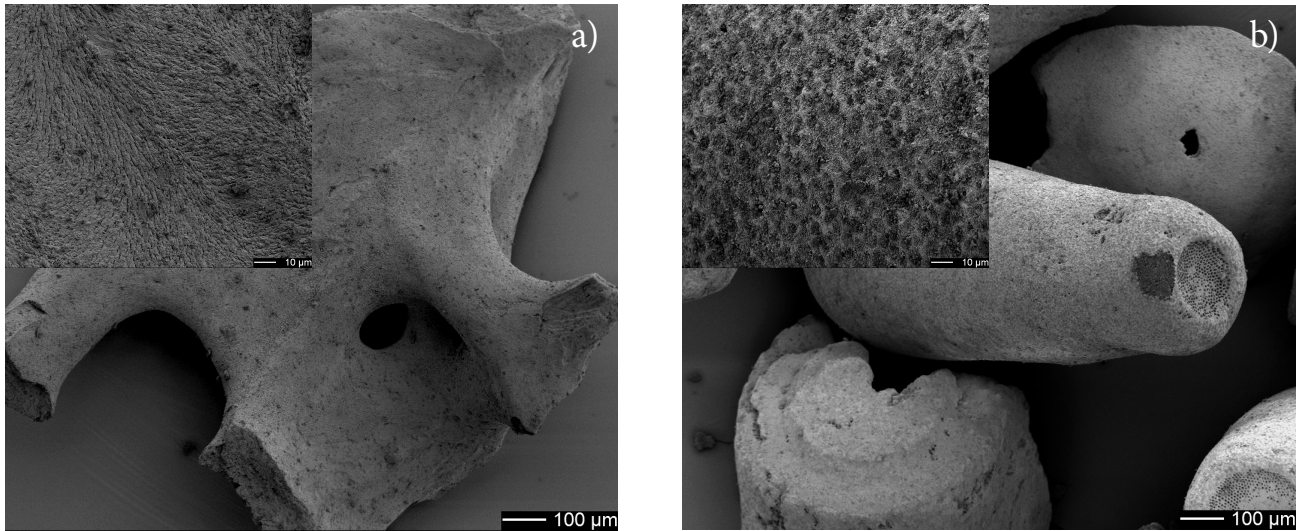


**Figure 5:** SEM images of a single particle of BioOss® (a) and Algipore® (b) as obtained from the manufacturer. Scale bar of close up = 10 µm

Most of the Algipore® particles had a cylindrical structure with uniformly distributed pores around 5 µm in diameter. The pores had a honeycomb like structure and were all of similar size. Most of the pores at the surface of the particles appeared to be covered by smaller particles in the submicron range whereas the pores at the ends of the cylindrical particles were open. The measured porosity was  $67 \pm 1 \%$ .

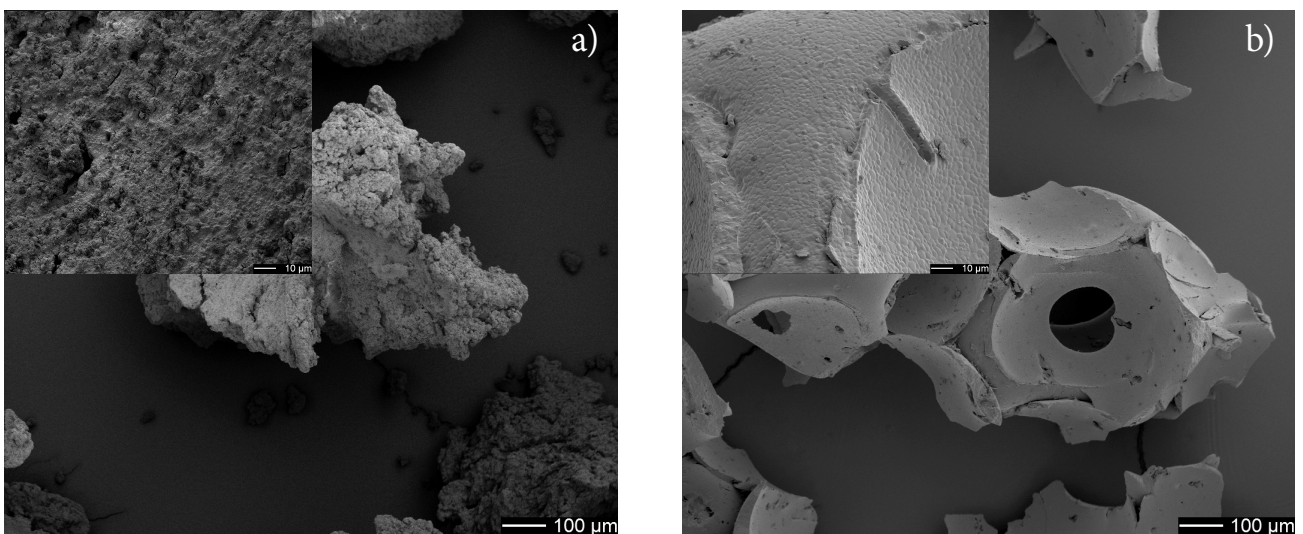


**Figure 6:** SEM images of a single particle of Nanobone®(a) and BoneCeramic®(b) as obtained from the manufacturer. Scale bar of close up = 10 µm

Nanobone<sup>®</sup> consisted of particles with a very rough surface but no visible pores. At higher magnitudes (close up in fig. 6a), some irregular shaped, not interconnected pores were visible. Nevertheless, a total porosity of  $66 \pm 3 \%$  was measured

BoneCeramic<sup>®</sup> consisted of irregularly shaped particles with a smooth surface that arised from the sintering procedure. It can be seen that the particles were made of concave spherical surfaces that stick together. The images reveal a high macroporosity whereas no micropores were visible on the surface. At higher magnitude it can be seen that the material was made of individual grains with a diameter of  $1 - 2 \mu\text{m}$ . No microporosity was detectable on the SEM images. Total porosity measured with MIP was  $72 \pm 8 \%$ .

At lower magnitudes Maxresorb<sup>®</sup> revealed a similar structure as BoneCeramic<sup>®</sup> with several concave surfaces per particle. Furthermore, the granules had macropores ranging from  $10 - 100 \mu\text{m}$ . At higher magnitudes, it became apparent that the particles were made of individual spherical grains with a diameter of  $0.5 - 2 \mu\text{m}$ . Since Maxresorb<sup>®</sup> was also sintered, the individual grains had a smooth surface like it was the case for BoneCeramic<sup>®</sup>. In contrary to BoneCeramic<sup>®</sup>, the individual grains were not packed as tight together leaving a large amount of micropores that seemed to be interconnected. Maxresorb<sup>®</sup> was the material with the highest measured porosity of all investigated materials with a total porosity of  $79 \pm 3 \%$ .

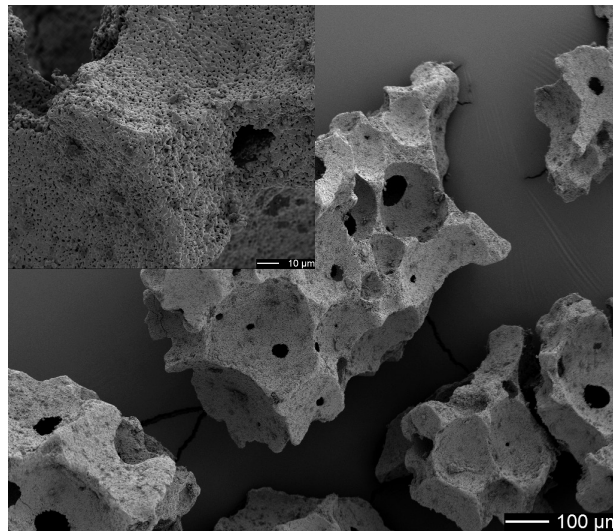


**Figure 7:** SEM image of Maxresorb<sup>®</sup> as obtained from the manufacturer. Scale bar of close up =  $10 \mu\text{m}$

#### 4.1.2. Phase and Elemental Composition

Maxresorb<sup>®</sup> and BoneCeramic<sup>®</sup> almost perfectly matched the patterns of synthetic HA and  $\beta$ -TCP obtained from the ICDD database (HA: PDF 01-076-0694 and  $\beta$ -TCP: PDF 00-055-0898) without any other detected crystalline phases (fig. 8). Both materials were highly crystalline as indicated by the clearly defined and sharp reflection peaks. To estimate the phase composition of the BCP materials, a semi-quantitative phase analysis was performed with the obtained XRD spectra. In table 5 it can be seen that BoneCeramic<sup>®</sup> had a higher HA/ $\beta$ -TCP ratio than Maxresorb<sup>®</sup>.

As expected, the spectrum for Nanobone<sup>®</sup> only shows reflections that were contributed to HA since the contained  $\text{SiO}_2$  was completely amorphous. It is worth to notice that all reflections of Nanobone<sup>®</sup> were shifted around  $0.1^\circ$  to higher angles compared to pure HA. Since this was the case

for all measured samples a sample displacement or a systematic shift was excluded to account for the measured reflection shift. In fact, the spectrum matched the patterns of fluor substituted HA ( $\text{Ca}_5(\text{PO}_4)_3((\text{OH})_{0.6}\text{F}_{0.4})$ ; PDF 01-074-4174) far better than the patterns for pure HA. Those fluoride ions affected the lattice parameters and therefore the reflection angle.<sup>79,80</sup> The broad peaks indicated a lower crystallinity compared to the other synthetic samples and the amorphous background was attributed to the contained silica.

The only material that was measured with a lower crystallinity was BioOss® as indicated by the broad and overlapping reflection peaks. The spectrum of BioOss® shows reflections typical for HA and three small peaks at 27.3°, 34.9° and 36.6° which were contributed to  $\text{CaCO}_3$  as already shown in other studies.<sup>42</sup> These peaks were minor and not visible in figure 8. A more detailed spectrum can be found in the appendix.

The spectrum of Algipore® showed all peaks characteristic for calcium-deficient fluorapatite (FHA) ( $\text{Ca}_{10}\text{F}_2\text{O}_{24}\text{P}_{6.05}$ , COD 5000041) and the same three small peaks like BioOss®. Furthermore, the spectrum was shifted to higher angles compared to stoichiometric HA which is contributed to a substitution of the hydroxyl groups with fluor, as mentioned above<sup>61,81,82</sup>

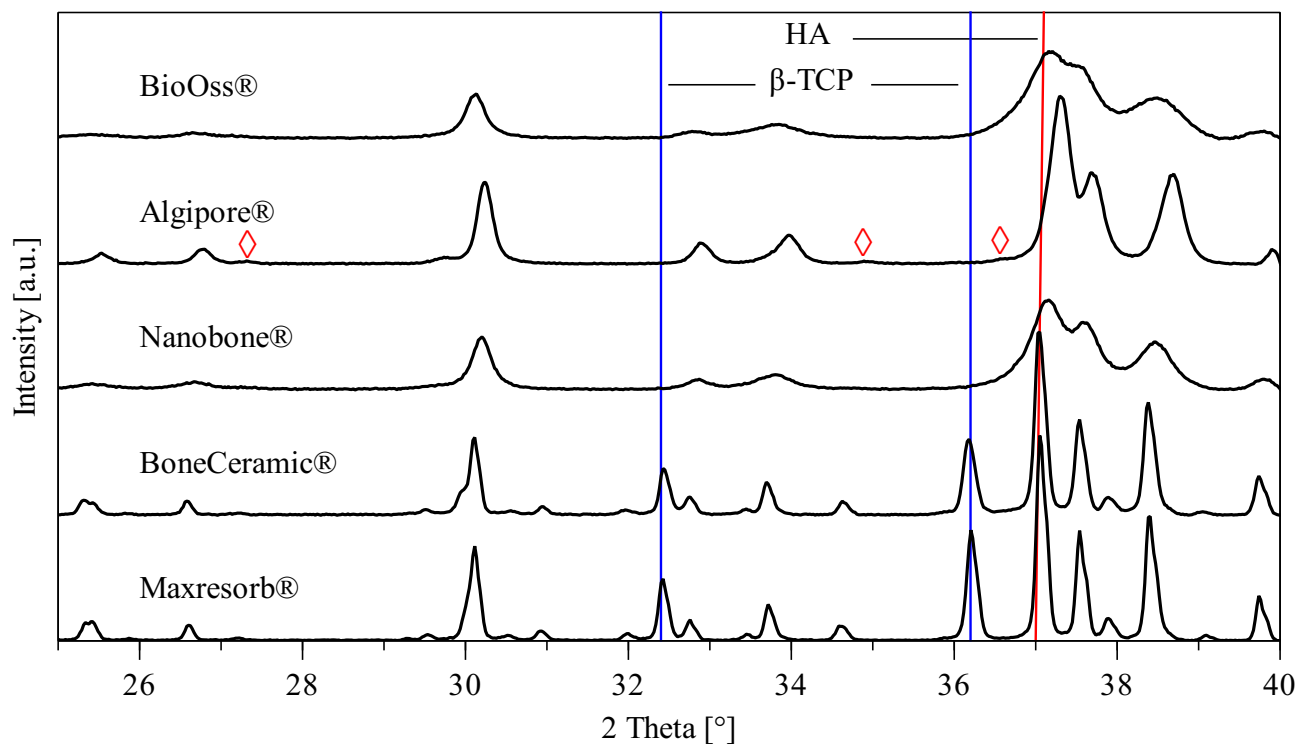


**Figure 8:** XRD spectra of the commercial materials as obtained from the manufacturer.  $\diamond$  indicates reflections of residual  $\text{CaCO}_3$ .

Elemental concentrations of Ca and P were measured by ICP-OES and are listed in table 5. Since the absolute values for percentage Ca and P content was affected by a weighing error, only the Ca/P ratios are shown that were solely affected by the internal error of the spectrometer. The comparison of the measured values and the calculated ones of HA and  $\beta$ -TCP shows that Maxresorb®, BoneCeramic® and Nanobone® were composed of stoichiometric HA and/or  $\beta$ -TCP respectively. The Ca/P ratio of BioOss® either indicated that it consisted of non-stoichiometric HA with an excess of Ca or that some phosphate ions were substituted with other ions. Algipore® consisted of Ca deficient FHA which was also consistent with the obtained XRD spectrum. Since only Ca and P were measured,

the phase composition of Nanobone® was calculated via the weighed amount of sample and the absolute values for Ca and P concentration as follows:

$$\text{HA ratio [\%]} = \frac{\text{Calcium concentration of the sample [wt.\%]}}{\text{Calcium concentration of HA [wt.\%]}} * 100 = \frac{30.977}{39.974} = 77.493\%$$

**Table 5:** Ca/P ratio of the raw commercial materials obtained by ICP-OES and HA/ $\beta$ -TCP ratio measured by semi-quantitative XRD analysis.

	HA : $\beta$ -TCP [wt%]	Ca/P [at%]
Maxresorb®	60.5 : 39.5	1.596 $\pm$ 0.009
BoneCeramic®	66.6 : 33.4	1.578 $\pm$ 0.020
Nanobone®	-	1.679 $\pm$ 0.011
BioOss®	-	1.717 $\pm$ 0.015
Algipore®	-	1.603 $\pm$ 0.014
HA (calculated)	-	1.667
60 % HA / 40 % $\beta$ -TCP (calculated)	-	1.600

#### 4.1.3. *In vitro* Bioactivity Test

In figure 9 the weight changes of the materials upon immersion in cell culture medium for different time intervals are shown. It has to be mentioned that the weight changes were affected by two processes. On the one hand, some compounds of the materials were soluble in aqueous solutions which lead to a mass loss of the samples. On the other hand, precipitation of HA lead to a mass gain.

Both BCPs behaved similarly in the bioactivity test. BoneCeramic® lost 0.5 % of its initial weight within 12 h of immersion. From 24 h to 336 h of immersion, the samples had continuously been gaining mass up to a final mass gain of around 0.9 % of the initial mass. Ignoring the statistical outlier of Maxresorb® after 12 h of immersion Maxresorb® exhibited almost the same behavior as

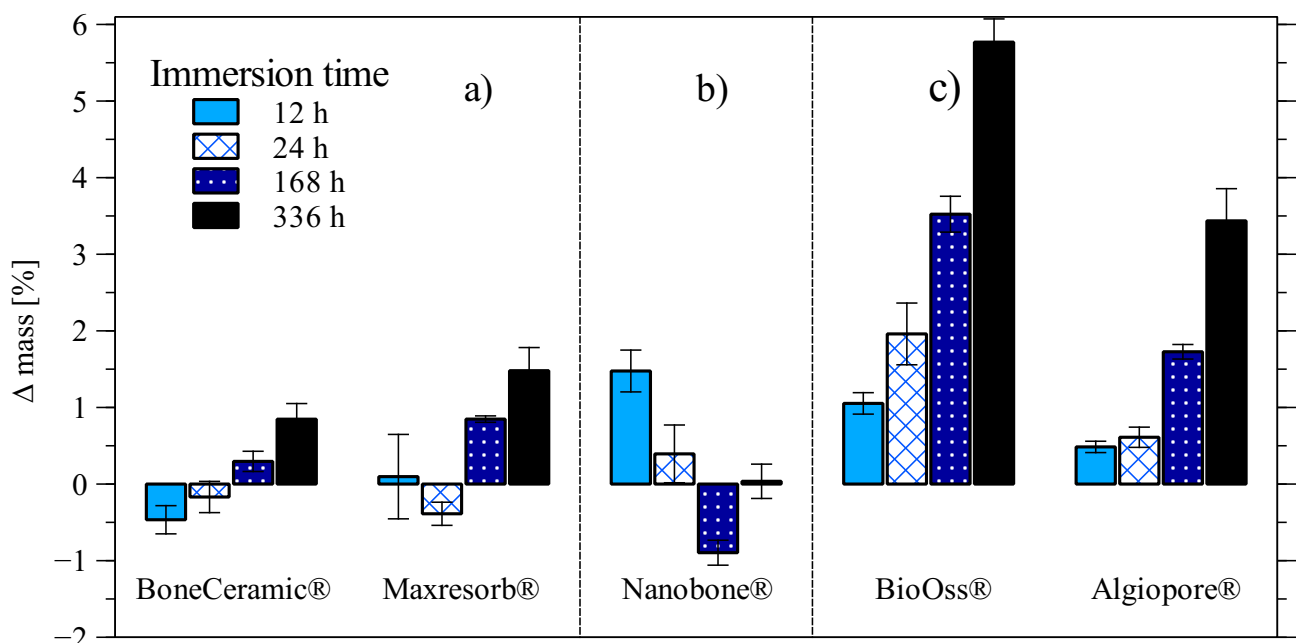


**Figure 9:** Mass change of the commercial materials in percent of initial sample mass as a function of immersion time. a) For the biphasic materials with a HA/  $\beta$ -TCP ratio of 60/40 wt%. b) 76 wt% HA and 24 wt% SiO<sub>2</sub>. c) Single phase HA materials.

BoneCeramic<sup>®</sup>. Also Maxresorb<sup>®</sup> was affected by a mass loss within the first 24 h and subsequent continuous mass gain. The difference between these two materials was the rate at which dissolution and precipitation had taken place. Maxresorb<sup>®</sup> lost more weight than BoneCeramic<sup>®</sup> within the first 24 h but also gained more mass after one week and two weeks respectively.

Nanobone<sup>®</sup> exhibited almost the reverse behavior than the two BPC materials. After 12 h a mass gain of around 1.5 % was measured. The sample mass then decreased within one week to - 0.9 % of the initial mass. After two weeks, the Nanobone<sup>®</sup> samples had almost the same mass as at the beginning of the experiment.

BioOss<sup>®</sup> revealed a continuous mass gain over the whole experiment time. After two weeks, the mass gain was around 5.8 % of the initial sample mass. It was the material with the most continuous and significant mass gain of the materials in granular form.

Algipore<sup>®</sup> behaved similarly to BioOss<sup>®</sup> with the difference that precipitation rate was lower within the first 24 h compared to BioOss<sup>®</sup>. After 24 h up to 336 h of immersion the HA precipitation rate was comparable to that of BioOss<sup>®</sup>. Due to the head-start of BioOss<sup>®</sup> the final mass gain of Algipore<sup>®</sup> was still lower than for BioOss<sup>®</sup>.

In figures 10 and 11 SEM images of the BCP materials are shown after different immersion times. For better representation, not all SEM images are shown (In the appendix a collection of all materials can be found). After 12 h of immersion there were no visible changes in surface morphology of BoneCeramic<sup>®</sup>. After 24 h, first signs of precipitation were visible. Several nucleation sites were detectable on the smooth surface. After one week, the nucleation sites seemed to spread over the surface. After two weeks of immersion, almost the whole surface was covered with a thin HA layer.

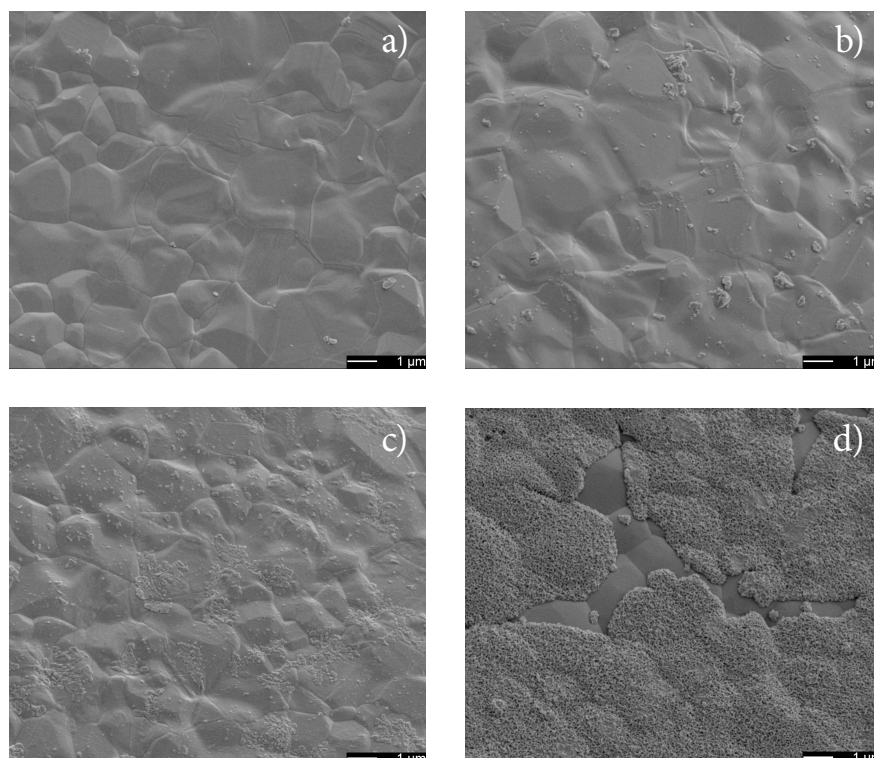


**Figure 10:** SEM images of the surface of BoneCeramic<sup>®</sup> particles after different immersion times. a) Raw material b) 24 h of immersion c) 168 h of immersion d) 336 h of immersion.

Maxresorb® showed first signs of nucleation already after 12 h of immersion. After 168 h it was clearly visible that some of the grains were covered with HA whereas other grains did not change their morphology. After two weeks, this behavior became even clearer although it seemed that also the grains that had not shown signs of precipitation after 168 h, had started to induce precipitation.

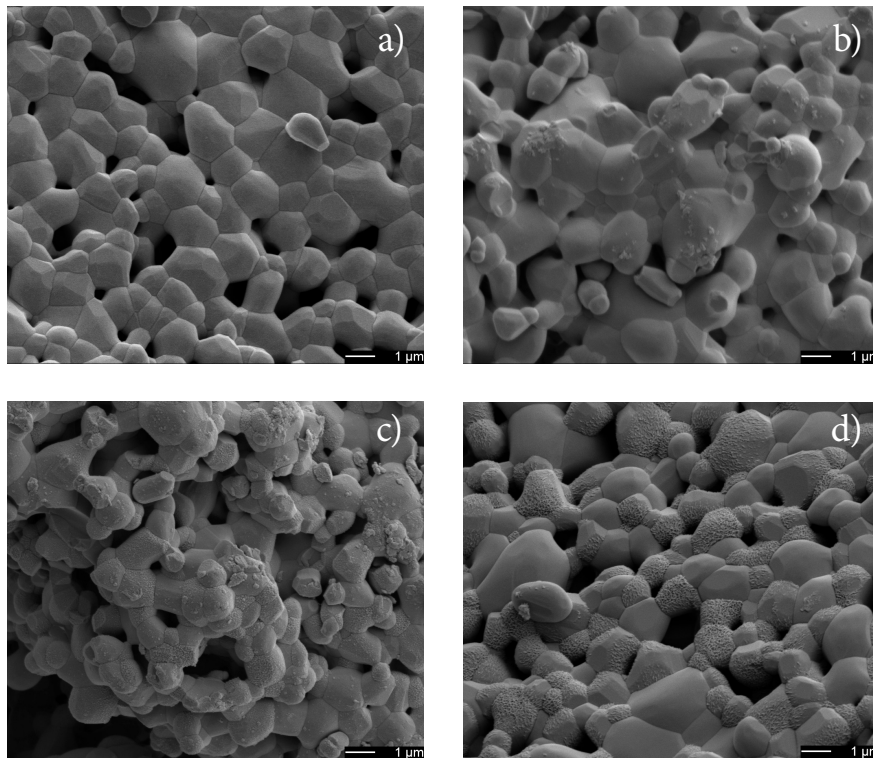


**Figure 11:** SEM images of the surface of Maxresorb® particles after different immersion times. a) Raw material b) 12 h immersion c) 168 h immersion d) 336 h immersion.

Since the surface of Nanobone® was rough and structurally similar to the expected precipitants from the beginning, it was difficult to tell from the SEM images whether precipitation had taken place or not. Nevertheless, it seemed that the surface was being covered with small cauliflower like crystals as immersion time prolonged.

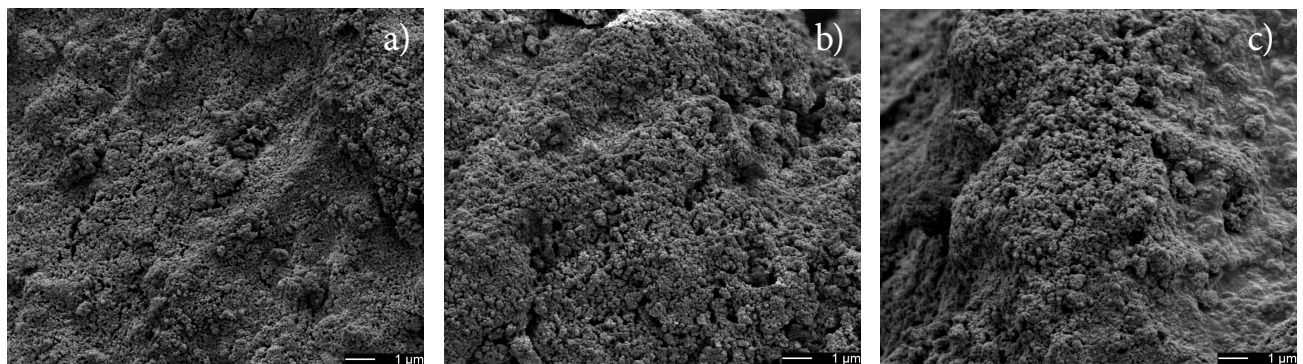


**Figure 12:** SEM images of the surface of Nanobone® particles after different immersion times. a) Raw material b) 168 h immersion c) 336 h immersion.

Although the surface of BioOss® was also quite rough, it was possible to detect precipitates due to the distinct morphology of the initial sample surface. Already after 12 h of immersion, cauliflower-like crystals were visible on the surface. The surface was further being covered with these crystals as immersion time prolonged.

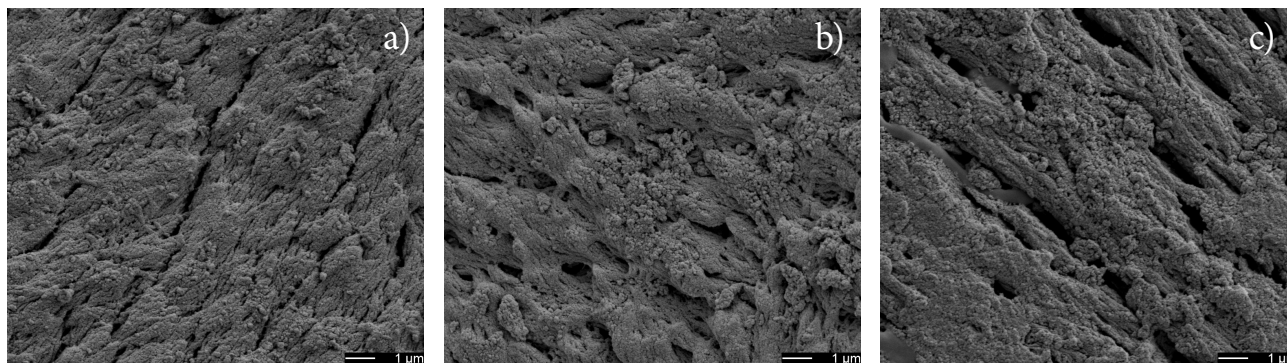


**Figure 13:** SEM images of the surface of BioOss® particles after different immersion times. a) Raw material b) 168 h immersion c) 336 h immersion.

The SEM images of Algipore® were also difficult to analyze with SEM images for the reasons outlined. However, the SEM images of the samples after 1 week of immersion clearly reveal that some structures precipitated on the surface that had not been present before immersion in SBF.

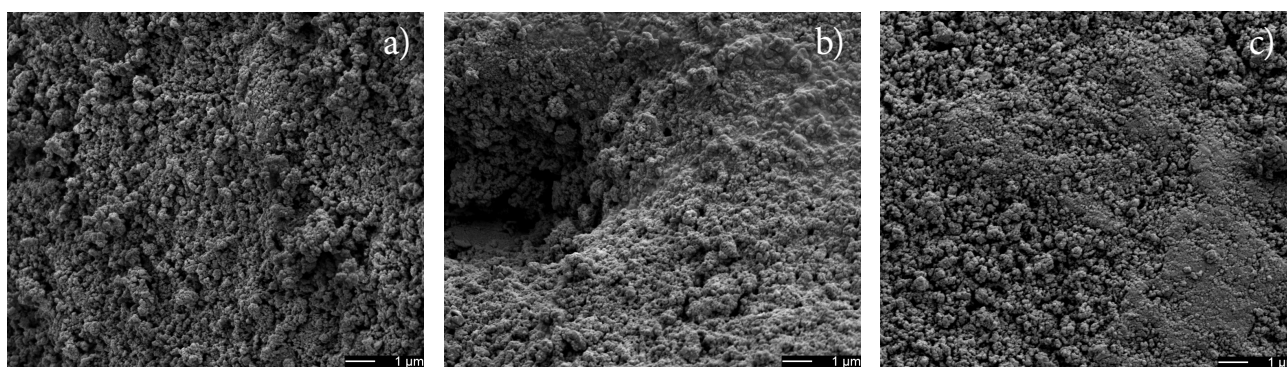


**Figure 14:** SEM images of the surface of Algipore® particles after different immersion times. a) Raw material b) 168 h immersion c) 336 h immersion.

XRD analysis of the samples after different immersion times did not show any differences since the phase analysis is not sensitive enough for small changes. No other peaks were visible after immersion indicating that nothing besides HA precipitated on the surface.

## 4.2. AlgOss® Series

### 4.2.1. Surface Morphology

In figure 15, SEM images of the materials in the AlgOss® series are shown. Since those materials had the same origin as Algipore®, namely calcifying algae, the surface morphology was found to be the same. The only difference that was detected was that AlgOss®3070 had a smaller average particle size. All the materials in this group were mostly composed of particles with a cylindrical structure and uniformly distributed pores with a mean diameter of around 5 µm. As it was the case for Algipore®, the honeycomb like pores on the surface seemed to be covered with smaller particles whereas the pores at the ends were open. MIP analysis revealed a total porosity of  $69 \pm 1 \%$ , except for AlgOss®2080 where a porosity of  $77 \pm 1 \%$  was measured.

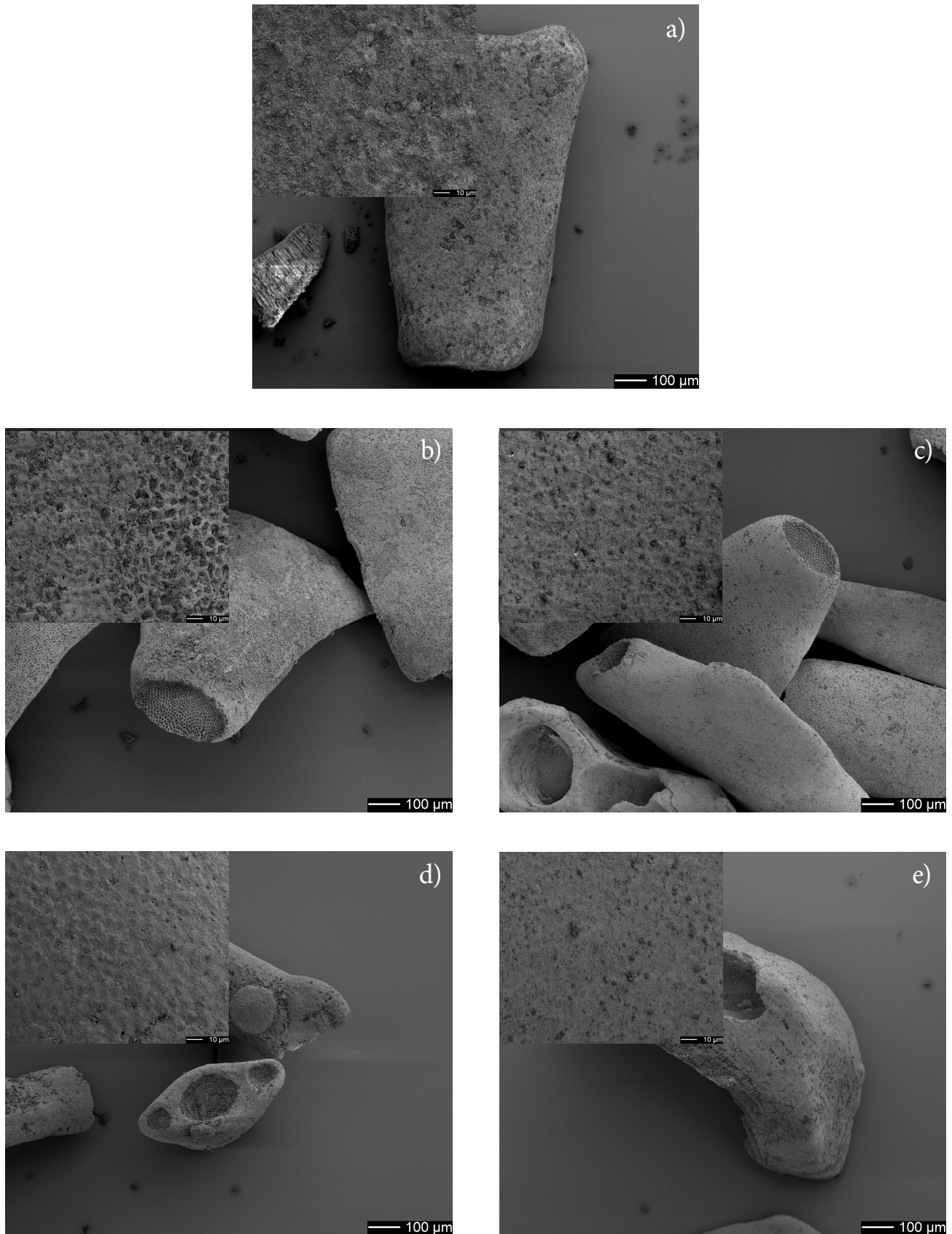


**Figure 15:** SEM images of a single particle of AlgOss® as obtained from the manufacturer. a) 100 % HA b) 50 % HA 50 %  $\beta$ -TCP c) 40 % HA 60 %  $\beta$ -TCP d) 30 % HA 70 %  $\beta$ -TCP e) 20 % HA 80 %  $\beta$ -TCP. Scale bar of close up = 10  $\mu$ m.

#### 4.2.2. Phase and Elemental Composition

XRD spectra of the materials within the AlgOss® series revealed the biphasic character of the materials (fig. 16). All reflections can be contributed either to fluor substituted HA or magnesium substituted  $\beta$ -TCP ( $\text{Ca}_{9.5}\text{MgO}_{28}\text{P}_7$ , COD 9012137). The pattern for Mg-substituted  $\beta$ -TCP matched

the obtained spectra for the AlgOss® series far better than that of pure  $\beta$ -TCP. Furthermore, Mg was detected with EDS and the ICP-OES results indicate a Ca deficiency in all AlgOss® samples.<sup>83,84</sup>

The spectrum of AlgOss®100 was almost identical to the spectrum of Algipore® and also showed three small peaks at  $2\theta = 27.3^\circ$ ,  $34.9^\circ$  and  $36.6^\circ$ . Comparisons with the other AlgOss® materials made it clear that these reflections are also present in the spectra of the biphasic AlgOss® materials where they were more dominant. Those additional peaks can be contributed to residual calcite. Shift of the HA peaks to higher values was more dominant in AlgOss®100 than in the other AlgOss® materials, indicating a higher substitution in AlgOss®100. The spectrum matched the same pattern like the Algipore® spectrum.

The HA peaks of biphasic AlgOss® materials were all shifted to higher angles compared to pure HA except the spectrum of AlgOss®4060 that matched the pattern of pure HA (PDF 01-076-0694). AlgOss®5050 matched with the same spectrum as Nanobone® with 0.4 F atoms per unit formula HA. The spectra of AlgOss®3070 and AlgOss®2080 matched the pattern of fluor substituted HA with 0.2 F atoms per unit formula (PDF: 01-074-4173). Comparison of the peak broadening revealed a similar crystallinity of all AlgOss® materials. The phase composition derived from the semi-quantitative analysis is shown in table 6. The obtained compositions were in agreement with the manufacturer's specifications.

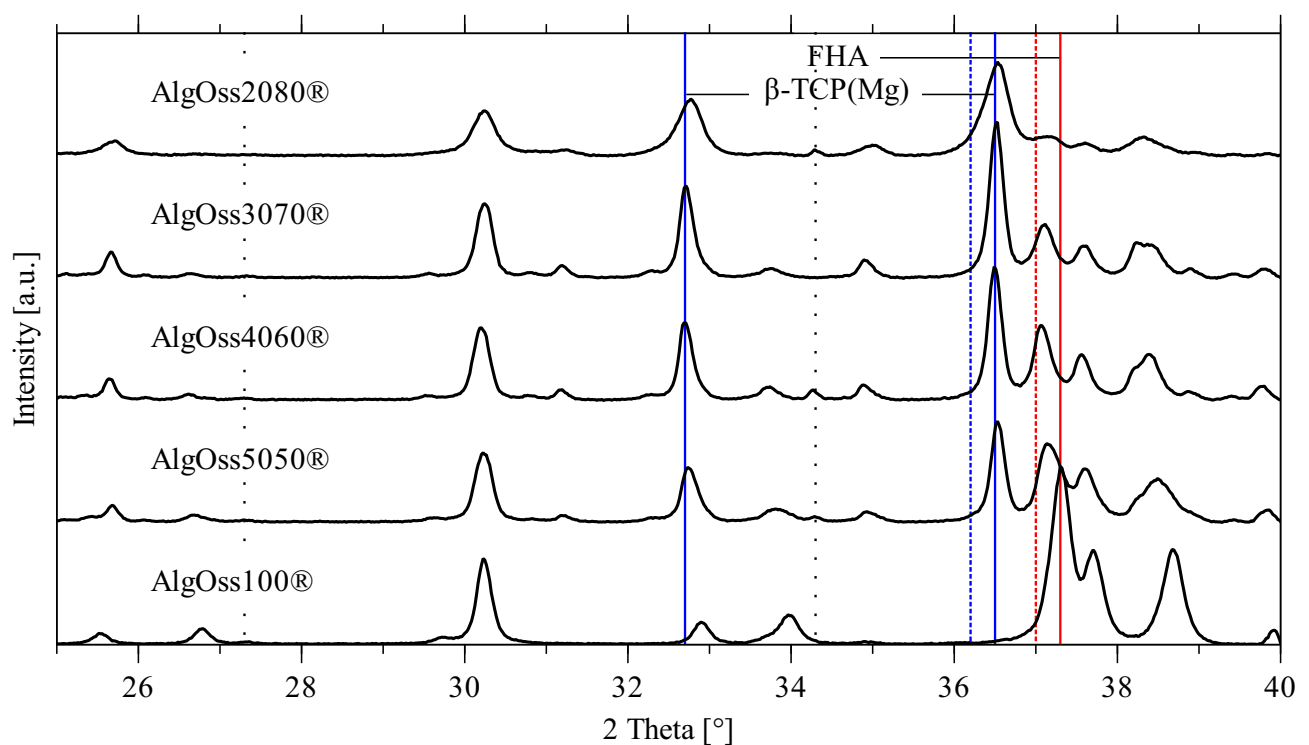


**Figure 16:** XRD spectra of the material from the AlgOss® series as obtained from the manufacturer. The dash-dotted lines left of the respective reflections of FHA and  $\beta$ -TCP (Mg), correspond to stoichiometric HA and  $\beta$ -TCP. It can be seen that substitution shifted the spectra to higher angles. The dotted lines correspond to residual  $\text{CaCO}_3$ .

Ca and P concentrations were measured for the AlgOss® series with ICP-OES and are listed in table 6. The measured values for the atomic Ca/P ratio are lower than the calculated ones for all samples, indicating a substitution of some ions either in the HA, the  $\beta$ -TCP or both phases. This result is in agreement with the obtained XRD spectra which also indicate a Ca substitution. It has to be mentioned that fluor substitution only affected the shift of the XRD reflections but not the Ca/P

ratio measured by ICP-OES. The partial substitution of  $\text{Ca}^{2+}$  with  $\text{Mg}^{2+}$  in the  $\beta$ -TCP phase and the  $\text{Ca}^{2+}$  deficiency in the HA phase determined by XRD were in agreement with the values for Ca/P ratio determined by ICP-OES.

Even though AlgOss®5050 had a higher HA content than AlgOss®4060 determined by X-ray analysis, the Ca/P ratio was higher in AlgOss®4060 compared to AlgOss®5050. This behavior can be attributed to a different amount of substituted ions within the two materials.

**Table 6:** Ca/P ratio of the raw AlgOss® materials obtained by ICP-OES and HA/ $\beta$ -TCP ratio measured by semi-quantitative XRD analysis.

	HA: $\beta$ -TCP [wt%]	Ca/P [at%]
AlgOss®5050	50.8 : 49.2	1.479 ± 0.015
AlgOss®4060	42.6 : 57.4	1.514 ± 0.015
AlgOss®3070	31.4 : 68.6	1.398 ± 0.016
AlgOss®2080	21.2 : 78.8	1.388 ± 0.018
HA/ $\beta$ -TCP 50/50 (calculated)	-	1.584
HA/ $\beta$ -TCP 40/60 (calculated)	-	1.567
HA/ $\beta$ -TCP 30/70 (calculated)	-	1.550
HA/ $\beta$ -TCP 20/80 (calculated)	-	1.533

#### 4.2.3. *In vitro* Bioactivity Test

The weight changes upon immersion in SBF of the AlgOss® series are shown in figure 17. It can clearly be seen that all materials behaved similarly with different rates of dissolution and precipitation. All measured samples were continuously gaining weight over the whole experiment time, indicating that HA precipitation rate was higher than dissolution of  $\beta$ -TCP. Within the first 24 h all materials gained around 0.5 % of their initial weight except AlgOss®5050, which hardly changed weight, and AlgOss®2080, where a mass gain of 1 % was measured.

After one week, a clear trend was observed. From AlgOss®100 to AlgOss®4060, the mass gain decreased from 2.2 % to 1.2 % and rose again for the samples with higher  $\beta$ -TCP ratios to 1.7 % for AlgOss®3070 and 2.7 % for AlgOss®2080. A similar trend was observed after two weeks of immersion when the least mass gain of 2 % was measured for AlgOss®4060 and AlgOss®3070. AlgOss®100 and AlgOss®2080 were the samples that gained most weight of 3.1 % and 4.9 % respectively, with AlgOss®5050 in between with a mass gain of 2.8 %. In other words, there was a minimum mass gain for samples with a HA/TCP ratio of around 1 : 1 and a maximum for samples with either a high HA or a high TCP ratio.

The obtained data of the weight changes revealed another trend. The minimum mass gain after 12 h and 24 h of immersion was measured for AlgOss®5050. After one week of immersion the least mass gain was observed for AlgOss®4060 and after two weeks of immersion the minimum weight was measured for AlgOss®4060 and AlgOss®3070. It seems like the minimum mass gain was moving towards higher  $\beta$ -TCP ratios as immersion time was prolonged (fig. 18).

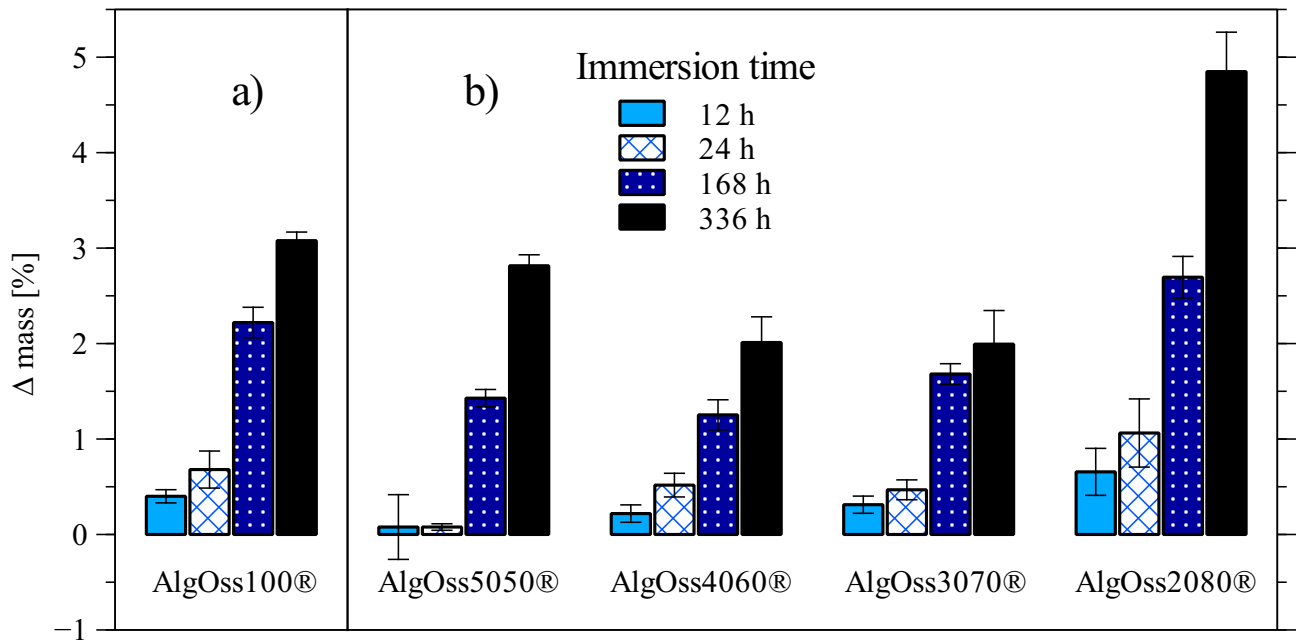


**Figure 17:** Mass change of the AlgOss® materials in percent of initial sample mass as a function of immersion time. a) single phase HA b) Biphasic calcium phosphates with different HA/  $\beta$ -TCP ratios.

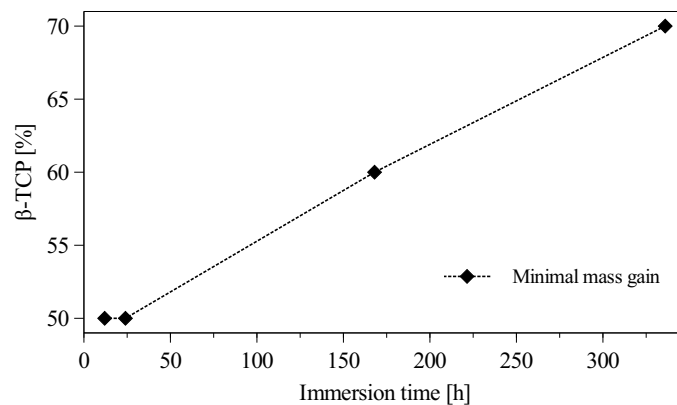


**Figure 18:** BCP with the minimum mass gain as a function of immersion time. Minimal mass gain after 12 h and 24 h was measured for AlgOss®5050. After 168 h AlgOss®6040 revealed the minimum mass gain and after 336 h AlgOss® 3070 was the sample with the minimal measured mass gain.

The change in surface morphology for different immersion times is shown in figure 19. It was hard to distinguish between the initial surface morphology of AlgOss® and the precipitated HA, especially after only 12 h immersion. Therefore, only the raw materials and the materials after 336 h of immersion are shown. A more detailed collection of SEM images of the samples can be found in the appendix. Almost no differences in surface morphology for different HA/ $\beta$ -TCP ratios were observed for the BCP of the AlgOss® series. Only for AlgOss®100, the particle clusters at the surface were larger compared to the other materials and therefore the surface appeared rougher. After 168 h of immersion, it seemed like the particle clusters became larger and rougher, indicating that some precipitation took place. After 336 h of immersion all materials seemed to have changed their surface morphology. Particularly AlgOss®100 and AlgOss®2080 showed precipitates on the clusters that were not present before immersion. The XRD spectra of the materials after different immersion times were all identical with the spectra of the respective raw spectrum.

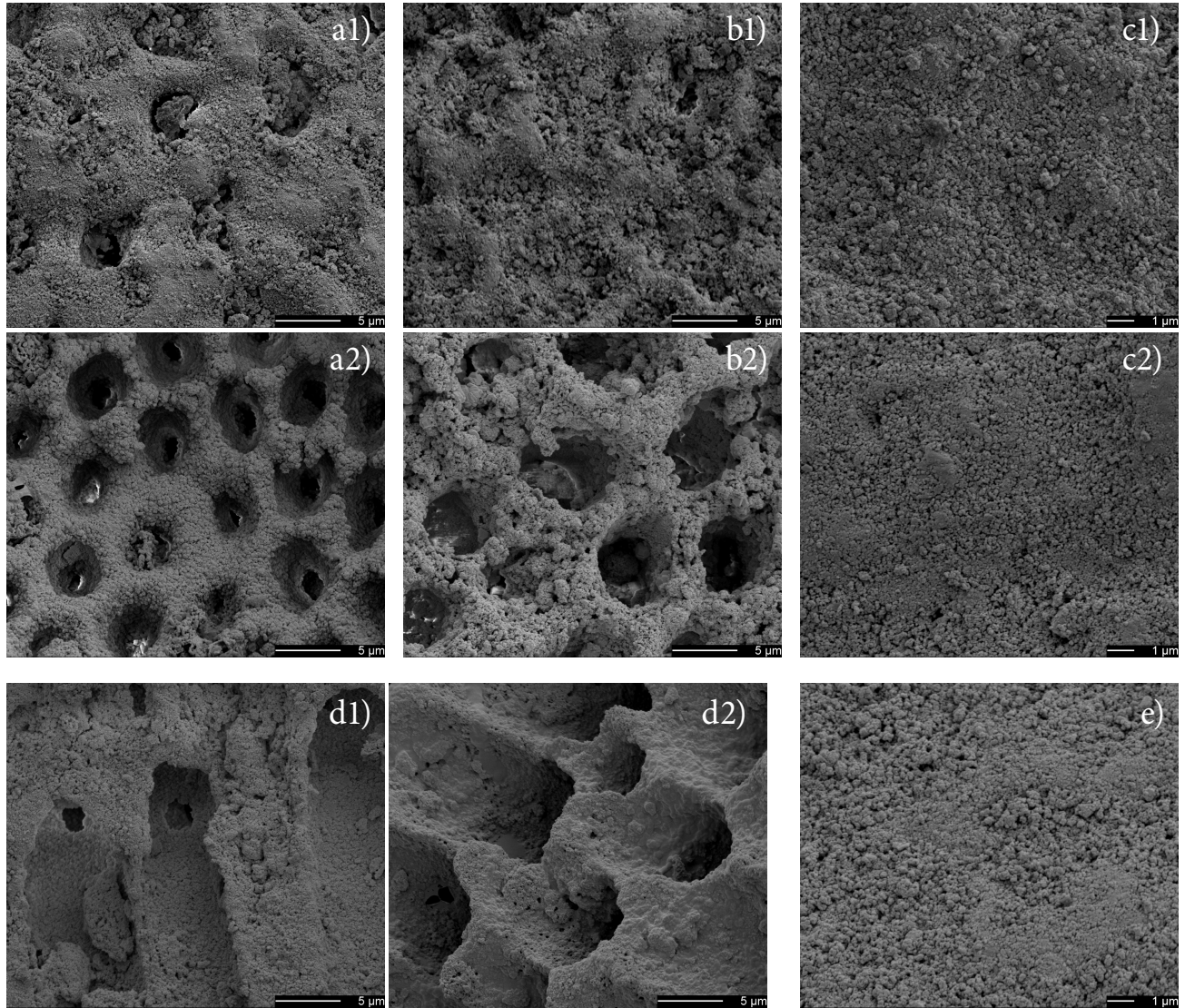


**Figure 19:** SEM images of the AlgOss® materials as obtained from the manufacturer and after 336 h immersion. a1) AlgOss®5050 raw. a2) AlgOss®5050 336 h. b1) AlgOss®4060 raw. b2) AlgOss®4060 336 h. c1) AlgOss®3070 raw. c2) AlgOss®3070 336 h immersion. d1) AlgOss®2080 raw. d2) AlgOss®2080 336 h. e) AlgOss®100 after 336 h immersion.

### 4.3. Composite Materials

#### 4.3.1. Surface Morphology

The morphology of the electrospun PLGA/ATCP composite materials and of pure PLGA can be seen in figure 20. The materials consisted of porous fibers with a diameter between 1 and 5  $\mu\text{m}$ . A smooth surface was observed for pure PLGA fibers at lower magnitudes. At higher magnitudes the porous surface of the fibers became clear which can be attributed to the evaporation of solvent during the electrospinning process. For both PLGA/ATCP composites, it can be seen that the fibers were not as homogeneous and regularly spun as pure PLGA fibers. There were many ruptured fibers, accumulations of PLGA and larger variation in fiber diameters compared to pure PLGA. On the surface of the PLGA/ATCP composites, small ATCP particles were observed (fig. 25). Bonewool®6040 seemed to have less and smaller pores than the other two samples and accumulations of ATCP were observed.

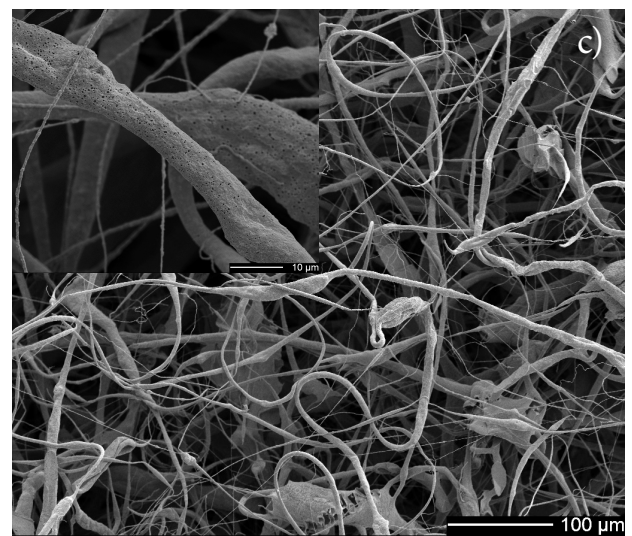
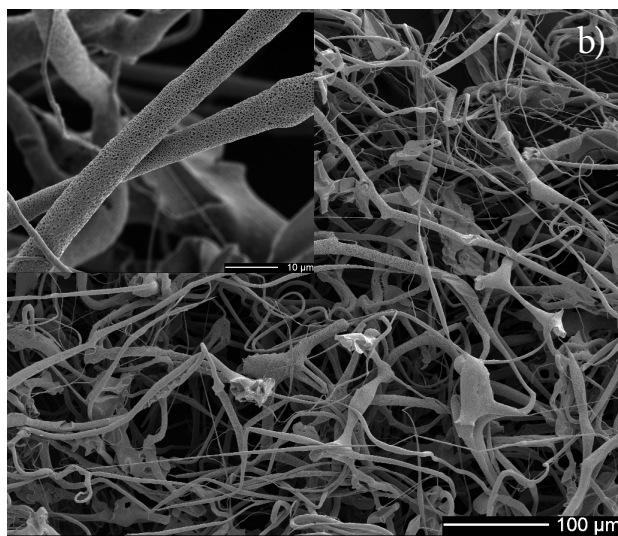
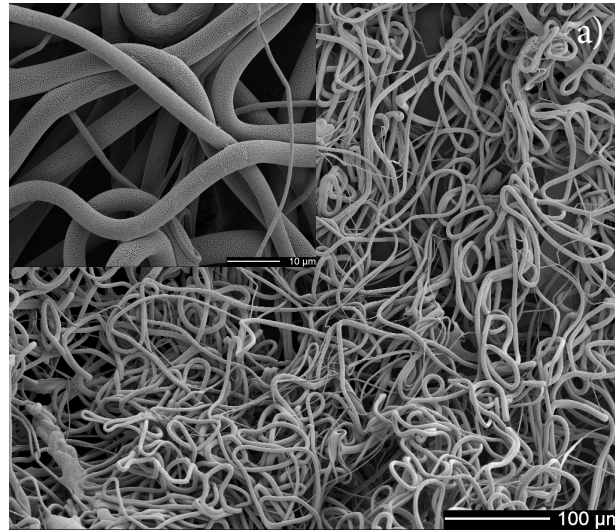


**Figure 20:** SEM images of a) pure electrospun PLGA fibres and ATPC/PLGA composite materials. b) PLGA/ATCP ratio of 80/20. c) PLGA/ATCP ratio of 60/40. Scale bar of close up = 10  $\mu\text{m}$ .

### 4.3.2. Phase and Elemental Composition

Due to a lack of material, no XRD and elemental analysis was performed with the Bonewool® samples before immersion in SBF. X-ray diffraction patterns and EDS spectra of the inorganic content after combustion of PLGA can be found in section 4.3.3.

### 4.3.3. *In vitro* Bioactivity Test

Pure electrospun PLGA fibers gained 6 % of their initial mass within 12 h as can be seen in figure 21. EDS analysis of the precipitates after combustion of PLGA revealed that this weight gain was mainly due to precipitation of sodium chloride and some magnesium salts (fig. 25) and is therefore not a measure of bioactivity. The same is true for the weight gain after 24 h and 168 h. After 336 h of immersion a weight loss of 1.8 % was measured which is contributed to dissolution of water soluble Tween20.<sup>84</sup> Ignoring the weight gain at the beginning due to sodium chloride precipitation, the mass of pure PLGA fibers hardly changed over the observed time span which is in agreement with previous studies.<sup>52,85</sup>

A significant mass gain of 6 % and 10 % of the initial sample mass was measured for

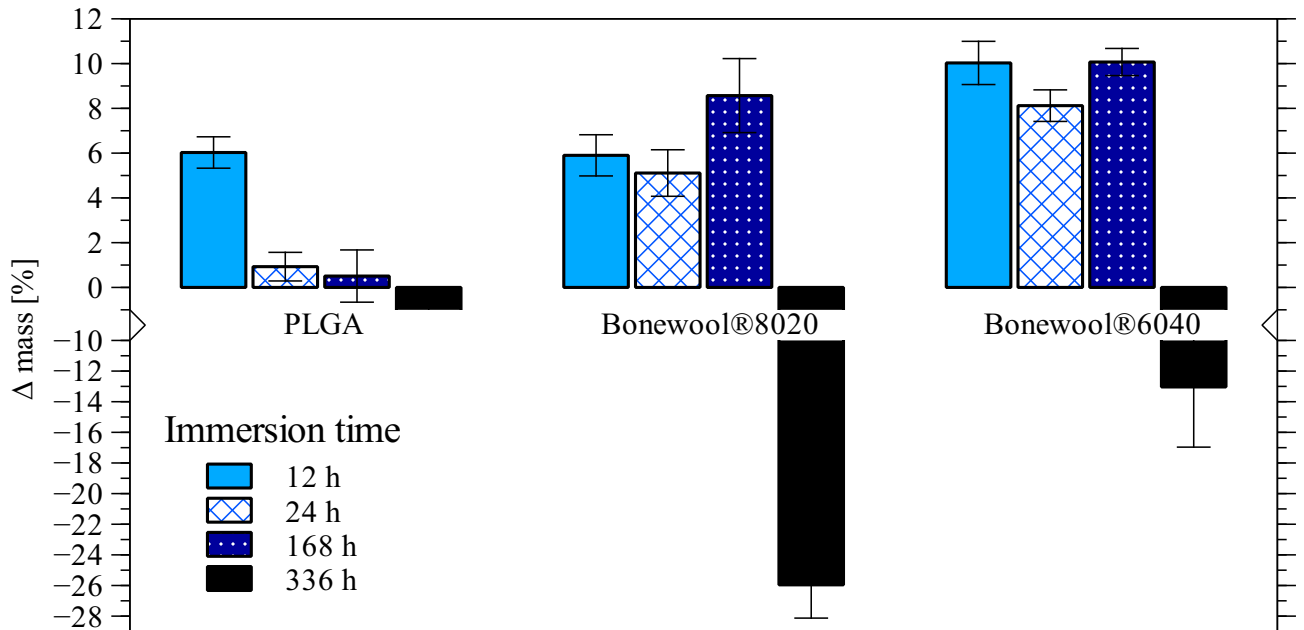


**Figure 21:** Mass change of pure PLGA and PLGA/ATCP composites in percent of initial sample mass as a function of immersion time.

Bonewool®8020 and Bonewool®6040 after 12 h respectively. After 24 h Bonewool®8020 and Bonewool®6040 lost weight, compared to the results after 12 h, to 5.1 % and 8.1 % of the initial sample mass which is contributed to degradation of PLGA9. The highest weight gain for the two composite samples was measured after 168 h of immersion. This result indicates that precipitation rate of HA was higher than the degradation rate of PLGA and ATCP within this time span. This effect was obviously more pronounced with Bonewool®6040 since more nucleation sites for HA depositions were available.

A significant weight loss of 26 % and 13 % of the initial sample mass was detected for Bonewool®8020 and Bonewool®6040 respectively. Degradation of PLGA and ATCP could be one reason for the mass loss of the composite materials. Since the rate of HA precipitation is higher for Bonewool®6040 than for Bonewool®8020 it lost less mass.

To determine the amount of residual ATCP plus deposited HA the PLGA was removed by combustion and the inorganic residuals were weighed (fig. 22). It can be seen that the inorganic mass increased with immersion time for both ATCP doped samples whereas the mass of PLGA hardly changed over the experiment time ignoring the sodium chloride deposition at the beginning. The nucleation rate was higher for Bonewool®6040 than for Bonewool®8020, as can be seen at the slope between 168 h and 336 h. SEM images of the samples after different immersion times (fig. 23-25) and XRD spectra of the inorganic components after combustion confirmed the weight gain due to HA deposition (fig. 27) for ATCP doped samples.

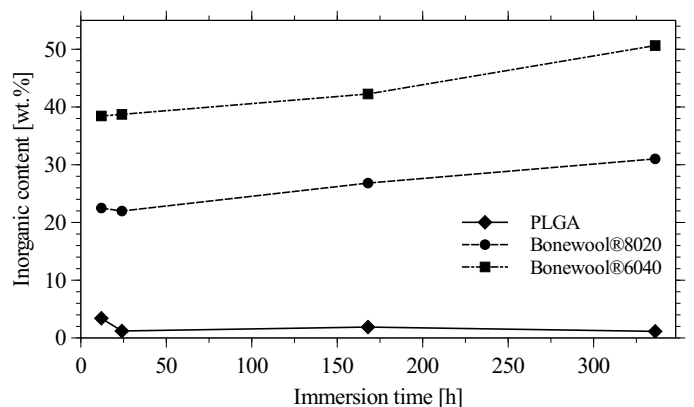


**Figure 22:** Inorganic content (TCP + HA deposition + other inorganic precipitates) in percent as a function of immersion time related to the weight before immersion.

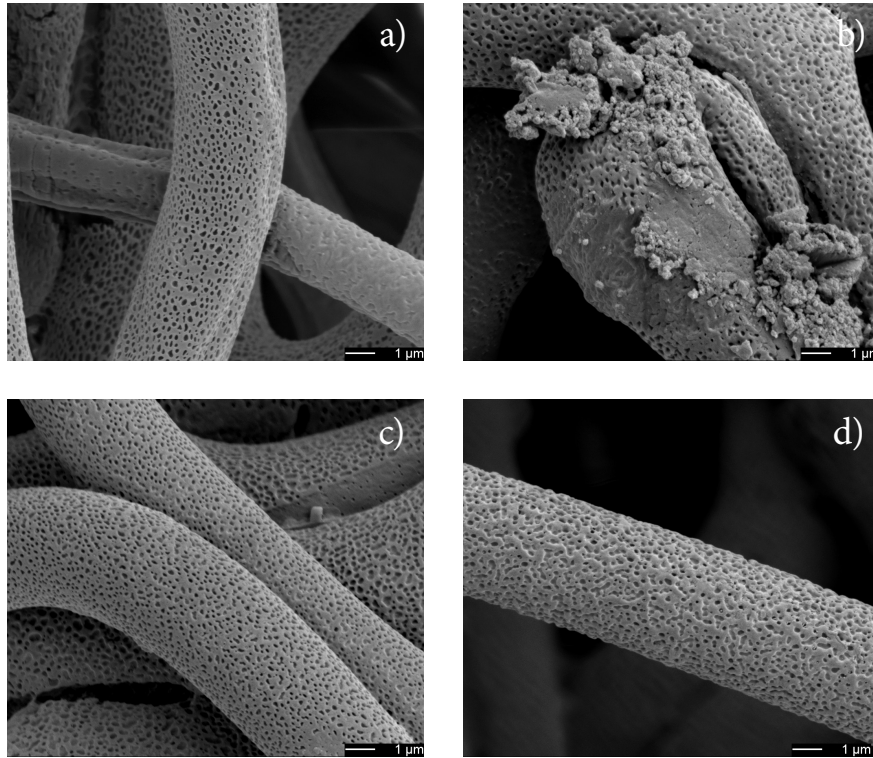


**Figure 23:** SEM images of the surface of electrospun PLGA fibres after different immersion times. a) Raw material b) 12 h of immersion c) 168 h of immersion d) 336 h of immersion.

The surface of pure PLGA fibers hardly changed over the experiment time, except that the pore diameter increased with longer immersion times. The images taken after 12 h of immersion confirmed that the weight gain was due to crystal precipitation. EDS analysis of those precipitates indicates that these crystals are composed of sodium chloride and small amounts of magnesium salts (fig. 26).

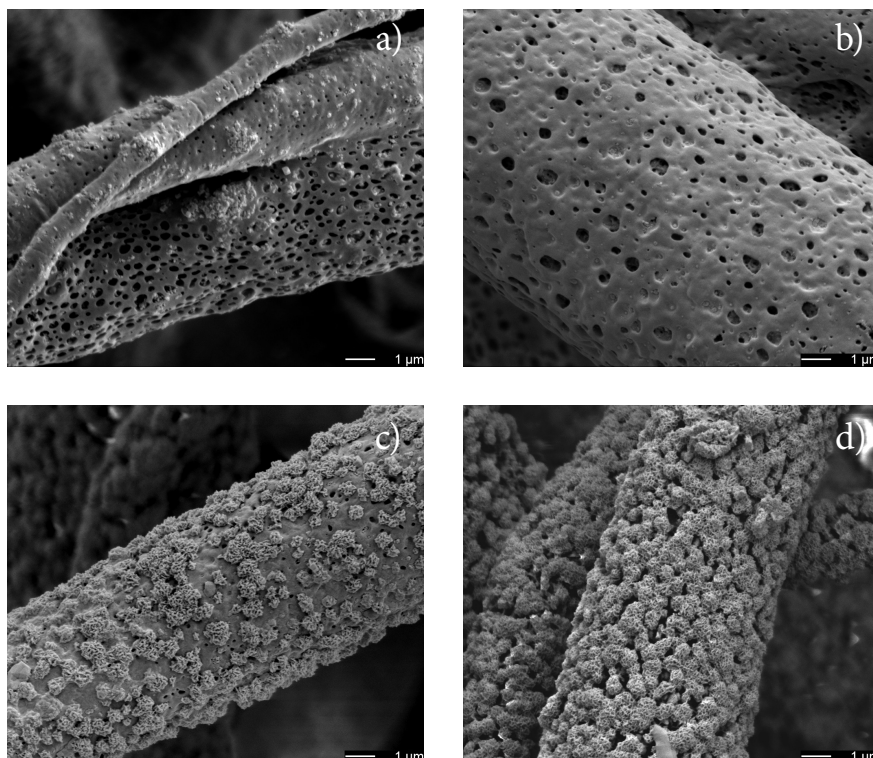


**Figure 24:** SEM images of the surface of Bonewool8020 after different immersion times. a) 12 h immersion b) 24 h of immersion c) 168 h of immersion d) 336 h of immersion.

Despite the measured weight gain of Bonewool®8020 upon immersion in SBF, only small amounts of precipitates were detected with SEM after 12 h and 24 h. After 168 h of immersion, about half of the fiber surface was covered with cauliflower like HA crystals and after 336 h almost the complete surface of the fibers was covered with HA crystals.

Immediate HA deposition took place on the surface of Bonewool®6040 as can be seen in figure 25b. Already after 12 h the majority of the fibers was almost covered with HA crystals. After 24 h of immersion, the surface of the fibers was completely covered with a HA layer. HA deposition continued for longer immersion times and the crystals became larger.

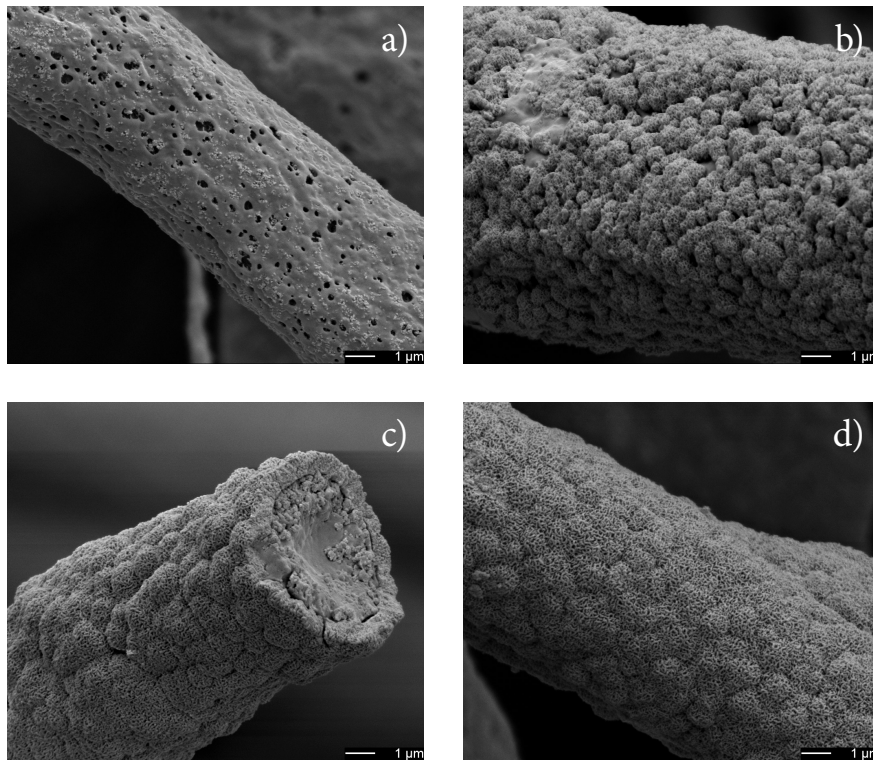


**Figure 25:** SEM images of the surface of Bonewool®6040 after different immersion times. a) Raw material b) 12 h of immersion c) 24 h of immersion d) 336 h of immersion.

XRD spectra of the inorganic components after combustion of PLGA for different time intervals are shown in figure 27 for the ATCP doped samples. The spectra confirm that the weight gain was mainly due to precipitation of HA although other reflections can be seen for some samples. For Bonewool®8020 after 12 h and 168 h (appendix) of immersion, three additional peaks ( $2\theta = 31.8^\circ$ ,  $36.8^\circ$  and  $39.4^\circ$ ) were found that may be contributed to precipitated sodium chloride (COD 4300180). The same peaks were visible for Bonewool®6040 after 12 h and 168 h of immersion (appendix) and for Bonewool®8020 after 336 h of immersion where they were less prominent.

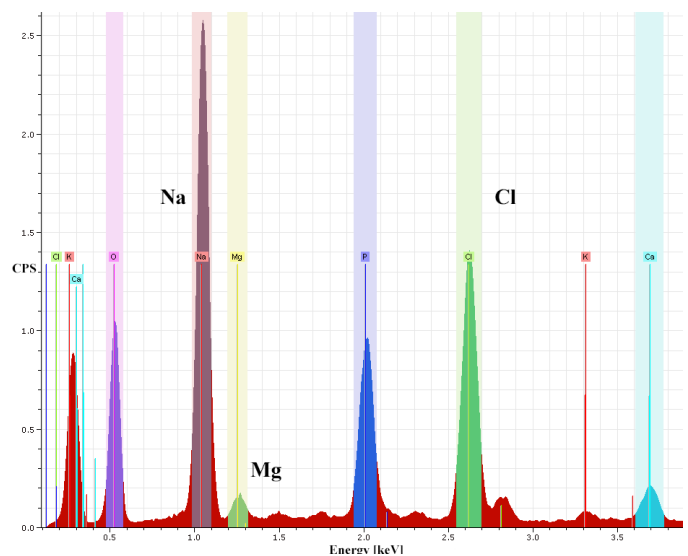


**Figure 26:** EDS spectrum of the inorganic content of pure PLGA after 12 h immersion.

Two small peaks between  $2\theta = 26.9^\circ$  and  $27.3^\circ$  were measured for all samples that could not be assigned. Although it seemed that other precipitates than HA were deposited on the Bonewool® samples, the XRD spectra revealed that the major phase was HA which therefore contributed most to the mass change. EDS analysis of the inorganic components showed that small amounts of sodium, chloride and some magnesium were present. From the XRD and EDS spectra it can be seen that beside HA also other crystal phases precipitated.

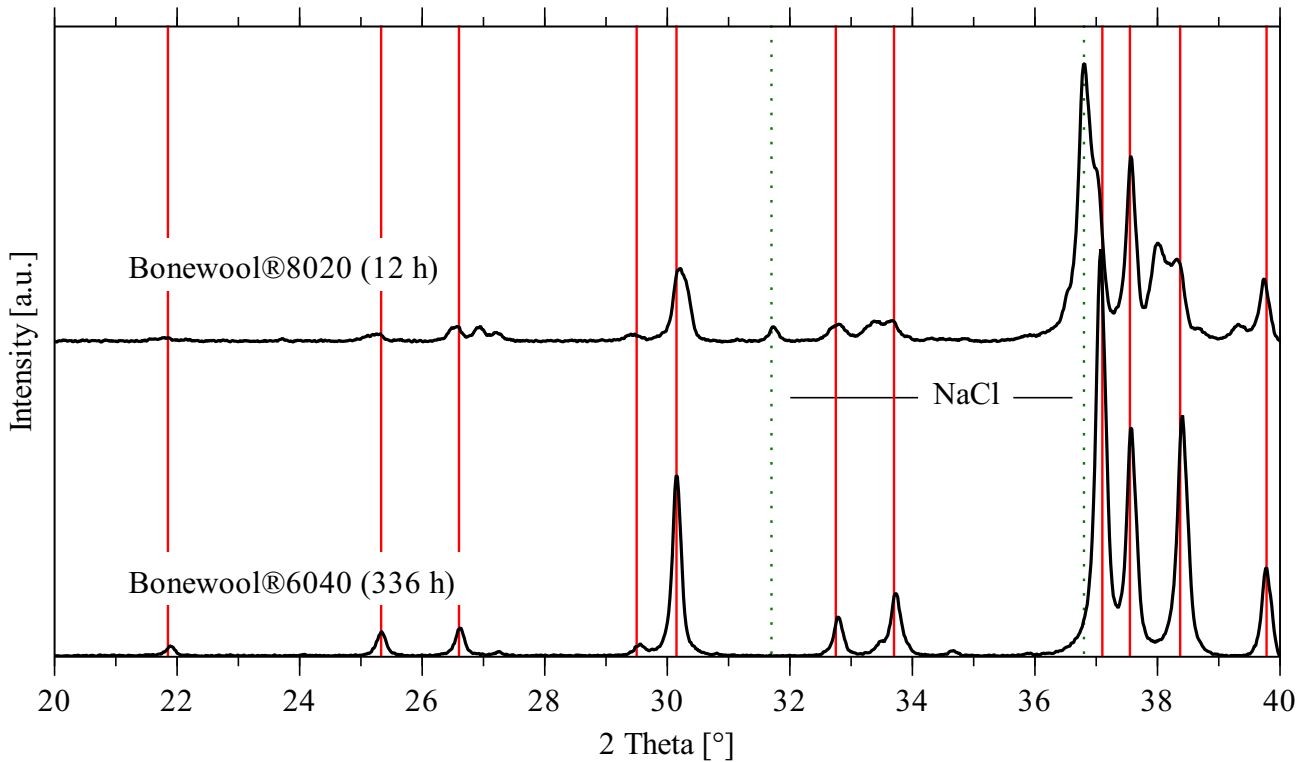


**Figure 27:** XRD spectra of the inorganic content after combustion. Only the spectra of the sample with fewest amount of precipitates besides HA and of the sample with most precipitates that could not be assigned to HA. Further spectra can be found in the appendix. The solid lines could be assigned to HA and the dotted lines to sodium chloride. The other peaks could not be assigned.

## 5. Discussion

The bioactivity test in this study measured the differences in dissolution and precipitation behavior of the different bone graft materials in physiological environment that are crucial factors for *in vivo* bone graft performance. Dissolution and precipitation are mainly affected by the chemical composition and the specific surface area in contact with the medium. The latter is predominantly related to microporosity and surface morphology. The two processes were working in opposite direction. Dissolution of compounds with higher solubility, compared to HA, lowered the sample mass. On the other hand precipitation of HA increased the mass. According to the nucleation theory a rough surface with grains and edges could facilitate nucleation and therefore precipitation by removing the need of the formation of a critical size nucleus (formulas 11 and 12). The effect of edges being a favorite site for precipitation could be nicely observed on the smooth surface of BoneCeramic® (fig. 27). Furthermore the surface area in contact with the medium, which is related to microporosity, was obviously a key factor since crystal formation starts at the liquid-solid interface<sup>86</sup> Another effect that favored HA precipitation was the release of  $\text{Ca}^{2+}$  and  $\text{PO}_4^{2-}$  ions due to dissolution of soluble calcium phosphate phases since rise of phosphate and calcium ions moved the supersaturation level towards HA. It was attempted to correlate the results obtained from the physicochemical analysis with the performance of the different bone graft substitutes in the bioactivity test according to the dissolution and precipitation theory of calcium phosphates.

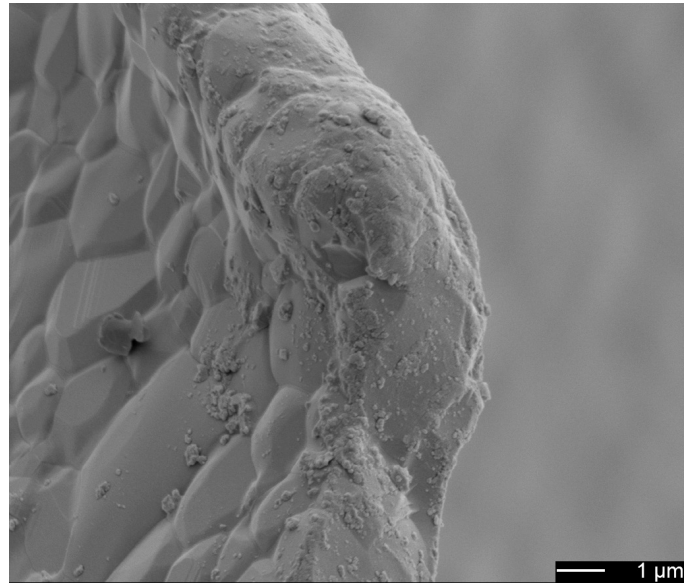


**Figure 27:** SEM image of BoneCeramic® after 24 h immersion. It can be seen that precipitation is favoured at edges.

### 5.1. Commercial Materials

The five examined commercial materials had major differences in dissolution and precipitation behavior although the results of the two BCP materials and the two pure HA materials were comparable.

#### 5.1.1. Commercial BCP

The initial weight loss of BoneCeramic® and Maxresorb® can be explained with dissolution of  $\beta$ -TCP, which has a higher solubility compared to HA (table 3). Furthermore the SEM images showed that almost no HA precipitation took place within the first 24 h. This can be explained by the fact that the materials were sintered and therefore had a smooth surface (fig. 27). Sintering altered the mechanical properties of the materials<sup>30</sup> but also made them more resistant to precipitation due to lower surface area and less nucleation sites compared to the unsintered materials. The smooth sintered surface explains the low precipitation rate after 336 h of immersion compared to the other materials. SEM images revealed that Maxresorb® featured many micropores whereas BoneCeramic® had no visible microporosity which can be attributed to the higher sinter temperatures for BoneCeramic®. This could be an explanation for why dissolution and precipitation rates were slightly higher for Maxresorb®

than for BoneCeramic®. Microporosity goes together with a higher surface area in contact with the medium and therefore favors dissolution as well as nucleation.

The XRD data showed that both sintered materials were highly crystalline which also explains the low dissolution and precipitation rates.<sup>87</sup> Nevertheless, cauliflower like HA crystals were detected for both materials after two weeks immersion. The SEM images showed that only some of the grains were covered with a HA layer for the Maxresorb® samples (fig 11d). This behavior can be explained by the assumption that the individual grains were either composed of HA or  $\beta$ -TCP and that precipitation was favored on the HA grains because they already had the same crystal structure as the precipitate.<sup>86</sup> Dissolution of  $\beta$ -TCP might have amplified this effect by increasing the  $\text{Ca}^{2+}$  and  $\text{PO}_4^{2-}$  concentrations around the HA grains (formula 12). Although BoneCeramic® was also a BCP composed of individual grains, SEM images showed that there were no favored grains for precipitation which might indicate that the individual grains have biphasic character rather than being separated.

Although XRD analysis revealed a higher HA/ $\beta$ -TCP ratio for BoneCeramic® than for Maxresorb®, Maxresorb® showed a more significant weight gain. This relation indicates that microporosity and a larger surface area are more relevant for the weight gain than the higher solubility caused by the higher  $\beta$ -TCP ratio. A difference in phase composition was not detected after immersion because the percentage change due to HA deposition was lower than the sensitivity of the semi-quantitative XRD analysis.

### 5.1.2. Nanobone®

A rapid weight gain of the Nanobone® samples within the first 12 hours was measured. This can be explained by the extremely rough surface of the particles revealed by SEM. The particles had many grains and edges in the submicron range that facilitated nucleation and precipitation by removing the need of the formation of a critical size nucleus (formula 12). Furthermore, ICP-OES analysis of Nanobone® showed that the contained HA was stoichiometric while the XRD spectrum was shifted to higher angles. This can be explained by a partial substitution of the  $\text{OH}^-$  groups with  $\text{F}^-$  ions<sup>82</sup> which lowered the solubility of Nanobone® compared to pure HA (table 3). The continuous weight loss after 24 h and 168 h immersion can be attributed to the dissolution of the amorphous silica matrix. The rate of dissolution was obviously faster than HA precipitation because the total sample mass decreased. The weight gain between 168 h and 336 h indicates that the dissolution rate of  $\text{SiO}_2$  decreased and precipitation dominated the weight change.

### 5.1.3. Commercial HA Based Materials

The two pure HA based materials BioOss® and Algipore® showed the most significant mass gain within this group with no mass loss over the whole experiment time. These results indicate that the precipitation rate was significantly higher than the dissolution rate at any point in time. Since the materials were only composed of HA, weight loss due to dissolution was little compared to the other materials as it is reflected in the respective  $pK_s$  values (table 3). Furthermore, both materials had a rough surface with many nucleation sites and they were equipped with macro- and micropores increasing the specific surface area.

The XRD data showed broad diffraction peaks which indicates that BioOss<sup>®</sup> consisted of HA with a significant portion of amorphous phase as already shown by other studies.<sup>42</sup> ICP-OES analysis revealed a Ca/P ratio of 1.717 which is slightly higher than the ratio of stoichiometric HA. This can be explained with the amorphous phase because amorphous calcium phosphates can have Ca/P ratios from 1.2 – 2.2 and a much higher solubility than crystalline HA (table 3). A substitution of the phosphate ions was not probable because this would have caused a shift in the XRD reflections. Furthermore, the contained CaCO<sub>3</sub> leads to a higher Ca/P ratio.

The X-ray reflections of Algipore<sup>®</sup> were typical for calcium deficient FHA (Ca<sub>10</sub>F<sub>2</sub>O<sub>24</sub>P<sub>6.05</sub>). Apart from that, the reflections indicate a small amount of residual CaCO<sub>3</sub> that has also been measured in other studies for Algipore<sup>®</sup> and BioOss<sup>®</sup>. The results of the ICP-OES measurements showed a calcium deficiency in agreement with the XRD spectra. Those deviations of the composition of BioOss<sup>®</sup> and Algipore<sup>®</sup> according to dissolution can be interpreted as follows: Amorphous calcium phosphates are more soluble than HA and CaCO<sub>3</sub>. Furthermore, the solubility of FHA is even lower than of HA indicating that BioOss<sup>®</sup> is more soluble than Algipore<sup>®</sup>. The mass gain, on the other hand, was more significant for BioOss<sup>®</sup> indicating that the higher precipitation rate due to the surface structure is much more dominant than weight loss due to dissolution.

## 5.2. AlgOss<sup>®</sup> Series

The surface morphology and the porosity were almost the same for the materials within the AlgOss<sup>®</sup> series, except for AlgOss<sup>®</sup>4060 that had a higher total porosity (77 ± 1 %) compared to the other AlgOss<sup>®</sup> materials (69 ± 1 %). The different weight changes during the bioactivity test is therefore not influenced by the surface morphology, except that HA precipitation was maybe favored for AlgOss<sup>®</sup>4060 due to the higher porosity.

XRD analysis revealed that the β-TCP phase in all biphasic AlgOss<sup>®</sup> materials was magnesium substituted. This is in agreement with the ICP-OES results that showed a lower Ca/P ratio for the biphasic AlgOss<sup>®</sup> materials than expected for pure HA/β-TCP mixtures (table 6). Magnesium substituted β-TCP (Ca<sub>9.5</sub>MgO<sub>28</sub>P<sub>7</sub>) has a Ca/P ratio of 1.357 which is in agreement with the elemental analysis (table 6). The HA phases of the different materials had different degrees of substitution as can be seen in the peak shift of the spectra. It has been shown in other works that with higher fluor substitution the peaks shift to higher angles.<sup>79,80</sup> The only material that matched its HA peaks with the pattern for stoichiometric HA was AlgOss<sup>®</sup>4060. AlgOss<sup>®</sup>100 had almost the exact spectrum like Algipore<sup>®</sup> matching the pattern of calcium deficient FHA (Ca<sub>10</sub>F<sub>2</sub>O<sub>24</sub>P<sub>6.05</sub>). The spectra of AlgOss<sup>®</sup>5050 is in agreement with the pattern obtained for partially substituted FHA (Ca<sub>5</sub>(PO<sub>4</sub>)<sub>3</sub>((OH)<sub>0.6</sub>F<sub>0.4</sub>)) with 0.4 fluor atoms per formula unit. AlgOss<sup>®</sup>3070 and AlgOss<sup>®</sup>2080 matched the patterns obtained for partially substituted FHA with a lower substitution of 0.2 fluor atoms per formula unit. Comparison with the ICP-OES results indicates that not only AlgOss<sup>®</sup>100 is calcium deficient but also the biphasic AlgOss<sup>®</sup> materials except for AlgOss<sup>®</sup>4060. The differences between the materials do not seem to affect the dissolution behavior because fluor substitution was observed for all samples and the difference in solubility compared to HA is minor (table 3). Calcium deficiency, on the other hand, could affect the dissolution properties because calcium deficient HA is more soluble than stoichiometric HA. AlgOss<sup>®</sup>4060 was the only material in this series that did not have calcium deficiency in the HA phase and may have been less soluble. However, the differences in the bioactivity test only seem to be affected by the different phase composition. If anything, the

mass change for AlgOss®4060 would have been lower compared to the other samples, if it would have been also composed of calcium-deficient HA with a porosity comparable to the other AlgOss® materials, which again would emphasize the observed trend.

As already described, a higher  $\beta$ -TCP ratio leads to higher solubility and therefore to a more dominant weight lost which explains the trend observed for a  $\beta$ -TCP ratio between 0 % and 60 %. This trend is emphasized by the fact that the higher the HA ratio is the more nucleation sites are available according to the nucleation theory. The reason why the BCP materials within the AlgOss® series did not lose weight within the first 24 h like BoneCeramic® and Maxresorb® is simply that they were not sintered and HA precipitation took place immediately. On the other hand, there was a third effect that explained the rise of mass gain for AlgOss®3070 and AlgOss®2080.

Dissolution of  $\beta$ -TCP leads to a local raise of  $\text{Ca}^{2+}$  and  $\text{PO}_4^{2-}$  ions which increases the supersaturation level ( $L_{sat}$ ) and therefore favors HA precipitation. This effect seemed to dominate over the higher solubility and less nucleation sites for a  $\beta$ -TCP ratio of around 50 % to 80 %.

It seems that the minimal mass change shifts to higher  $\beta$ -TCP ratios as immersion time prolongues. This observation indicates that the effect of raising the supersaturation level to favor HA precipitation is reduced for longer immersion times. This can be explained with the fact that the longer the immersion time was, the less  $\beta$ -TCP had been available to raise the ion concentrations. Furthermore, the surface was covered with a HA layer that hindered dissolution of  $\beta$ -TCP.

### 5.3. Composite Materials

Two competing processes changed the mass of pure PLGA and ATCP doped PLGA during immersion in cell culture medium. On the one hand, degradation of PLGA via dissolution lead to a mass loss. It has been shown in other works that the degradation rate of PLGA is strongly related to the ATCP content and is faster for highly doped PLGA fibers.<sup>52</sup> On the other hand, precipitation of HA lead to a mass gain that was more prominent for composites with a higher ATCP/PLGA ratio. Furthermore, in the case of the composite samples, dissolution of ATCP played a role in mass change.

The SEM images and the weight change of pure PLGA fibers after 12 h immersion showed that precipitation took place. That goes against the findings of other studies that have shown that pure PLGA does not induce HA precipitation in SBF. EDS analysis of the precipitates after combustion revealed that they consisted mainly of sodium chloride and some magnesium salts. It seems that NaCl precipitation has been induced due to the fluctuation of the pH value (7.2 – 7.6) that influenced the saturation levels for different salts. Because of the high surface area of the fibers, it appears that precipitation, not only for HA, was extremely altered in comparison to the materials in granular form. The used cell culture medium had a slightly higher sodium content than conventional SBF and blood plasma (table 4) which may also favor the precipitation of NaCl. Furthermore, it is probable that the samples were not rinsed carefully enough prior to analysis leaving crystals on the surface.

XRD spectra and EDS analysis of the inorganic content of the composites after combustion indicate that also Bonewool®8020 after 12 h and 168 h of immersion had induced significant precipitation of sodium chloride and traces of magnesium salts. Only Bonewool®6040 after 24 h and 336 h showed XRD reflections for HA without any other peaks. Although even those samples showed small peaks at 26.9°, 27.3° and 39.2° which could not be identified. Also SEM images revealed crystal

formation on the surface of some samples that can be identified as NaCl and some magnesium precipitates with EDS analysis. Therefore, the results in figure 21 have to be interpreted carefully to not account NaCl precipitation for a measure of bioactivity. From the XRD spectra it can be seen that especially Bonewool®8020 after 12 h of immersion has significantly fewer HA deposits than indicated by the weight change that has also been confirmed with the SEM images. However, the precipitates on the other samples are mainly HA as can be seen from the dominant HA peaks compared to the peaks of the other detected phases. Therefore, weight change can mainly be attributed to HA precipitation for all samples except pure PLGA and Bonewool®8020 after 12 h of immersion where the mass gain due to HA precipitation was overestimated in the bioactivity test. HA precipitation was estimated by subtracting a significant portion of the mass gain from Bonewool®8020 after 12 h of immersion and a smaller portion of Bonewool®8020 after 168 h and Bonewool®6040 after 12 h, because these samples showed the most intense peaks for sodium chloride.

In figure 28 an estimate of the weight change without NaCl precipitation can be seen. With this estimation the results of the bioactivity test showed a different behavior. Pure PLGA does not seem to induce HA precipitation and therefore hardly changed mass during the experiment time. This can also be confirmed with the SEM images. Some loss of the mass after longer immersion times can be explained by dissolution of PLGA.

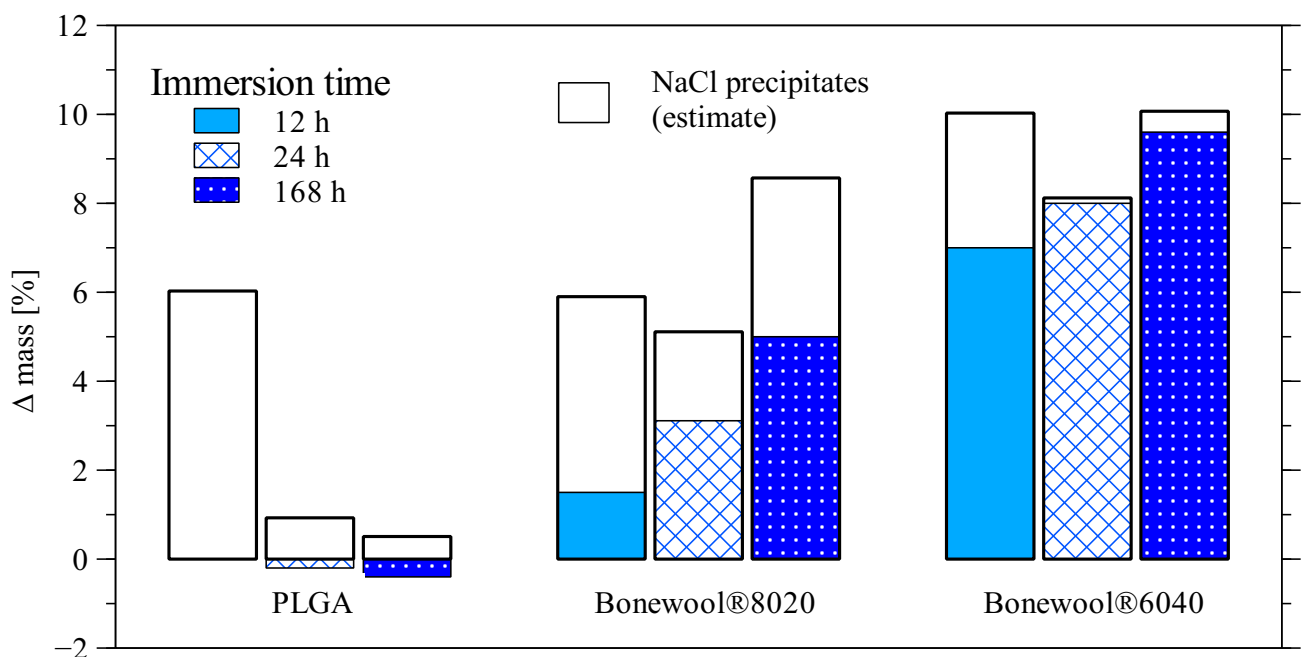


**Figure 28:** Weight change of PLGA and PLGA/ATCP composites after subtraction of estimated amount precipitated NaCl based on SEM images and XRD analysis.

The estimated HA precipitation for Bonewool®8020 and Bonewool®6080® continuously lead to a mass gain within the first week of immersion for both samples. This mass gain was more significant for the samples with 40 wt% ATCP because more nucleation sites were available and more ATCP was available that rose the saturation level for HA due to a release of  $\text{Ca}^{2+}$  and  $\text{PO}_4^{2-}$  ions. This finding is in agreement with other studies.<sup>52,85</sup>

A higher ATCP content appears to correlate with higher degradation rates and ATCP itself is more soluble than HA which are both effects leading to mass loss. The higher degradation was qualitatively observable by eye as the higher doped samples decomposed during immersion,

whereas pure PLGA almost did not change its appearance. In contrary, the effect of accelerated HA precipitation compared to less doped samples seems to dominate the weight change.

The significant mass loss after two weeks of the doped samples seems to correlate with the higher degradation rate of ATCP doped PLGA as observed by eye and shown by other studies.<sup>52</sup> Since the SEM images revealed a continuous HA precipitation for doped samples, ratio of inorganic content rose continuously, and XRD analysis showed strong HA reflections, the weight loss after two weeks was attributed to the method being unsuitable for those materials. It can be assumed that sample material was removed from the tubes with every change of the cell culture medium. Especially after one week, it was apparent that the doped samples decomposed significantly and the medium became bleared due to tiny floating particles. The tubes were centrifuged prior to removal of the medium but it could be that 2 min at 2500 rpm was not enough and there were still particles floating within the medium and got removed with the change of the medium. This explanation seems most probable considering that other studies have not showed such a significant weight loss. Although statistically more material was removed from the 40 wt.% doped samples since they decomposed more than the less doped samples, the weight loss was more significant for Bonewool®8020. This can be explained by the much higher precipitation rate of Bonewool®6040 that was also confirmed by SEM.

## 6. Conclusion and Outlook

In this study a method was described to investigate the degradation and the bioactivity of different bone graft materials. Dissolution and precipitation of HA were tested and correlated to physicochemical characteristics of the materials. According to the nucleation theory it became obvious that two processes affect the weight change upon immersion in cell culture medium. On the one hand, sample loss via dissolution, on the other hand, precipitation of HA that lead to a mass gain. From the comparison of the results of all materials it can be concluded that HA precipitation is favored on materials with a rough surface, high porosity and a minor content of components with a  $pK_s$  lower than HA. This effect of surface roughness, high porosity, and low solubility promoting HA precipitation can be seen in the continuous and most significant weight gain of BioOss® within the materials in granular form.

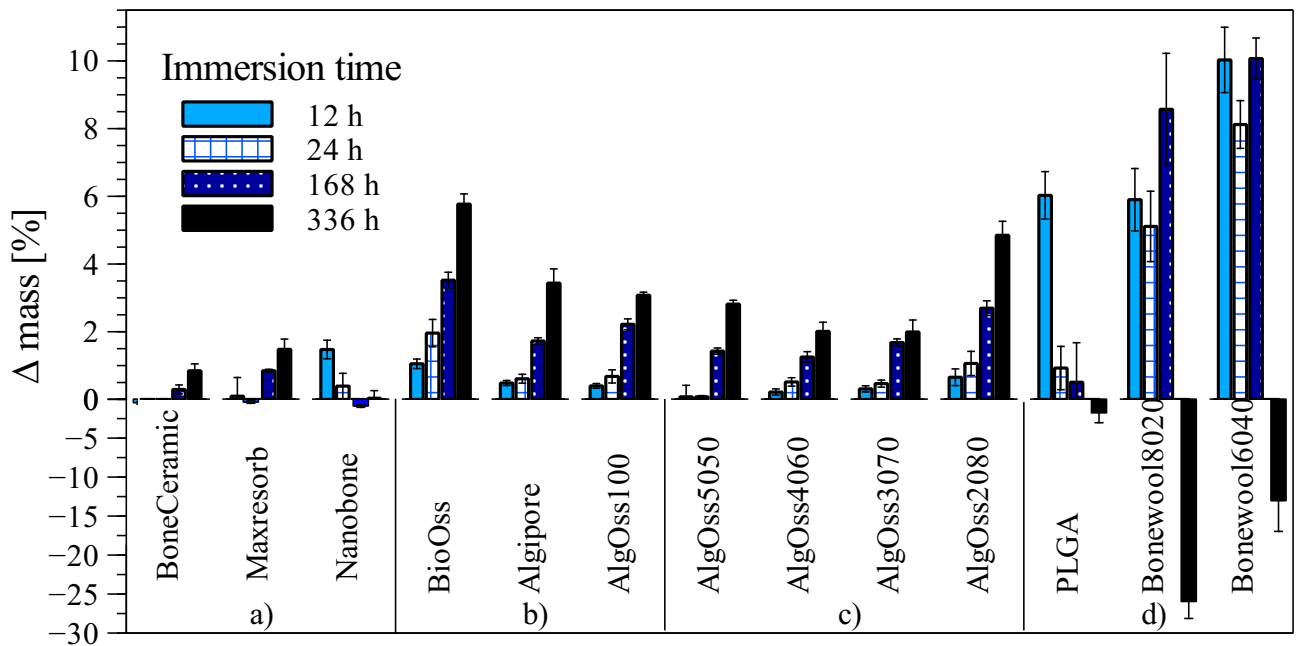


**Figure 29:** Weight changes of all investigated materials as a function of immersion time. a) Biphasic calcium phosphates with HA/ $\beta$ -TCP ratio of 60/40 wt% and Nanobone® with 76 wt% HA and 24 wt% amorphous silica. b) Single phase HA materials. c) Biphasic calcium phosphates with ratios between 50 and 80 wt%  $\beta$ -TCP. d) PLGA/ATCP composite materials and pure PLGA.

An exception is the group of composite materials that are made of compounds more soluble than HA. The dissolution effect was overcome within this group with an extremely high surface area, many nucleation sites and a fast elevation of the supersaturation level towards HA due to the fast release of  $\text{Ca}^{2+}$  and  $\text{PO}_4^{2-}$  ions from amorphous TCP. Since Bonewool®6040 was the material with the most significant HA precipitation, it seems that this is the most promising approach to accelerate HA deposition.

Other exceptions were AlgOss®3070 and AlgOss®2080 that also have a high content of phases more soluble than HA. From this observation it can be concluded that raising the supersaturation level towards HA through a fast release of  $\text{Ca}^{2+}$  and  $\text{PO}_4^{2-}$  ions, from dissolution of less stable calcium phosphates, is an important and maybe underestimated strategy to raise the HA precipitation rate and therefore bioactivity.

In general, it became clear that strategies raising the precipitation rate of HA are more important than strategies lowering the solubility.

Sintering of the materials seems to significantly hinder HA precipitation due to missing nucleation sites, lower porosity and surface area and slower release of ions. On the other hand, mechanical stability is much better for the sintered materials, which may compensate partly for the low HA precipitation rate. Those materials give immediate mechanical stability upon transplantation, which lowers the need of a fast HA precipitation rate. In contrary, the approach used for Bonewool® relies on a fast HA precipitation because the raw material does not promote much stability upon transplantation.

From the obtained results, it became clear that certain follow-up experiments should be done. For example it would have been interesting to complete the AlgOss® series with a pure  $\beta$ -TCP and a BCP with a HA/ $\beta$ -TCP ratio of 80/20 to see if the observed trends were confirmed over the whole spectrum of HA/ $\beta$ -TCP ratios. Furthermore, the experiment should be repeated for the Bonewool® series with an adapted method. For example higher volumes of medium could be used to eliminate the need for changing the medium regularly and therefore exclude sample removal. Also a different or adapted cell culture medium could be used to stabilize the pH value and lower the possibility of precipitates other than HA. Longer immersion times would have been interesting especially for BoneCeramic®, Maxresorb® and Nanobone® since it seemed like HA precipitation was just starting to dominate after 2 weeks immersion. Furthermore, it has to be mentioned that the mercury intrusion porosimeter had a problem with its high pressure station, why only a pressure range between 0.7 and 5.000 PSI (pore diameter between 300  $\mu$ m and 4.3  $\mu$ m) could be measured. Therefore, no information about microporosity, surface area and pore size distribution could be obtained. It is suggested that the measurements are repeated with a porosimeter working in the full pressure range. More accurate values for specific surface area could be obtained by nitrogen adsorption (BET).

The results obtained in this study are only a first step in the investigation of the *in vivo* performance of bone graft materials. Since only dissolution and precipitation properties were tested it was not possible to directly relate the obtained results with positive or negative *in vitro* behavior. There may be effects that favor HA precipitation and at the same time hinder positive cell response. Also, features like pore size and pore size distribution that are believed to be crucial for bone augmentation did not affect the performance in the bioactivity test and were therefore not tested. For the prediction of the *in vivo* performance, it can be suggested to perform a similar study with the addition of cell experiments. The correlations found in this study could then be compared to cellular response and reveal other important material properties for bone augmentation.

## 7. Acknowledgments

I would like to thank Prof. Dr. Dr. Jens Fischer (Division for Materials Science and Engineering of the University of Basel) for giving me the opportunity to write this thesis under his supervision. He supported me wherever he could and gave me valuable suggestions for a successful outcome.

This thesis would not have been realizable without the support of Prof. Dr. Michael de Wild wherefore I would like to acknowledge and thank him. He provided me with the analytical methods used for this thesis and was always helpful and patient when I consulted him for difficult questions. Furthermore, I would like to thank also his group at the Institute for Medical and Analytical Technologies (IMA, FHNW) for their helpfulness and a pleasant working atmosphere.

I am very thankful that Prof. Dr. Thomas Pfohl supported this master thesis as a member of the Chemistry Department of the University of Basel and therefore made collaboration between the institutes possible. With his theoretical background in thermodynamics, he was very valuable to set down the theoretical part of this thesis.

The team of the Centre for Microscopy (ZBM) at the University of Basel allowed me to use their facilities at any time which I am very thankful for. Special thanks go to Evi Bieler and Daniel Mathys for their patience and time which they invested to help me with every problem I had.

I give thanks to the companies Geistlich Pharma AG, Straumann AG, and Artoss GmbH for providing me with their respective bone graft products.

A special thank goes to Samuel Hess from the Functional Materials Lab at the ETH Zurich and to Prof. Dr. Markus Laub from the company AlgOss® Biotechnologies GmbH for providing me customized bone graft materials. The customized materials from the Bonewool® (S. Hess) and AlgOss® (Prof. Dr. M. Laub) series were a key component for this thesis.

Furthermore, I am thankful for the special support I received from my girlfriend Michelle, my flatmates Selim, and Sandro. They helped me overcome demanding phases during the process with mental support.

Finally, I would like to thank my family Acracio, Noel, and Evelin for the great support during my entire time as a student. It was invaluable to me and allowed me to pursue my passion for natural sciences.

## 8. References

1. Giannoudis, P. et al. Bone substitutes: an update. *Injury* **36S**, 20-27 (2005).
2. Murugan, R. et al. Development of nanocomposites for bone grafting. *Compos. Sci. Technol.* **65**, 2385–2406 (2005).
3. Greenwald, S. et al. Bone-Graft Substitutes: Facts, Fictions, and Applications. *JBJS* **83A** 98-103 (2001).
4. Retzepi, M. et al. Guided Bone Regeneration: Biological principle and therapeutic applications. *Clin. Oral Implants Res.* **21**, 567–576 (2010).
5. Calori, G. M. et al. The use of bone-graft substitutes in large bone defects: Any specific needs? *Injury* **42**, 56–63 (2011).
6. Scarano, A. et al. Maxillary sinus augmentation with different biomaterials: a comparative histologic and histomorphometric study in man. *Implant Dent.* **15**, 197–207 (2006).
7. Orsini, G. et al. Maxillary sinus augmentation with Bio-Oss particles: a light, scanning, and transmission electron microscopy study in man. *J. Biomed. Mater. Res. B. Appl. Biomater.* **74**, 448–457 (2005).
8. Velich, N. et al. Long-term results with different bone substitutes used for sinus floor elevation. *J. Craniofac. Surg.* **15**, 38–41 (2004).
9. Moy, P. K. et al. Maxillary sinus augmentation: histomorphometric analysis of graft materials for maxillary sinus floor augmentation. *J. Oral Maxillofac. Surg.* **51**, 857–862 (1993).
10. Habibovic, P. et al. Comparative *in vivo* study of six hydroxyapatite-based bone graft substitutes. *J. Orthop. Res.* **26**, 1363–1370 (2008).
11. Iezzi, G. et al. Comparative histological results of different biomaterials used in sinus augmentation procedures: A human study at 6 months. *Clin. Oral Implants Res.* **23**, 1369–1376 (2012).
12. Zhou, H. & Lee, J. Nanoscale hydroxyapatite particles for bone tissue engineering. *Acta Biomater.* **7**, 2769–2781 (2011).
13. Dorozhkin, S. V & Epple, M. Biological and medical significance of calcium phosphates. *Angew. Chem. Int. Ed. Engl.* **41**, 3130–3146 (2002).
14. Dorozhkin, S. V. Biocomposites and hybrid biomaterials based on calcium orthophosphates. *Biomatter* **1**, 3–56 (2011).
15. Dorozhkin, S. V. Biological and Medical Significance of Nanodimensional and Nanocrystalline Calcium Orthophosphates. *Biomed. Mater. Diagnostic Devices* **2**, 19–99 (2012).
16. Rogel, M. et al. The role of nanocomposites in bone regeneration. *J. Mater. Chem.* **18**, 4233–4241 (2008).
17. Yaszemski, M. J. et al. Evolution of bone transplantation: Molecular, cellular and tissue strategies to engineer human bone. *Biomaterials* **17**, 175–185 (1996).
18. Franceschi, R. T. et al. Biological Approaches to Bone Regeneration by Gene Therapy. *J. Dent. Res.* **12**, 1093–1103 (2005).
19. LeGeros, R. Z. Calcium phosphate-based osteoinductive materials. *Chem. Rev.* **108**, 4742–4753 (2008).
20. <http://myeclinic.com/wp-content/uploads/2014/10/BoneHealing.jpg> (12.16.2015)
21. Cypher, T. J. & Grossman, J. P. Biological principles of bone graft healing. *J. Foot Ankle Surg.* **35**, 413–417 (1996).
22. Hing, K. A. Bone repair in the twenty-first century: biology, chemistry or engineering? *Philos. Trans. A. Math. Phys. Eng. Sci.* **362**, 2821–2850 (2004).
23. Carano, R. a D. & Filvaroff, E. H. Angiogenesis and bone repair. *Drug Discov. Today* **8**, 980–989 (2003).
24. Schindeler, A. et al. Bone remodeling during fracture repair: The cellular picture. *Semin. Cell Dev. Biol.* **19**, 459–466 (2008).
25. Bauer, T. W. et al. Bone Graft Materials: An Overview of the Basic Science. *Clin. Orth. Rel. Res.* **371**, 10-27 (2000)
26. Clayton, P. R. Bone Repair Techniques, Bone Graft, and Bone Graft Substitutes. *Clin. Orth. Rel. Res.* **360**, 71-86 (1999)
27. Frost, H. M. The biology of Fracture Healing: An Overview for Clinicians. Part 1. *Clin. Orth. Rel. Res.* **248**, (1989)
28. Finkemeier, C. G. Bone-Grafting and Bone-Graft Substitutes. *J. Bone Jt. Surg.* **84**, 454–464 (2002).
29. Moore, W. R. et al. Synthetic bone graft substitutes. *Anz. J. Surg.* **71**, 354–361 (2001).
30. Dorozhkin, S. V. Calcium orthophosphate-based bioceramics. *Materials* **6**, 3840–3942 (2013).
31. Hing, K. A. Bioceramic bone graft substitutes: Influence of porosity and chemistry. *Int. J. Appl. Ceram. Technol.* **2**, 184–199 (2005).
32. Kübler, A. et al. Growth and Proliferation of Human Osteoblasts on Different Bone Graft Substitutes An *In Vitro* Study. *Implant Dent.* **13**, 171–179 (2004).
33. Samavedi, S. et al. Calcium phosphate ceramics in bone tissue engineering: A review of properties and their influence on cell behavior. *Acta Biomater.* **9**, 8037–8045 (2013).

34. Dorozhkin, S. V. Calcium orthophosphates in dentistry. *J. Mater. Sci. Mater. Med.* **24**, 1335-1363 (2013).
35. LeGeros, R. Z. Biodegradation and Bioresorption of Calcium Phosphate Ceramics. *Clin. Mat.* **14**, 65-88 (1993).
36. Brunner, T. J. et al. Effect of particle size, crystal phase and crystallinity on the reactivity of tricalcium phosphate cements for bone reconstruction. *J. Mater. Chem.* **17**, 4072-4078 (2007).
37. Como, A. M. & Enxerto, M. D. E. Commercial Hydroxyapatites for Medical- Dental Applications as Bone Graft. *J. Appl. Oral Sci.* **13**, 136-140 (2005).
38. Bohner, M. & Lemaître, J. Can bioactivity be tested *in vitro* with SBF solution? *Biomaterials* **30**, 2175-2179 (2009).
39. Kokubo, T. & Takadama, H. How useful is SBF in predicting *in vivo* bone bioactivity? *Biomaterials* **27**, 2907-2915 (2006).
40. Kawashita, M. et al. Apatite-forming ability of carboxyl group-containing polymer gels in a simulated body fluid. *Biomaterials* **24**, 2477-2484 (2003).
41. Yaszemski, M. J. et al. Evolution of bone transplantation: molecular, cellular and tissue strategies to engineer human bone. *Biomaterials* **17**, 175-185 (1996).
42. Tadic, D. A thorough physicochemical characterisation of 14 calcium phosphate-based bone substitution materials in comparison to natural bone. *Biomaterials* **25**, 987-994 (2004).
43. Bhatt, R. Bone Graft Substitutes. *Hand Clinics* **28**, 457-468 (2012).
44. Roberts, T. T. & Rosenbaum, A. J. Bone grafts, bone substitutes and orthobiologics: the bridge between basic science and clinical advancements in fracture healing. *Organogenesis* **8**, 114-124 (2012).
45. Balsly, C. R. et al. Effect of low dose and moderate dose gamma irradiation on the mechanical properties of bone and soft tissue allografts. *Cell Tissue Bank.* **9**, 289-298 (2008).
46. Vastel, L. et al. Effect of different sterilization processing methods on the mechanical properties of human cancellous bone allografts. *Biomaterials* **25**, 2105-2110 (2004).
47. Figueiredo, M. et al. Physicochemical characterization of biomaterials commonly used in dentistry as bone substitutes--comparison with human bone. *J. Biomed. Mater. Res. B. Appl. Biomater.* **92**, 409-19 (2010).
48. Ogunsalu, C. Bone Substitutes and Validation. *Impl. Dent.* 29-72 (2011)
49. Daculsi, G. et al. Current state of the art of biphasic calcium phosphate bioceramics. *J. Mat. Sci. Med.* **14**, 195-200 (1975).
50. Kalita, S. J. et al. Nanocrystalline calcium phosphate ceramics in biomedical engineering. *Mater. Sci. Eng.* **27**, 441-449 (2007).
51. Gaasbeek, R. D. et al. Mechanism of bone incorporation of  $\beta$ -TCP bone substitute in open wedge tibial osteotomy in patients. *Biomaterials* **26**, 6713-6719 (2005).
52. Loher, S. et al. Improved degradation and bioactivity of amorphous aerosol derived tricalcium phosphate nanoparticles in poly(lactide-co-glycolide). *Nanotechnology* **17**, 2054-2061 (2006).
53. Samavedi, S. et al. Calcium phosphate ceramics in bone tissue engineering: a review of properties and their influence on cell behavior. *Acta Biomater.* **9**, 8037-8045 (2013).
54. Hing, K. A. et al. Comparative performance of three ceramic bone graft substitutes. *Spine J.* **7**, 475-90 (2007).
55. Rich, J. et al. *In vitro* evaluation of poly( $\epsilon$ -caprolactone-co-DL-lactide)/bioactive glass composites. *Biomaterials* **23**, 2143-2150 (2002).
56. Armentano, I. et al. Biodegradable polymer matrix nanocomposites for tissue engineering: A review. *Polym. Degrad. Stab.* **95**, 2126-2146 (2010).
57. Rezwan, K. et al. Biodegradable and bioactive porous polymer/inorganic composite scaffolds for bone tissue engineering. *Biomaterials* **27**, 3413-31 (2006).
58. Schneider, O. D. et al. Flexible, silver containing nanocomposites for the repair of bone defects: antimicrobial effect against E. coli infection and comparison to tetracycline containing scaffolds. *J. Mater. Chem.* **18**, 2679 (2008).
59. Bigi, A. et al. Bonelike apatite growth on hydroxyapatite-gelatin sponges from simulated body fluid. *J. Biomed. Mater. Res.* **59**, 709-715 (2002).
60. Monteiro, M. et al. Dissolution properties of calcium phosphate granules with different compositions in simulated body fluid. *J. Biomed. Mater. Res.* **65**, 299-305 (2003).
61. Shchukarev, A. et al. To Build or Not to Build : The Interface of Bone Graft Substitute Materials in Biological Media from the View Point of the Cells. *Biomater. Sci. Eng.* 287-308 (1993).
62. Lu, X. & Leng, Y. Theoretical analysis of calcium phosphate precipitation in simulated body fluid. *Biomaterials* **26**, 1097-1108 (2005).
63. Oyane, A. et al. Preparation and assessment of revised simulated body fluids. *J. Biomed. Mater. Res. A* **65**, 188-95 (2003).
64. Lee, J. T. Y. et al. Cell culture medium as an

- alternative to conventional simulated body fluid. *Acta Biomater.* **7**, 2615–2622 (2011).
65. Mortimer, C. E. & Müller, M. (2005). *Chemistry*. Belmont, California: Wadsworth Publishing. ISBN: 978-3-13-484309-5.
66. Fernández, E. et al. Calcium phosphate bone cements for clinical applications. Part II: Precipitate formation during setting reactions. *J. Mater. Sci. Mater. Med.* **10**, 177–183 (1999).
67. Bell, L. C. et al. Synthetic hydroxyapatite-solubility product and stoichiometry of dissolution. *Arch. Oral Biol.* **23**, 329–336 (1978).
68. Dorozhkin, S. V. Dissolution mechanism of calcium apatites in acids: A review of literature. *World J. Methodol.* **2**, 1 (2012).
69. Dorozhkin, S. V. Calcium orthophosphates: occurrence, properties, biomineralization, pathological calcification and biomimetic applications. *Biomater* **1**, 121–164 (2011).
70. Ben-Nissan, B. (2014). *Advances in Calcium Phosphate Biomaterials*. Springer Heidelberg. DOI 10.1007/978-3-642-53980-0.
71. Handschel, J. et al. A histomorphometric meta-analysis of sinus elevation with various grafting materials. *Head Face Med.* **5**, 12 (2009).
72. Schneider, O. D. et al. *In vivo* and *in vitro* evaluation of flexible, cottonwool-like nanocomposites as bone substitute material for complex defects. *Acta Biomater.* **5**, 1775–1784 (2009)
73. Jensen, T. et al. Maxillary sinus floor augmentation with Bio-Oss or Bio-Oss mixed with autogenous bone as graft: a systematic review. *Clin. oral impl. res.* **23**, 263–273 (2012)
74. Mladenovic, Z. *In vitro* study of the biological interface of Bio-Oss: implications of the experimental setup. *Clin. oral impl. res.* **24**, 329–335 (2013)
75. [http://www.straumann.ch/content/dam/internet/straumann\\_ch/resources/brochurecatalogue/brochures/de/portfolio\\_DE\\_140819\\_LOW.pdf](http://www.straumann.ch/content/dam/internet/straumann_ch/resources/brochurecatalogue/brochures/de/portfolio_DE_140819_LOW.pdf) (12.16.2015)
76. [http://www.straumann.ch/content/internet/straumann\\_ch/de/professionals/products-and-solutions/regenerative-solutions-incl-botiss/bone-substitutes/synthetic-bone-substitutes/Maxresorb\\*\\_jcr\\_content/subnav/downloadlist\\_93fe/linklist/Maxresorb\\*\\_file.res/Maxresorb\\*\\_DE\\_140815\\_LOW.pdf](http://www.straumann.ch/content/internet/straumann_ch/de/professionals/products-and-solutions/regenerative-solutions-incl-botiss/bone-substitutes/synthetic-bone-substitutes/Maxresorb*_jcr_content/subnav/downloadlist_93fe/linklist/Maxresorb*_file.res/Maxresorb*_DE_140815_LOW.pdf) (12.16.2015)
77. Dietze, S. The ultrastructural and processing properties of Straumann Bone Ceramic and Nanobone®. *Folia Morphol.* **65**, 63–65 (2006)
78. [http://www.artoss.com/fileadmin/pdf/download/Nanobone\\*\\_bibliografie.pdf](http://www.artoss.com/fileadmin/pdf/download/Nanobone*_bibliografie.pdf) (12.16.2015)
79. Loher, S. et al. Fluoro-apatite and Calcium Phosphate Nanoparticles by Flame Synthesis. *Chem Mater.* **17**, 725–731 (2005).
80. LeGeros, R. Z. Calcium phosphate-based osteoinductiv materials. *Chem. Rev.* **108**, 4742–4753 (2008).
81. Shchukarev, A. et al. Surface characterization of bone graft substitute materials conditioned in cell culture medium. 2. Protein adsorption. *Surf. Interface Anal.* **44**, 919–923 (2012).
82. Shchukarev, A. et al. To Build or Not to Build : The Interface of Bone Graft Substitute Materials in Biological Media from the View Point of the Cells. *Biomater. Sci. Eng.* 289–318 1993).
83. Nathanael, A. J. et al. Influence of fluorine substitution on the morphology and structure of hydroxyapatite nanocrystals prepared by hydrothermal method. *Mater. Chem. Phys.* **137**, 967–976 (2013).
84. Enderle, R. et al. Influence of magnesium doping on the phase transformation temperature of beta-TCP ceramics examined by Rietveld refinement. *Biomaterials* **26**, 3379–3384 (2005).
85. Marchi, J. et al. Influence of Mg-substitution on the physicochemical properties of calcium phosphate powders. *Mater. Res. Bull.* **42**, 1040–1050 (2007).
86. Schneider, O. D. et al. Cotton wool-like nanocomposite biomaterials prepared by electrospinning: *in vitro* bioactivity and osteogenic differentiation of human mesenchymal stem cells. *J. Biomed. Mater. Res. B. Appl. Biomater.* **84**, 350–62 (2008).
87. Meyerson, A. S. *Concluding Remarks*. *Roy. Soc. Chem.* **179**, 543–547 (2015)
88. Okazaki, M. Solubility Behavior of CO<sub>3</sub> Apatites in Relation to Crystallinity. *Car. Res.* **15** (1981)
89. Carrodeguas, R. G. α-Tricalcium phosphate: Synthesis, properties and biomedical applications. *Acta Biomater.* **7**, 3536–3546 (2011).

## 9. Appendix

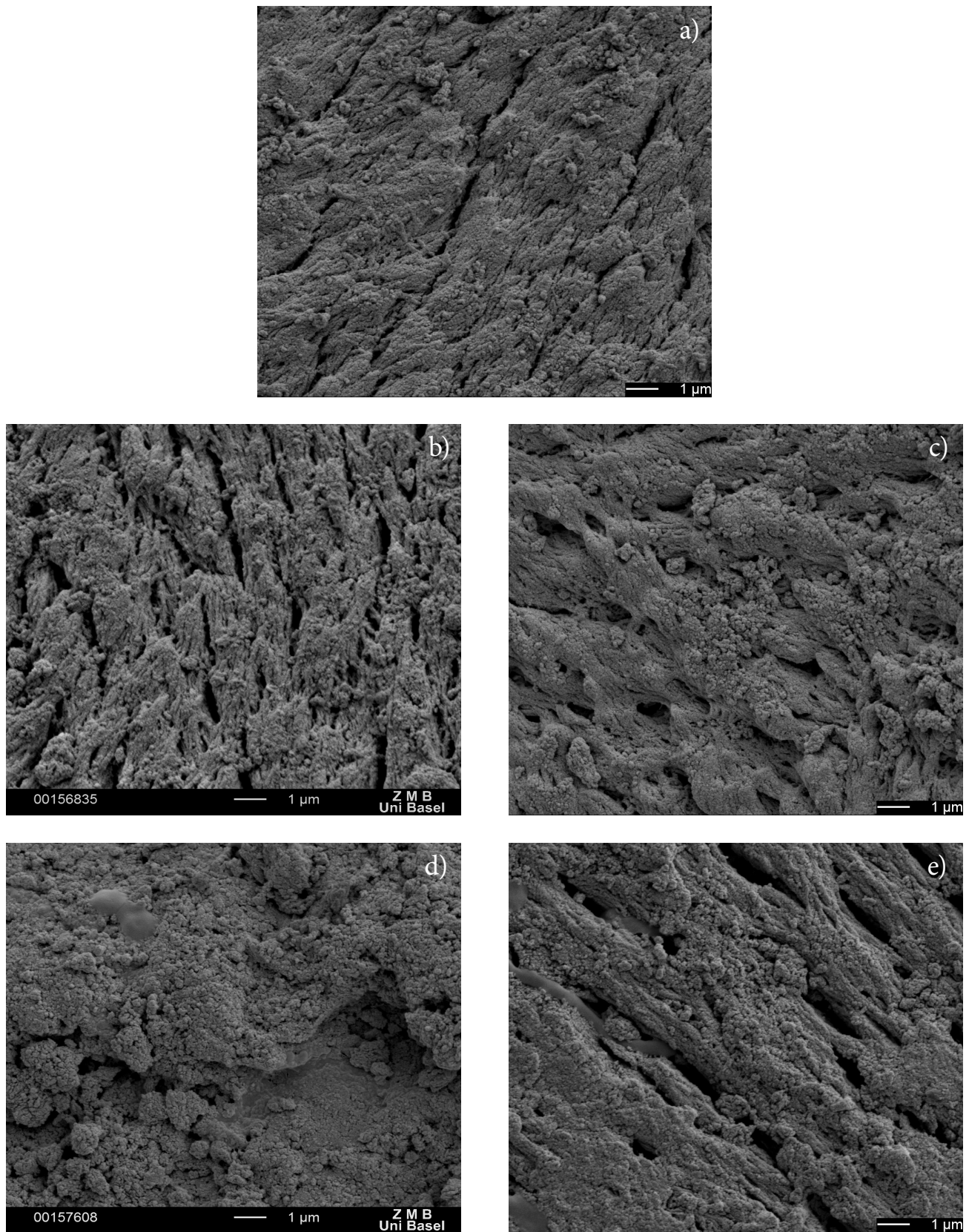


**Figure 30:** SEM images of BioOss® after different immersion times. a) raw material. b) 12 h immersion. c) 24 h immersion. d) 168 h immersion. e) 336 h immersion

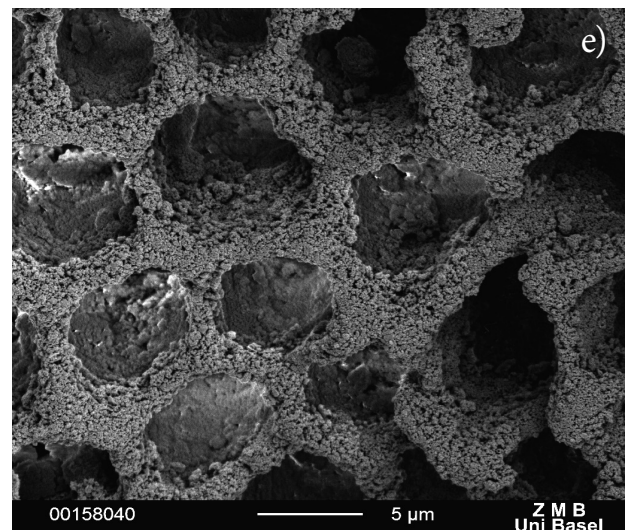
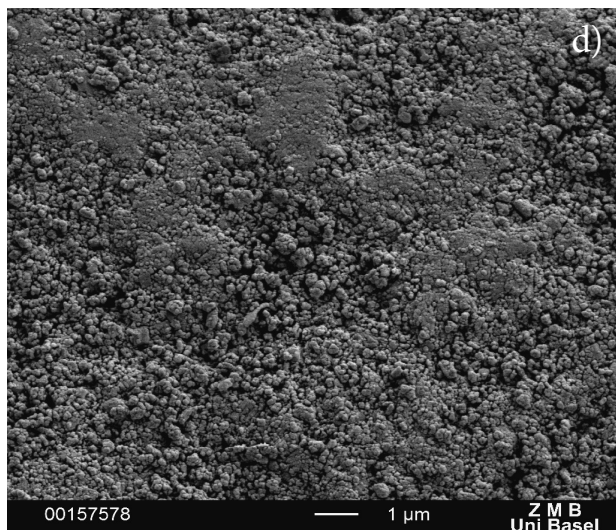
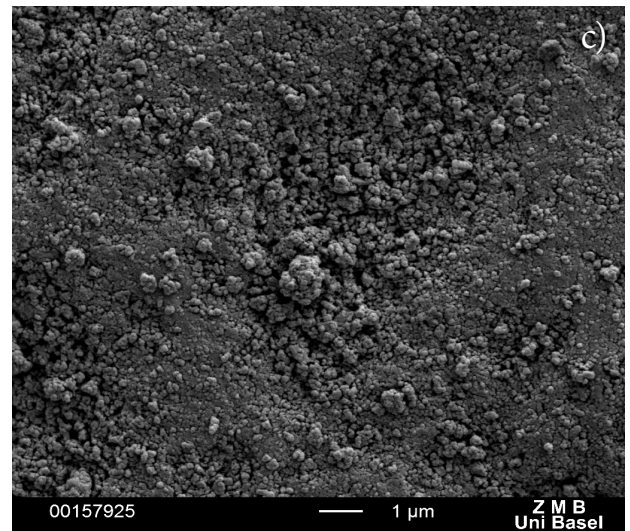
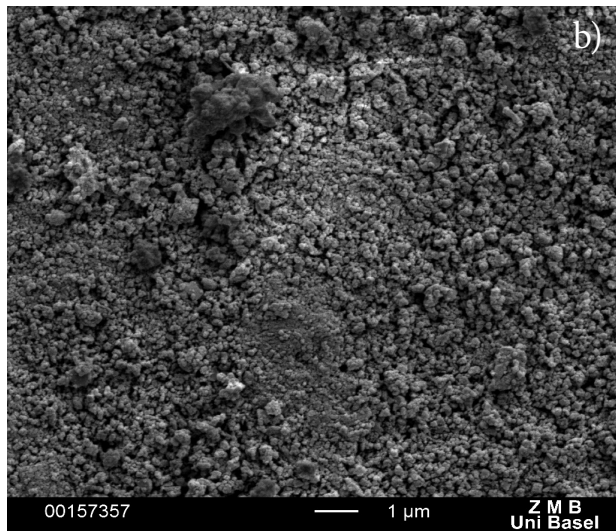
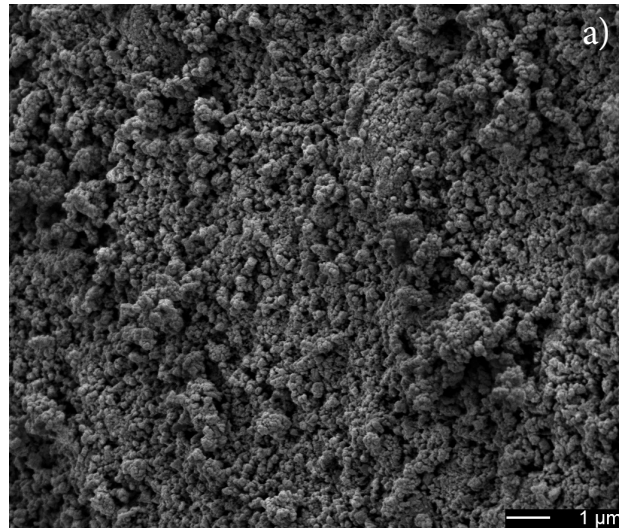


**Figure 31:** SEM images of Algipore® after different immersion times. a) raw material. b) 12 h immersion. c) 24 h immersion. d) 168 h immersion. e) 336 h immersion

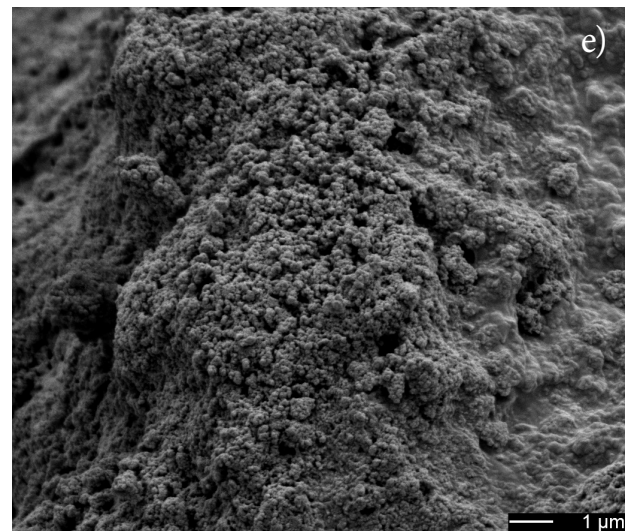
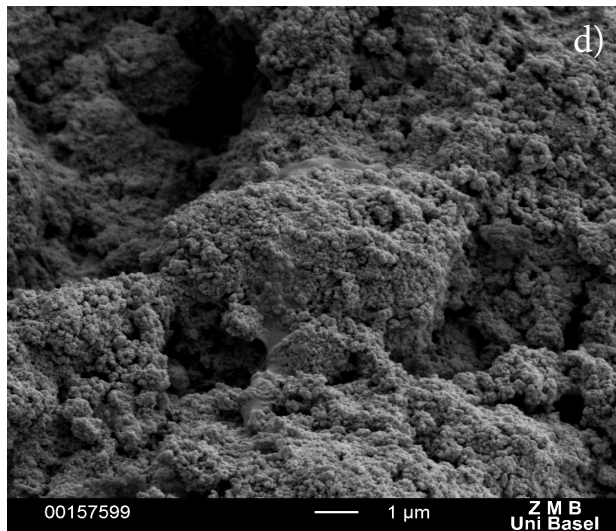
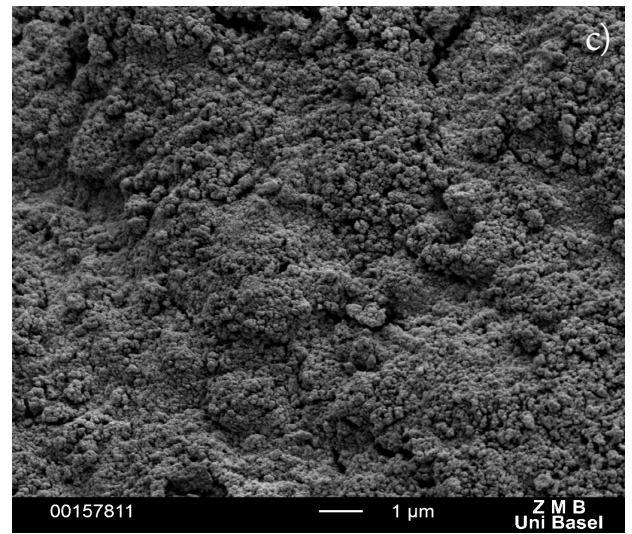
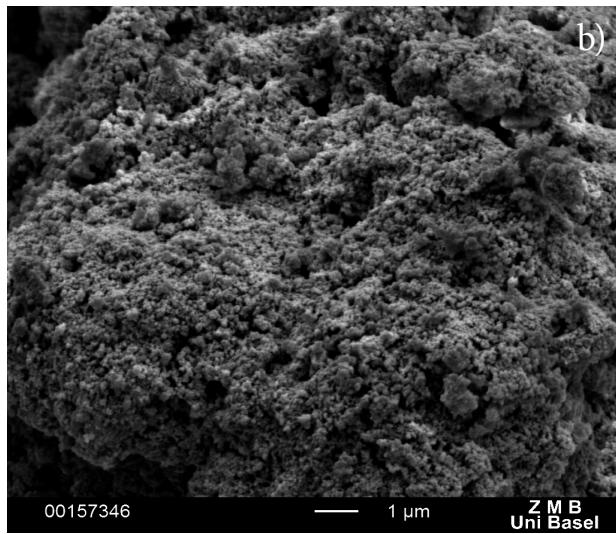
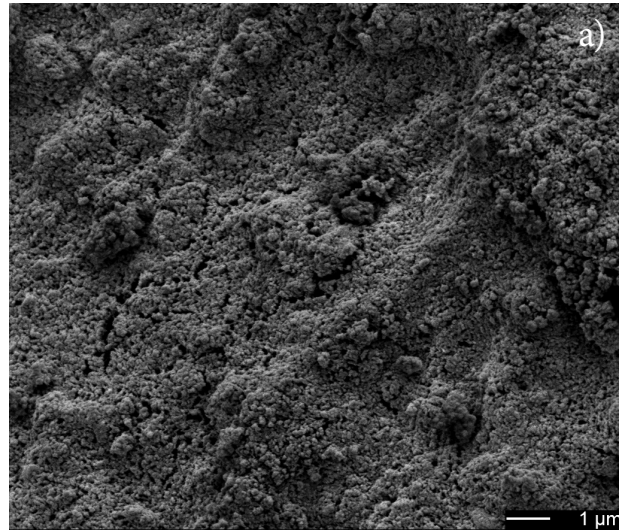


**Figure 32:** SEM images of Nanobone® after different immersion times. a) raw material. b) 12 h immersion. c) 24 h immersion. d) 168 h immersion. e) 336 h immersion

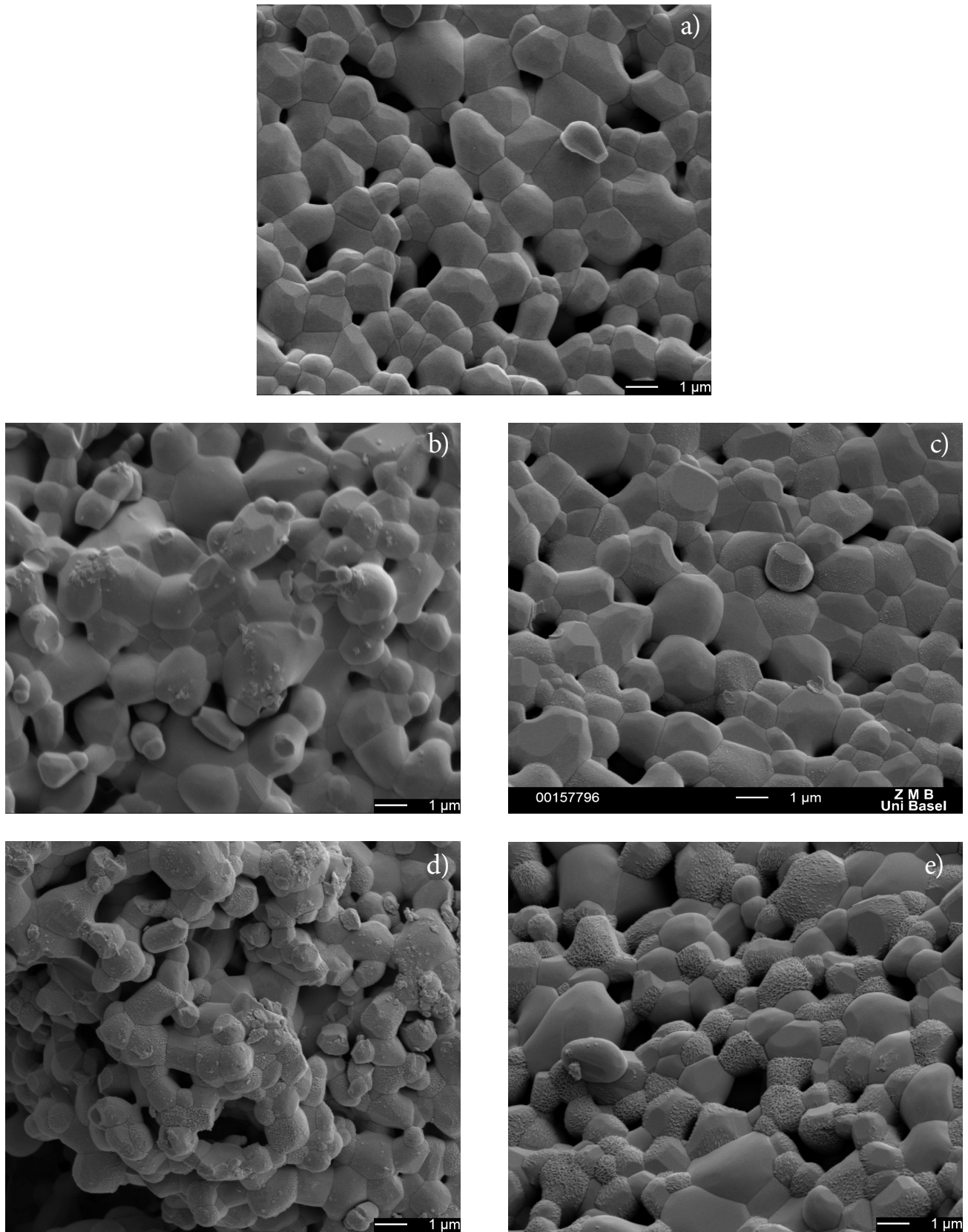


**Figure 33:** SEM images of Maxresorb® after different immersion times. a) raw material. b) 12 h immersion. c) 24 h immersion. d) 168 h immersion. e) 336 h immersion

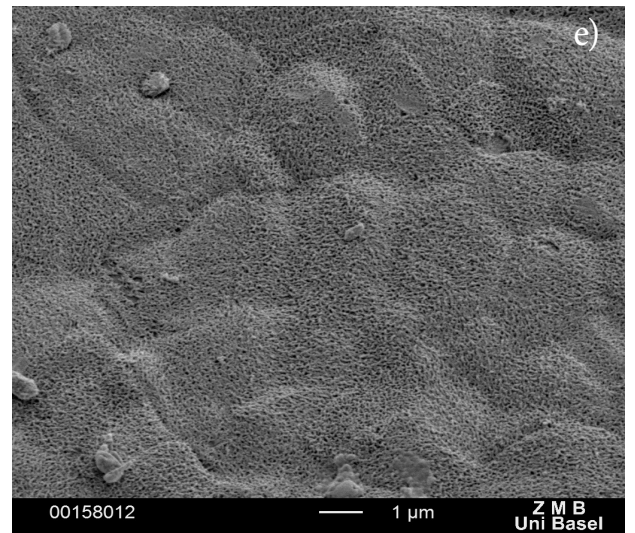
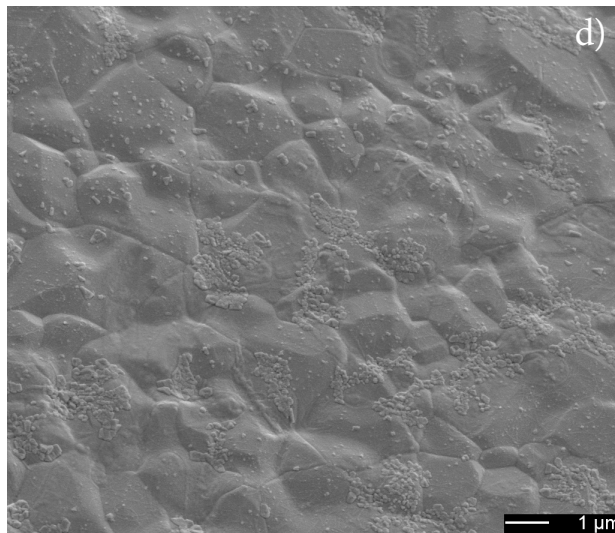
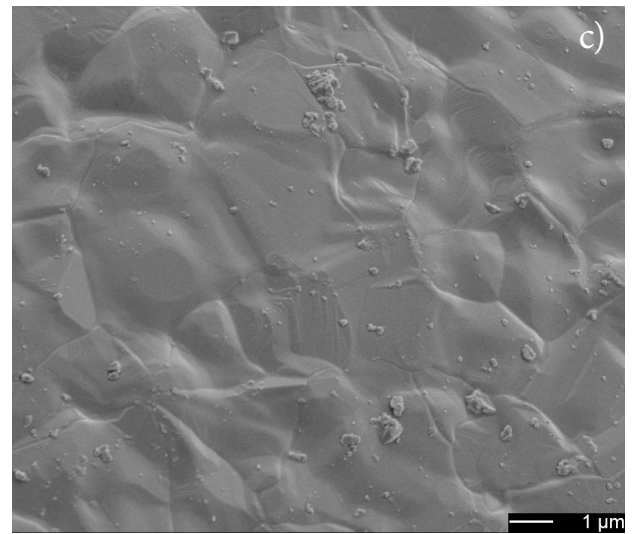
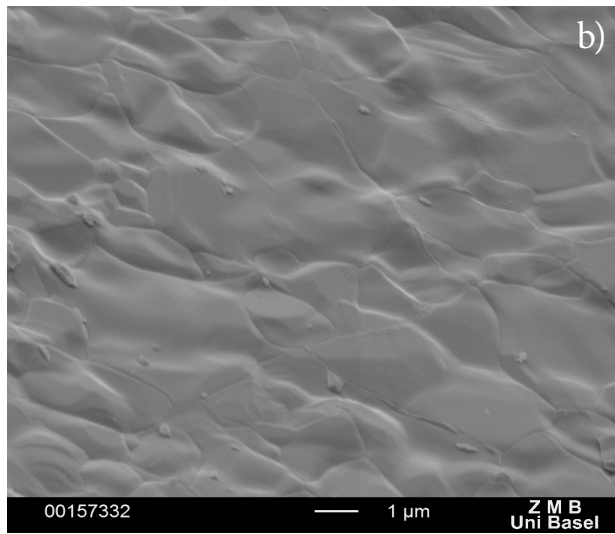
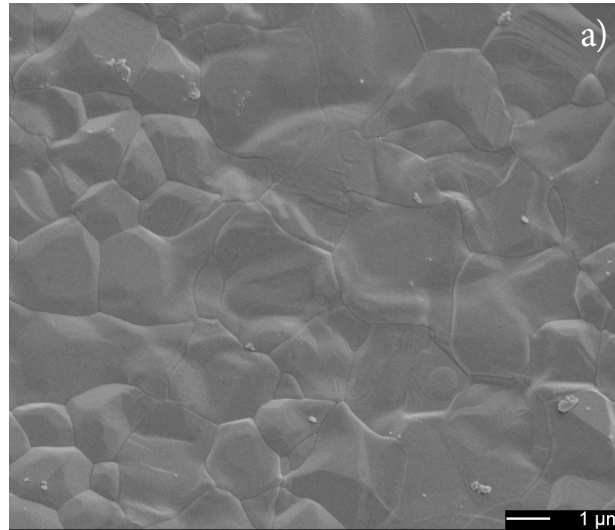


**Figure 34:** SEM images of BoneCeramic® after different immersion times. a) raw material. b) 12 h immersion. c) 24 h immersion. d) 168 h immersion. e) 336 h immersion

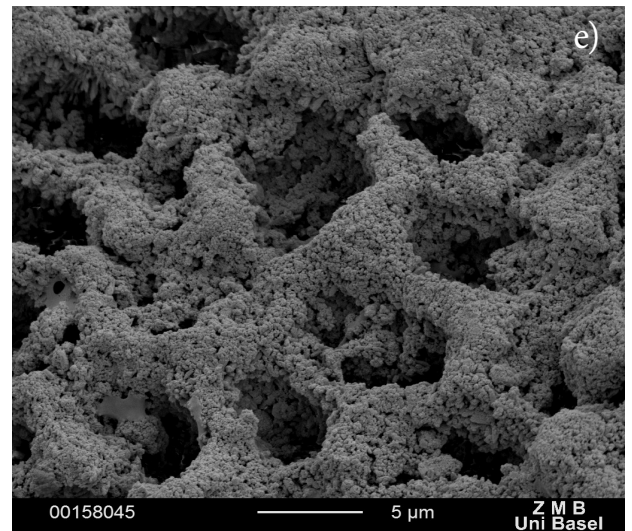
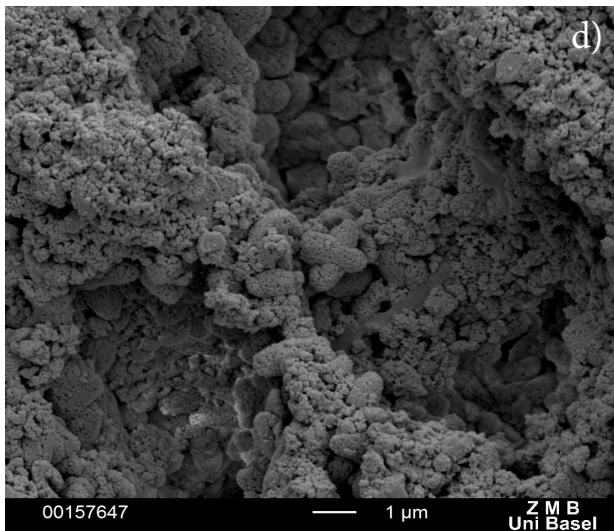
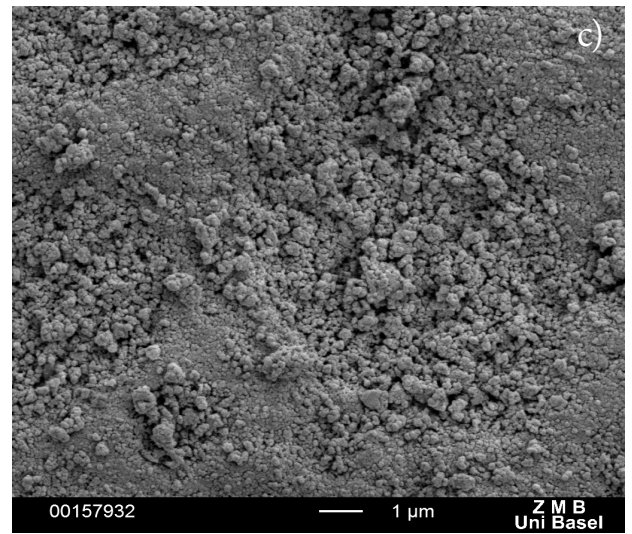
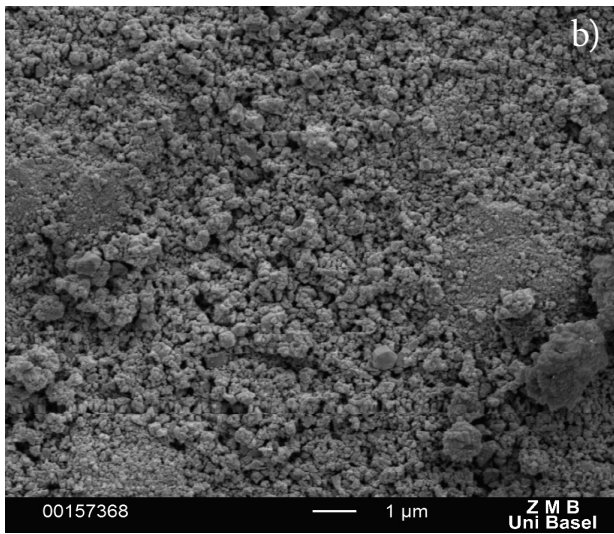
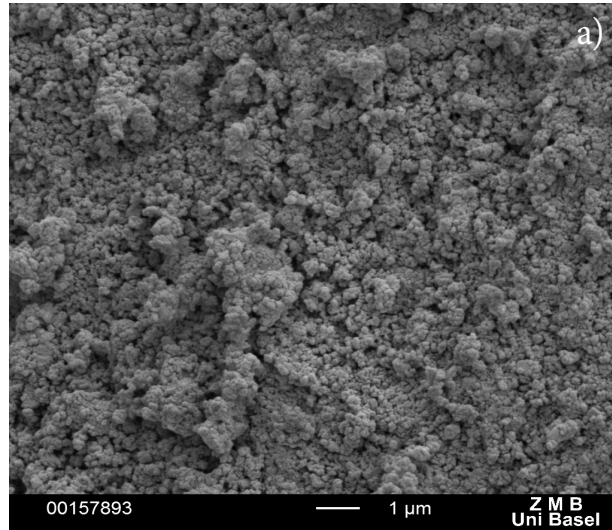


**Figure 35:** SEM images of AlgOss\*100 after different immersion times. a) raw material. b) 12 h immersion. c) 24 h immersion. d) 168 h immersion. e) 336 h immersion

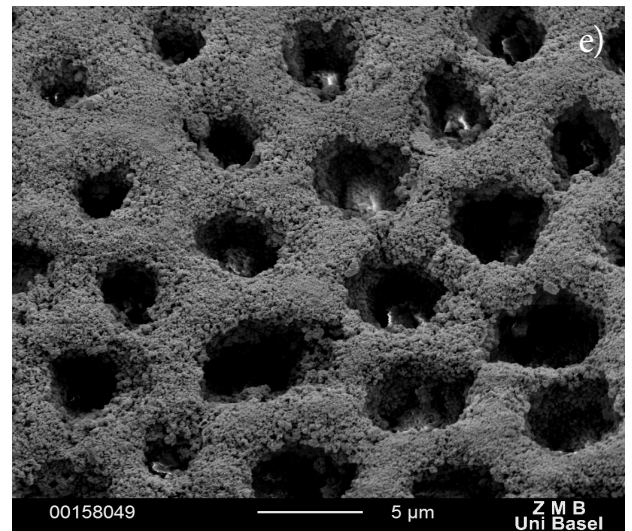
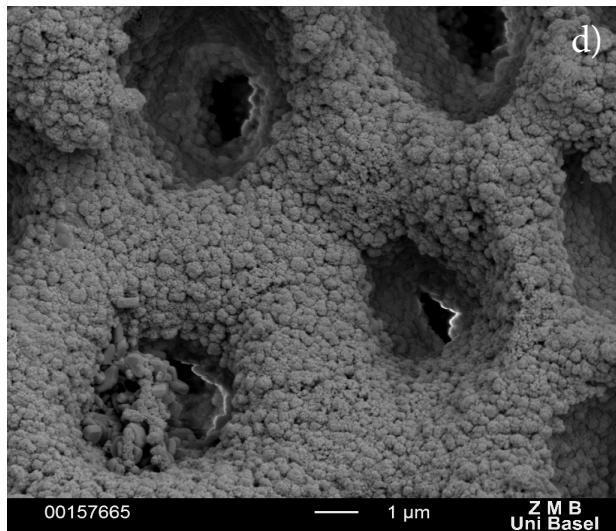
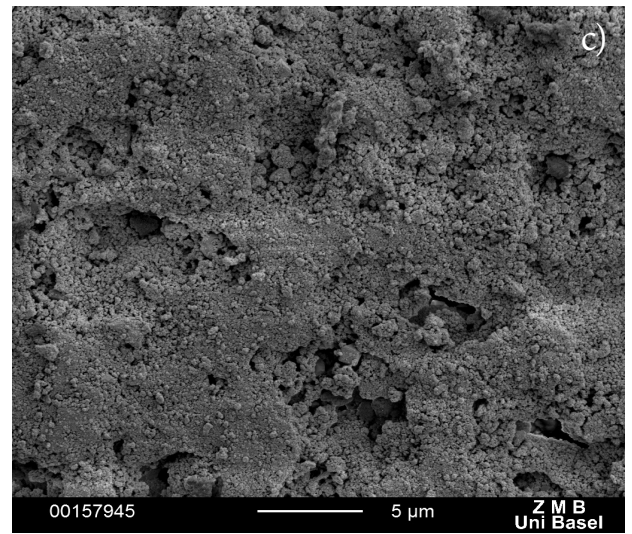
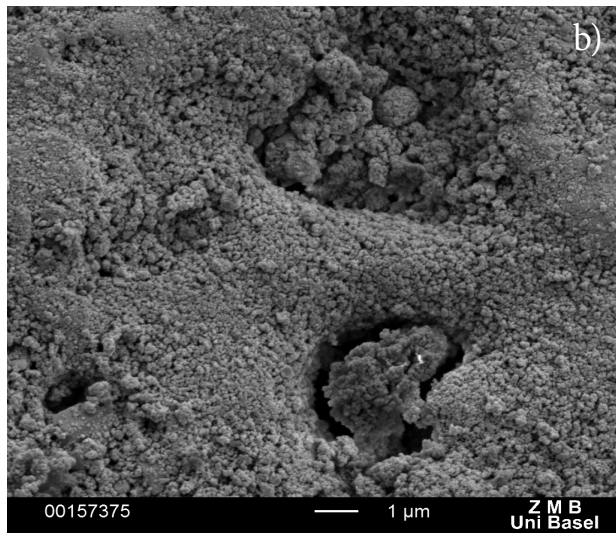
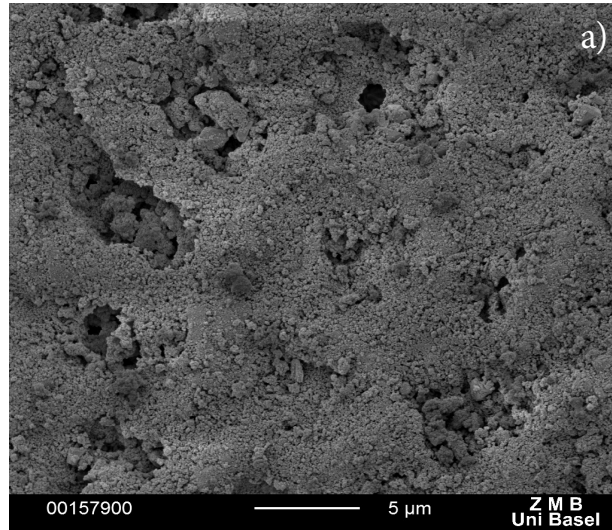


**Figure 36:** SEM images of AlgOss\*5050 after different immersion times. a) raw material. b) 12 h immersion. c) 24 h immersion. d) 168 h immersion. e) 336 h immersion

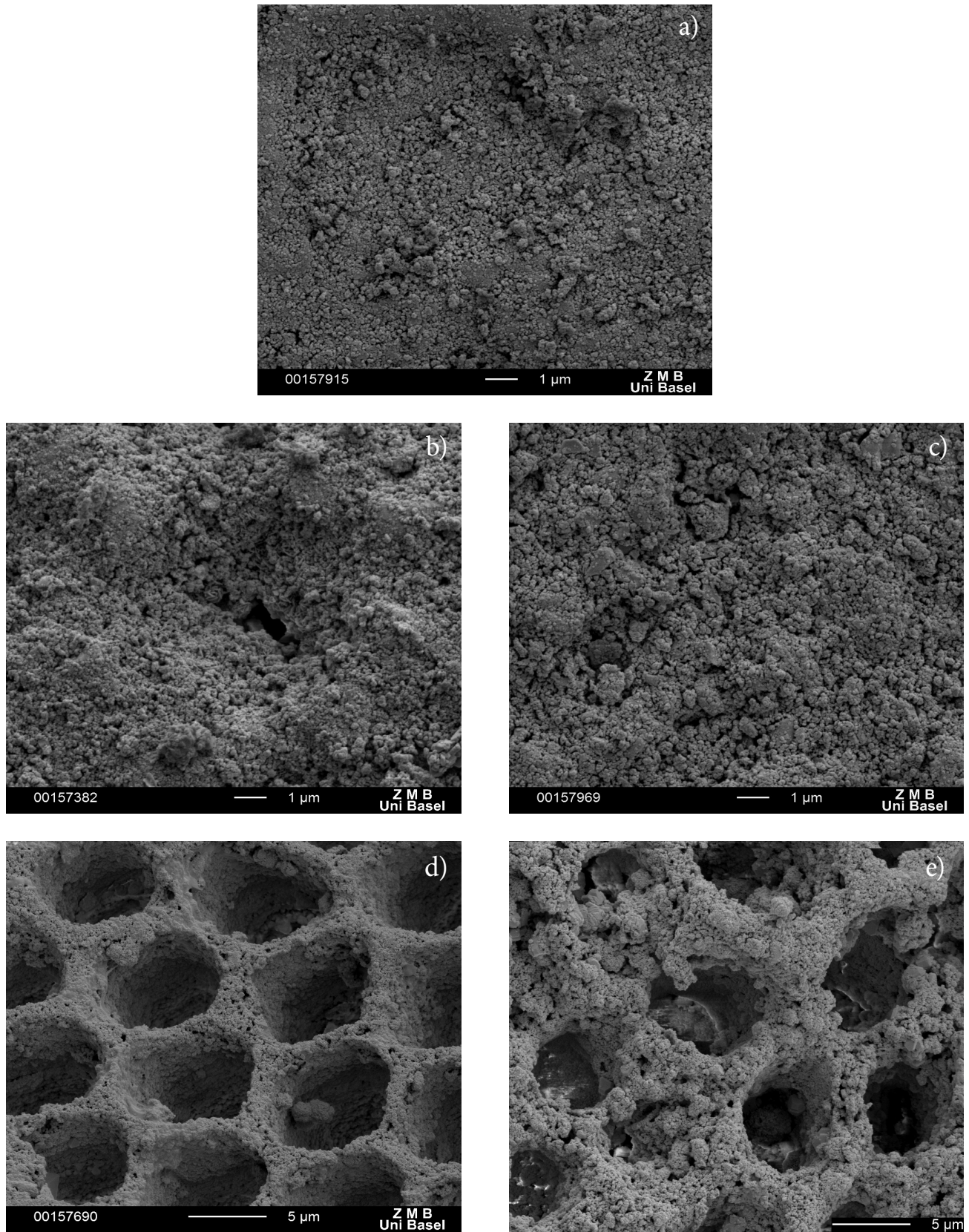


**Figure 37:** SEM images of AlgOss\*4060 after different immersion times. a) raw material. b) 12 h immersion. c) 24 h immersion. d) 168 h immersion. e) 336 h immersion

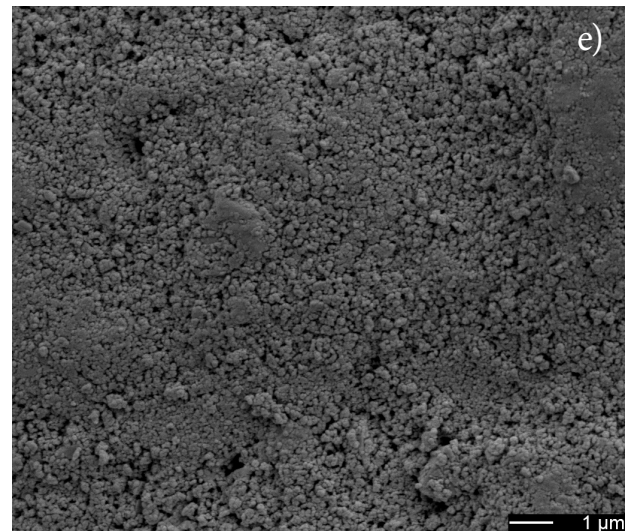
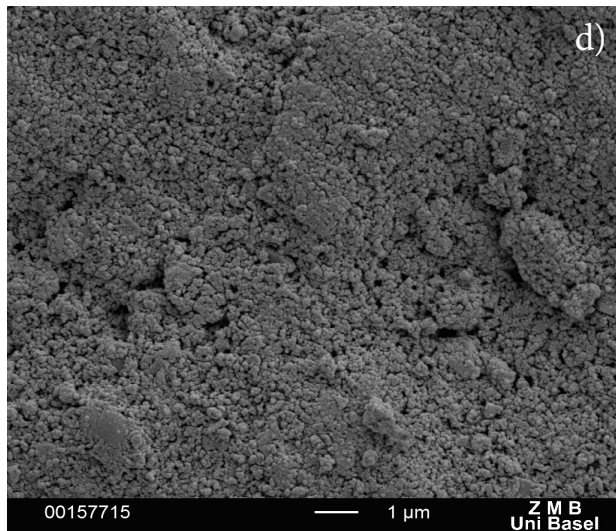
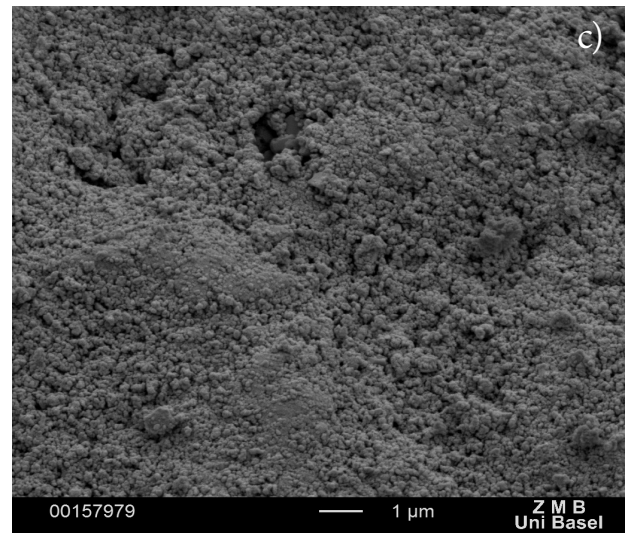
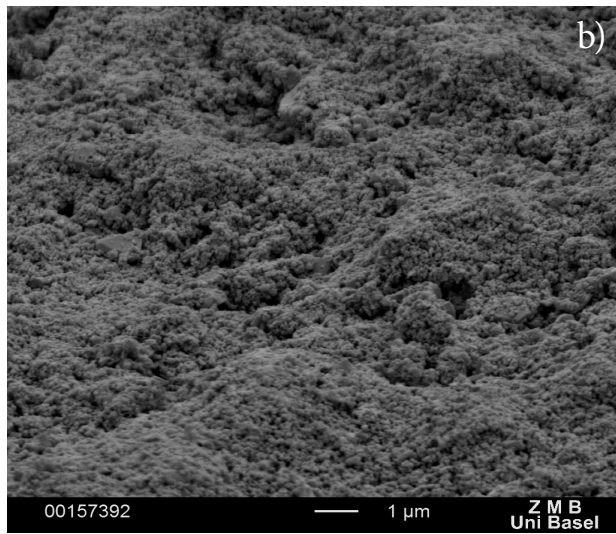
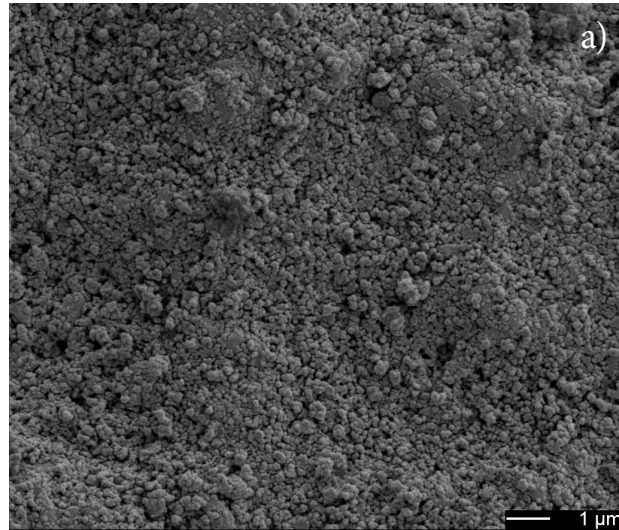


**Figure 38:** SEM images of AlgOss\*3070 after different immersion times. a) raw material. b) 12 h immersion. c) 24 h immersion. d) 168 h immersion. e) 336 h immersion

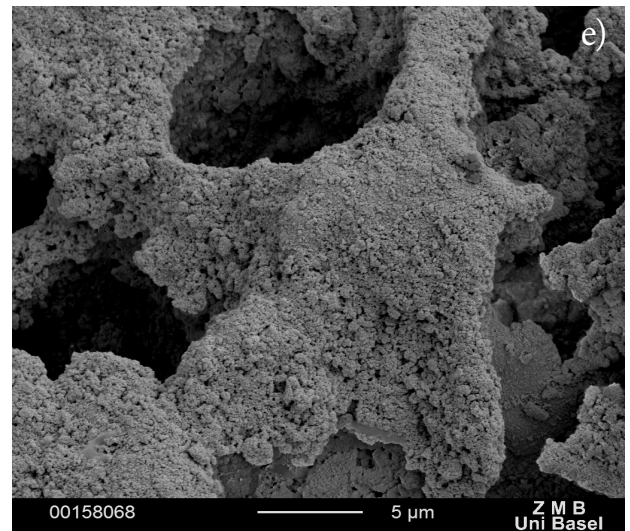
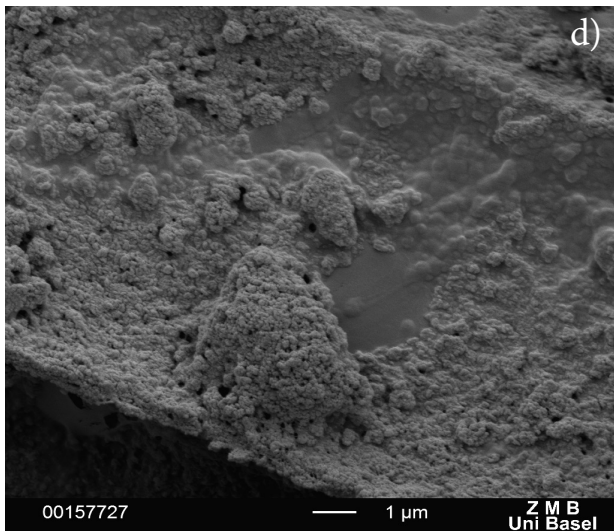
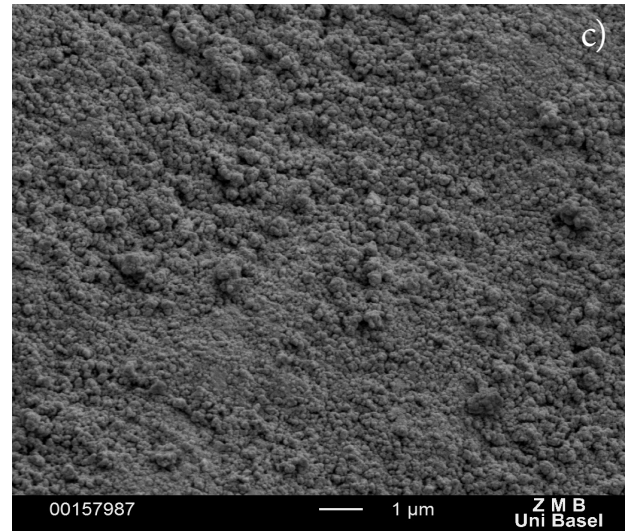
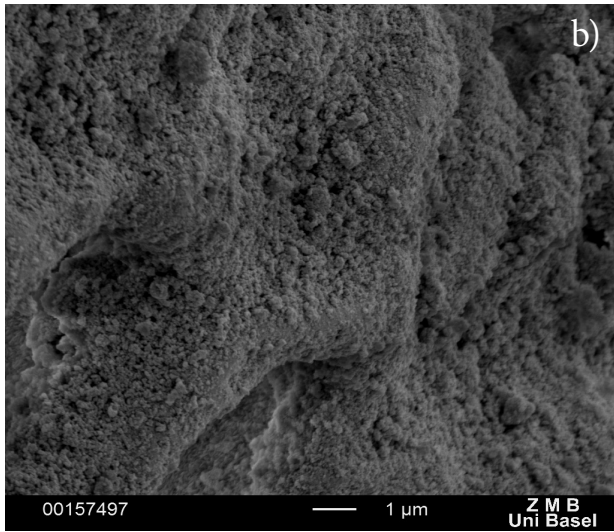
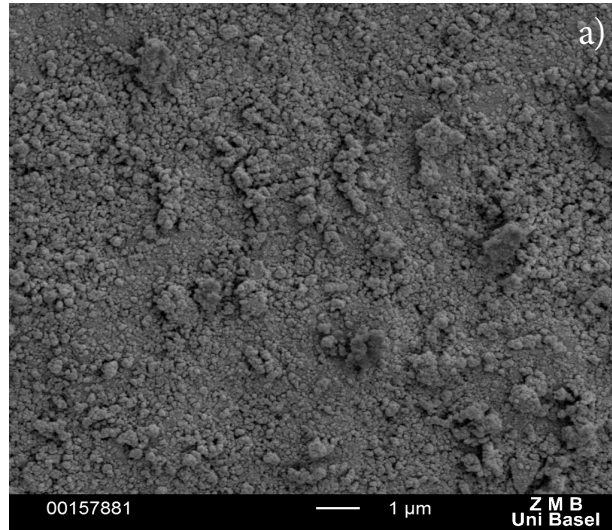


**Figure 39:** SEM images of AlgOss®2080 after different immersion times. a) raw material. b) 12 h immersion. c) 24 h immersion. d) 168 h immersion. e) 336 h immersion

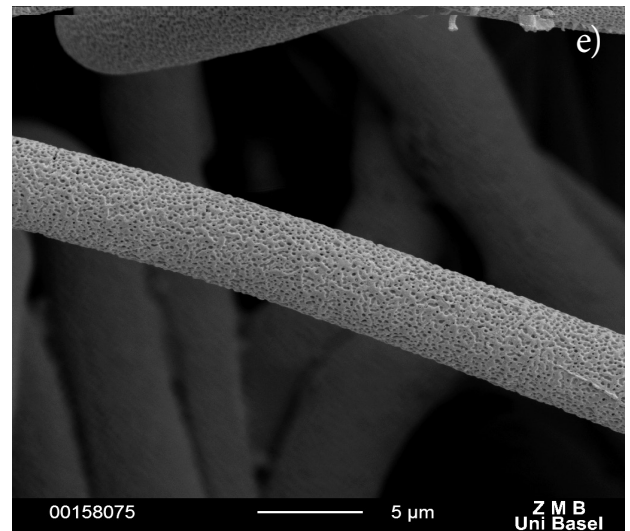
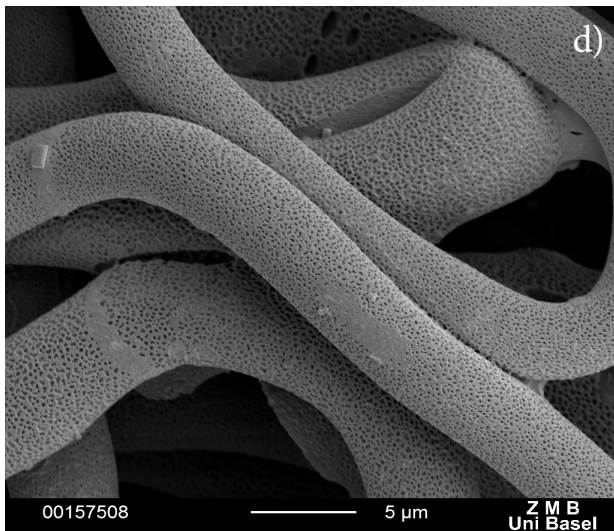
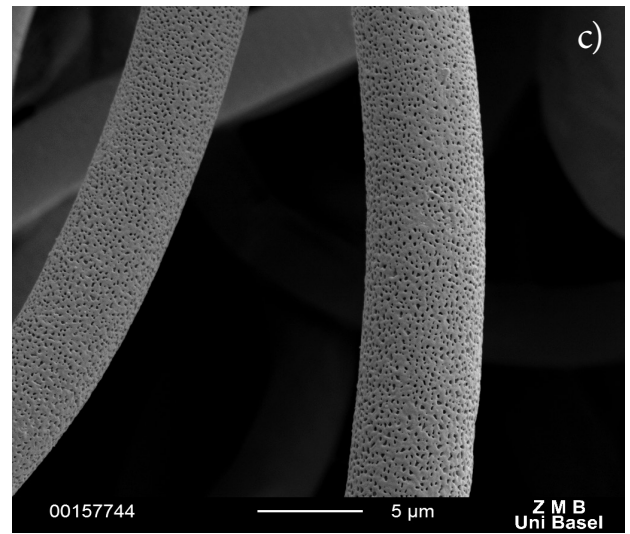
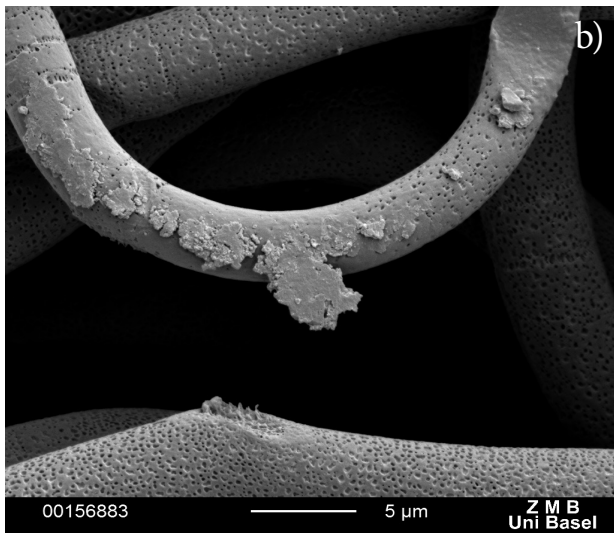
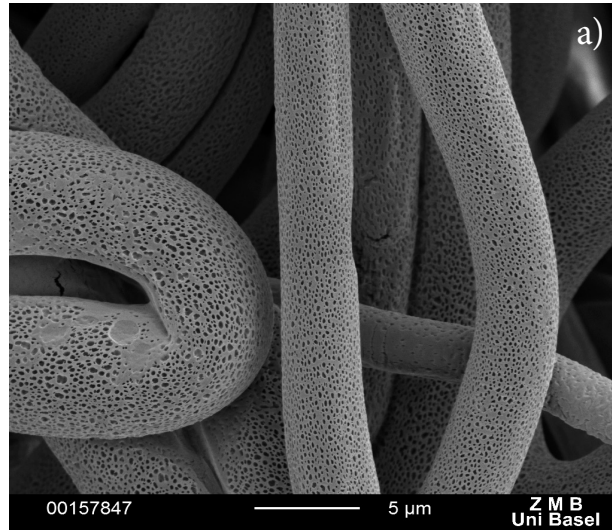


**Figure 40:** SEM images of pure PLGA fibres after different immersion times. a) raw material. b) 12 h immersion. c) 24 h immersion. d) 168 h immersion. e) 336 h immersion

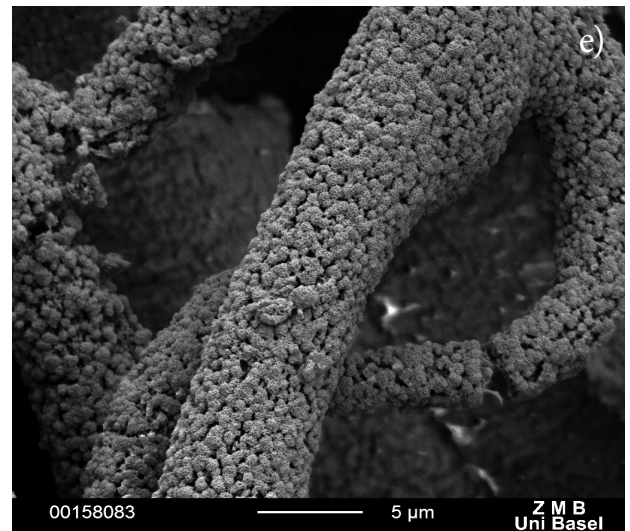
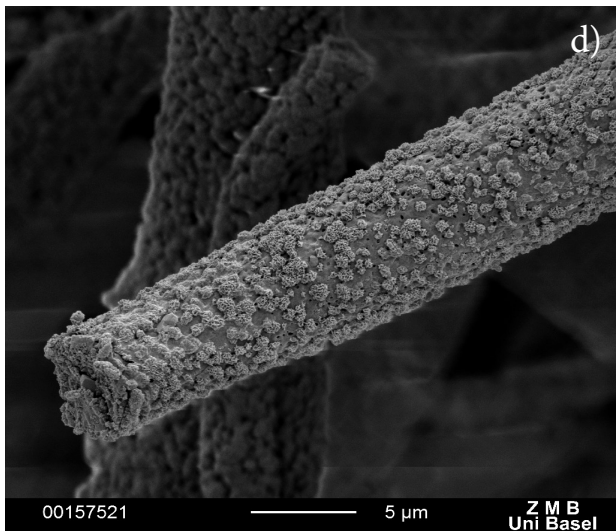
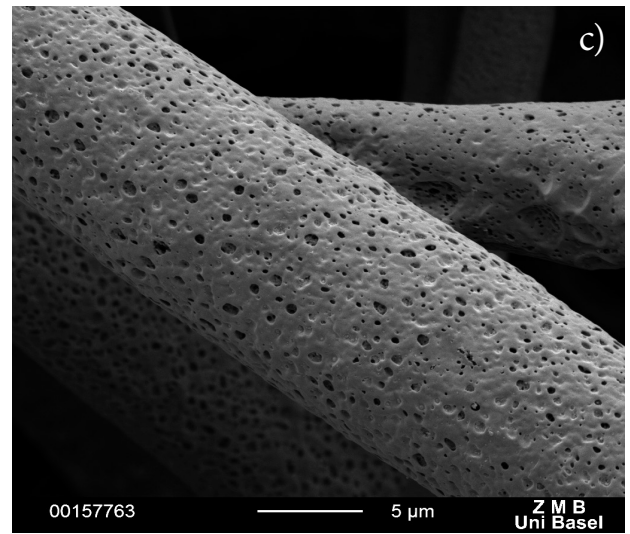
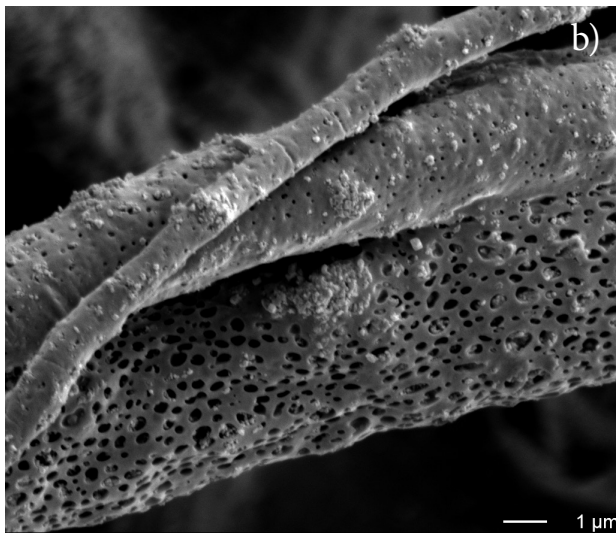
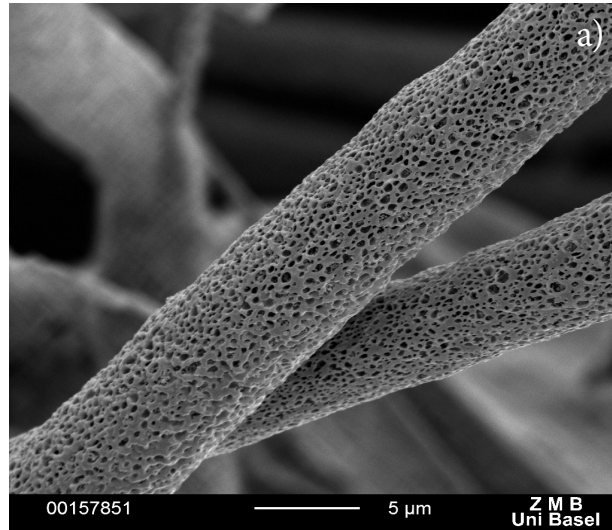


**Figure 41:** SEM images of Bonewool®8020 after different immersion times. a) raw material. b) 12 h immersion. c) 24 h immersion. d) 168 h immersion. e) 336 h immersion

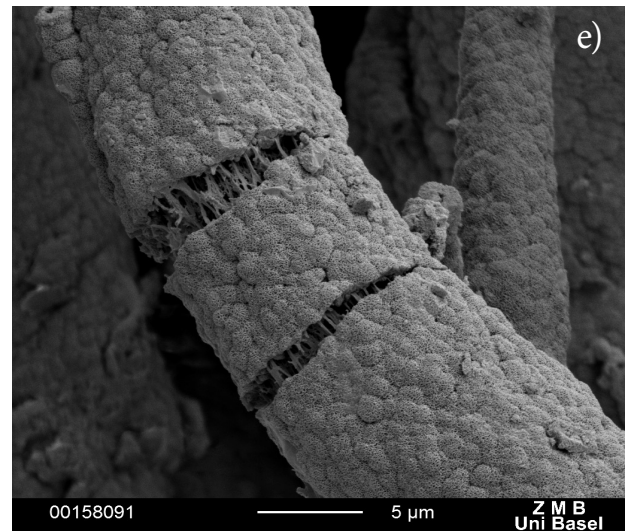
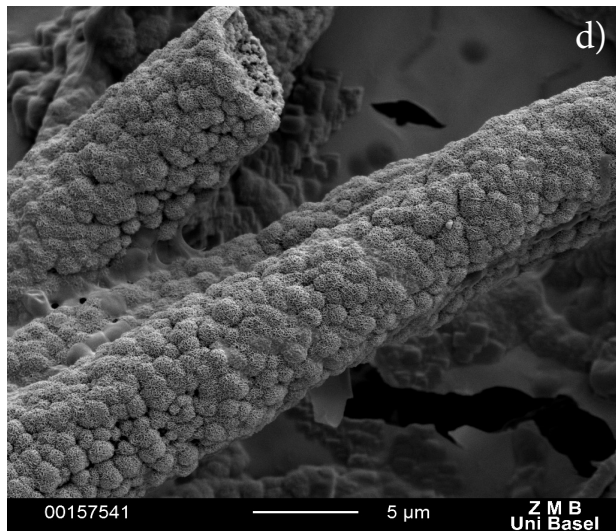
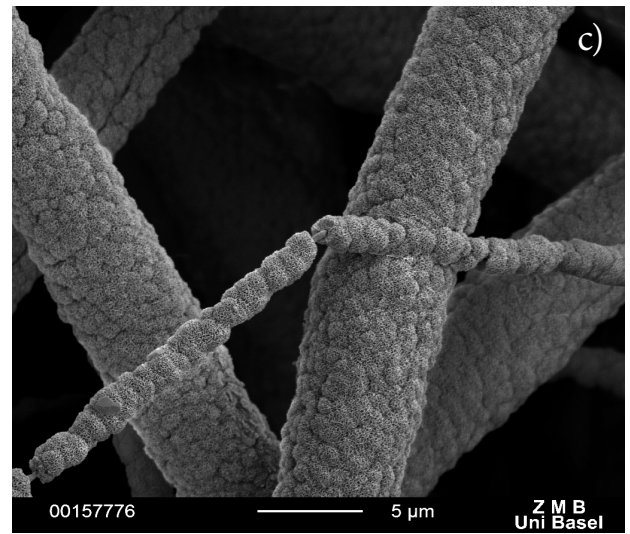
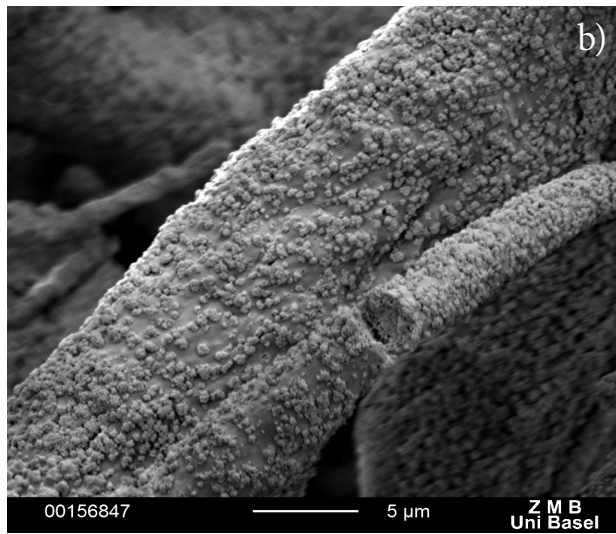
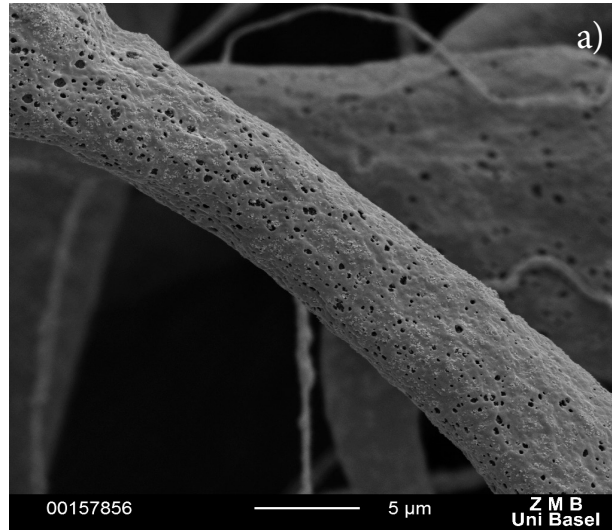


**Figure 42:** SEM images of Bonewool®6040 after different immersion times. a) raw material. b) 12 h immersion. c) 24 h immersion. d) 168 h immersion. e) 336 h immersion

## Commercial HA materials

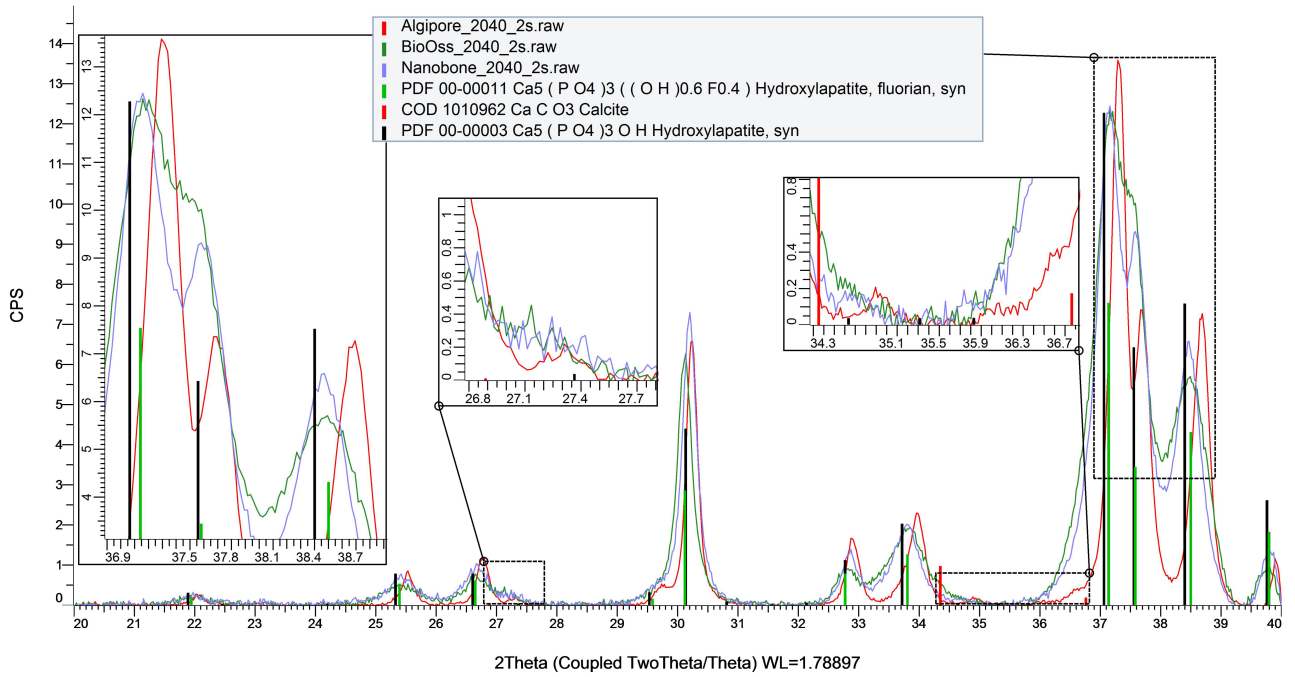


Figure 43: XRD spectra of the commercial materials Algipore®, BioOss® and Nanobone®.

## Synthetic BCP

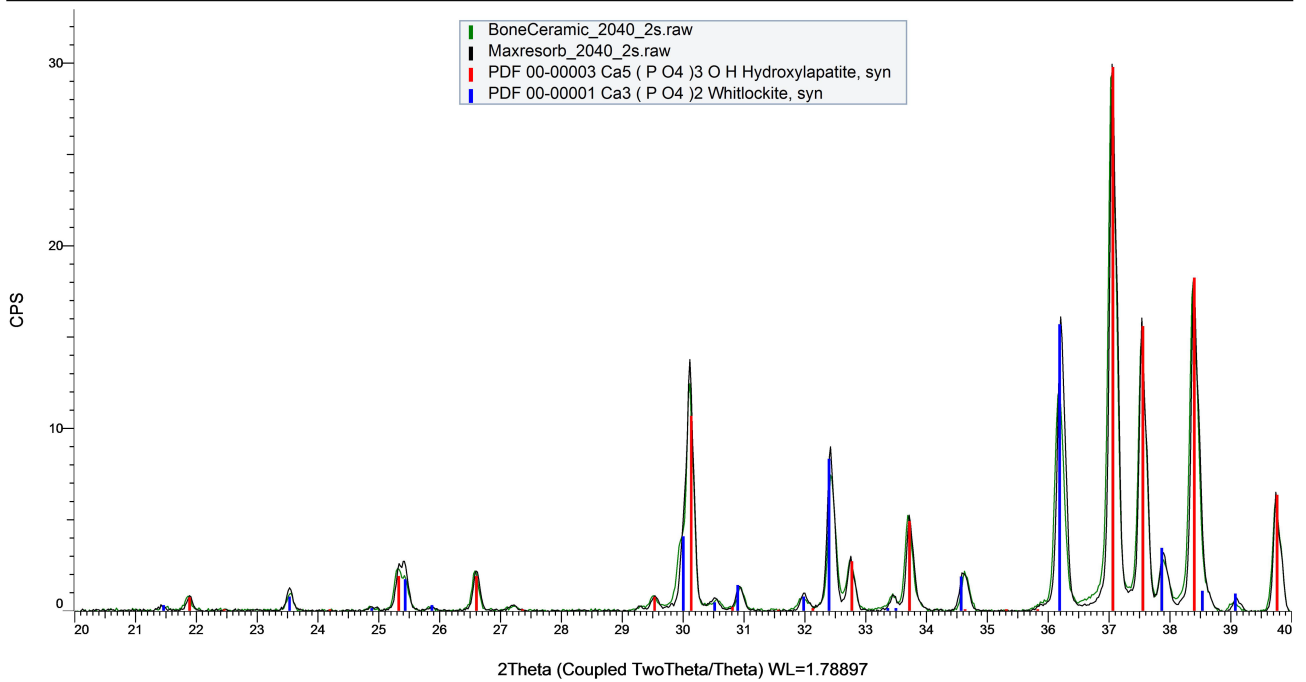


Figure 44: XRD spectra of the commercial biphasic calcium phosphates BoneCeramic® and Maxresorb®.

### ALgOss raw (BCP with different HA/ TCP ratios)

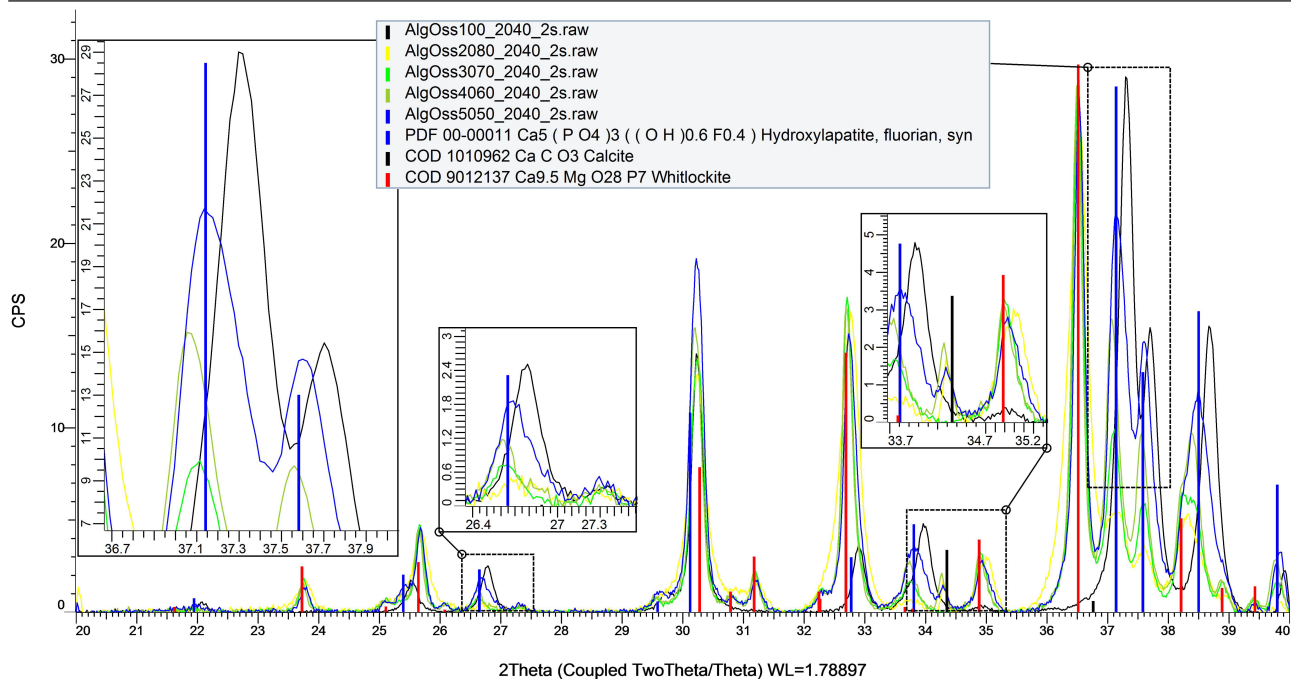


Figure 45: XRD spectra of the ALgOss® series.

### Bonewool8020 and 6040 after combustion of PLGA for different immersion times

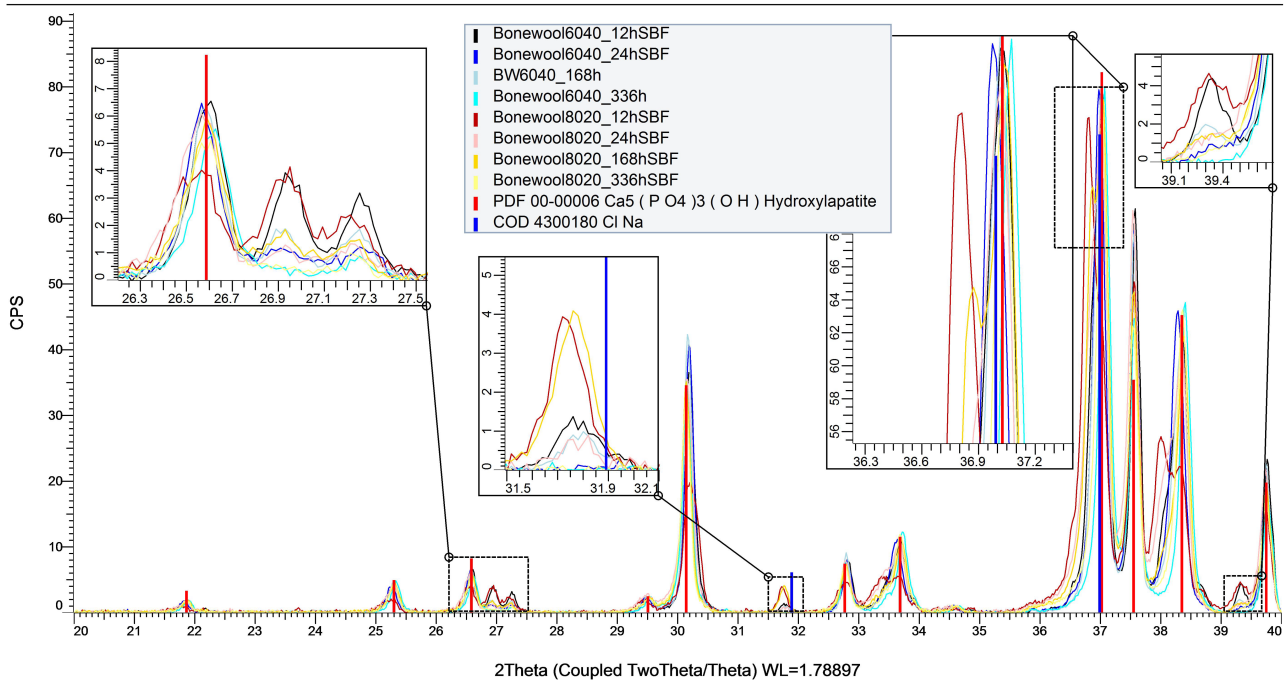


Figure 46: XRD spectra of the inorganic content of PLGA/ATCP composite materials after different immersion times.

### AlgOss 20% HA 80% TCP (different immersion times)

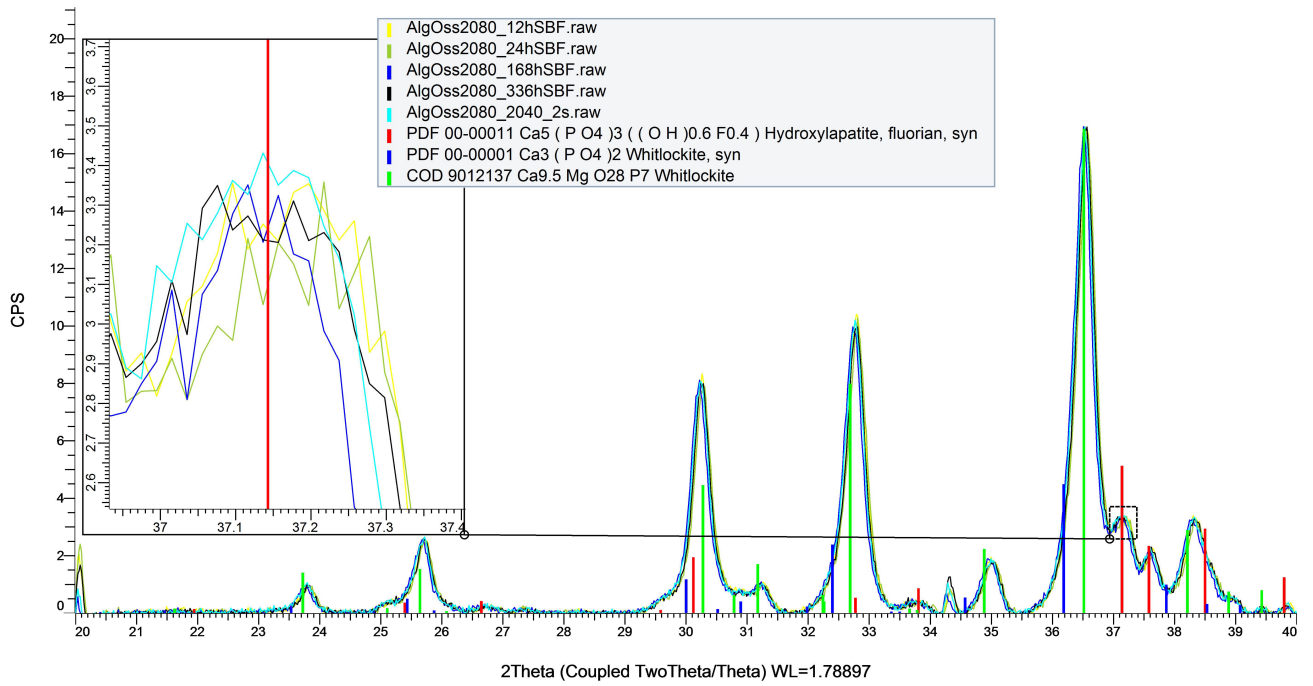


Figure 47: XRD spectra of AlgOss®2080 after different immersion times.

**Erklärung zur wissenschaftlichen Redlichkeit**

(beinhaltet Erklärung zu Plagiat und Betrug)

Bachelorarbeit / Masterarbeit (*nicht Zutreffendes bitte streichen*)

Titel der Arbeit (*Druckschrift*):

In vitro Evaluation of the Relevant Properties of Different Bone Graft Materials

---

---

---

Name, Vorname (*Druckschrift*): Bellon, Benjamin

Matrikelnummer: 09-059-452

Hiermit erkläre ich, dass mir bei der Abfassung dieser Arbeit nur die darin angegebene Hilfe zuteil wurde und dass ich sie nur mit den in der Arbeit angegebenen Hilfsmitteln verfasst habe.

Ich habe sämtliche verwendeten Quellen erwähnt und gemäss anerkannten wissenschaftlichen Regeln zitiert.

Diese Erklärung wird ergänzt durch eine separat abgeschlossene Vereinbarung bezüglich der Veröffentlichung oder öffentlichen Zugänglichkeit dieser Arbeit.

ja     nein

Ort, Datum: Basel, 18.12.2015

Unterschrift:



---

*Dieses Blatt ist in die Bachelor-, resp. Masterarbeit einzufügen.*